

LA-5412-T

THESIS

e.3

CIC-14 REPORT COLLECTION  
**REPRODUCTION  
COPY**

Polarization Transfer in  
Proton-Deuteron Elastic Scattering



**los alamos**  
**scientific laboratory**

of the University of California

LOS ALAMOS, NEW MEXICO 87544



This report was prepared as an account of work sponsored by the United States Government. Neither the United States nor the United States Atomic Energy Commission, nor any of their employees, nor any of their contractors, subcontractors, or their employees, makes any warranty, express or implied, or assumes any legal liability or responsibility for the accuracy, completeness or usefulness of any information, apparatus, product or process disclosed, or represents that its use would not infringe privately owned rights.

This report is a printed version of a thesis submitted as partial fulfillment of the requirement for an advanced academic degree and as such represents the independent work of the author. It has not been edited by the Technical Information staff.

Printed in the United States of America. Available from  
National Technical Information Service  
U. S. Department of Commerce  
5285 Port Royal Road  
Springfield, Virginia 22151  
Price: Printed Copy \$7.60; Microfiche \$1.45

LA-5412-T

Thesis

UC-34c

ISSUED: November 1973



# Polarization Transfer in Proton-Deuteron Elastic Scattering

by

Clyde Kenneth Mitchell



This report is derived from a dissertation submitted to the Department of Physics and Astronomy and the Graduate School of the University of Wyoming in partial fulfillment of requirements for the Degree of Doctor of Philosophy.

## TABLE OF CONTENTS

CHAPTER	Page
I. INTRODUCTION . . . . .	1
A. Description of Experiment . . . . .	1
B. Formalism . . . . .	6
1. Spin 1/2 . . . . .	6
2. Spin 1 . . . . .	9
C. Summary of Data to be Presented . . . . .	15
II. EXPERIMENTAL APPARATUS . . . . .	17
A. Experimental Situation . . . . .	17
B. "Cube" Scattering Chamber . . . . .	20
C. Deuteron Polarization Transfer Chamber and Polarimeter. . . . .	25
1. Early Design Considerations. . . . .	25
2. Polarization Transfer Chamber. . . . .	31
3. Accessory Lid for the ${}^3\text{He}(\vec{d}, p){}^4\text{He}$ Calibration. . . . .	37
4. Cryostat and Primary Gas Target. . . . .	37
5. Deuteron Polarimeter . . . . .	39
D. Associated Electronics . . . . .	43
III. MEASUREMENT OF PROTON-DEUTERON ANALYZING POWERS. . . . .	47
A. Experimental Procedure . . . . .	47
1. $\text{D}(\vec{p}, d)\text{H}$ . . . . .	47
2. $\text{H}(\vec{d}, p)\text{D}$ . . . . .	50
B. Results . . . . .	52

CHAPTER	Page
1. $D(\vec{p}, d)H$ . . . . .	52
2. $H(\vec{d}, p)D$ . . . . .	54
3. $D(p, \vec{d})H$ . . . . .	67
IV. CALIBRATION OF THE DEUTERON POLARIMETER . . . . .	74
A. Introduction . . . . .	74
B. Experimental Procedure . . . . .	80
C. Determination of Average Deuteron Inter- action Energy . . . . .	88
D. Unfolding Analyzing Powers from Thick Geometry . . . . .	96
E. Results . . . . .	97
V. MEASUREMENT OF PROTON-DEUTERON POLARIZATION TRANSFER . . . . .	104
A. Experimental Data Collection Procedure . . . . .	104
1. Experimental Arrangement . . . . .	104
2. Selection of Machine Energy via an Excitation Function . . . . .	108
3. Data Collection . . . . .	111
B. Data Reduction Procedures . . . . .	115
C. Results . . . . .	127
D. Summary . . . . .	131
1. Experimental . . . . .	131
2. Theoretical . . . . .	134

LIST OF TABLES

TABLE	Page
1. Measured Analyzing Powers ( $A_y$ ) for the Reaction $D(\vec{p}, d)H$ . . . . .	53
2. Measured Analyzing Powers for $H(\vec{d}, p)D$ at 7.98 MeV . . . . .	56
3. Measured Analyzing Powers for $H(\vec{d}, p)D$ at 10.00 MeV . . . . .	57
4. Measured Analyzing Powers for $H(\vec{d}, p)D$ at 12.00 MeV . . . . .	58
5. Measured Analyzing Powers for $H(\vec{d}, p)D$ at 14.00 MeV . . . . .	59
6. Measured Analyzing Powers for $H(\vec{d}, p)D$ at 16.00 MeV . . . . .	61
7. Measured Values of $A_{xz}$ for $H(\vec{d}, p)D$ at 17.00 MeV . . . . .	62
8. Polarization of Deuterons from p-d Elastic Scattering at 3.99 MeV . . . . .	70
9. Polarization of Deuterons from p-d Elastic Scattering at 5.00 MeV . . . . .	71
10. Polarization of Deuterons from p-d Elastic Scattering at 6.00 MeV . . . . .	72
11. Polarization of Deuterons from p-d Elastic Scattering at 7.00 MeV . . . . .	73
12. Measured ${}^3\text{He}(\vec{d}, p){}^4\text{He}$ Analyzing Powers in Thick Geometry . . . . .	98

TABLE	Page
13. Finite Geometry Corrected ${}^3\text{He}(\vec{d},p){}^4\text{He}$ Analyzing Powers . . . . .	99
14. Measured Outgoing Deuteron Polarizations Expressed in the Reaction Final Coordinate System at a Laboratory Angle of $22.5^\circ$ . . . . .	128
15. Analyzing Power, Polarization Functions, and Vector to Tensor Polarization Transfer Coefficients for $D(p,d)H$ Elastic Scattering . . . . .	129
16. Analyzing Power Measurements for the Reaction ${}^3\text{He}(\vec{d},p){}^4\text{He}$ for $1.03\text{MeV} \leq E_d \leq 4.00\text{MeV}$ . . . . .	144

CONTENTS OF APPENDICES

APPENDIX	Page
A. Measurement of Analyzing Powers in Reactions Induced by Polarized Deuterons via the Ratio Method . . . . .	138
B. Low Energy Analyzing Power Measurements in the Reaction ${}^3\text{He}(\vec{d},p){}^4\text{He}$ . . . . .	143
C. Finite Geometry Computer Code . . . . .	146

## LIST OF FIGURES

FIGURE	Page
1. Schematic of Experimental Facilities . . . . .	18
2. "Cube" Scattering Chamber . . . . .	21
3. "Cube" Detector Telescope Assembly . . . . .	23
4. Deuteron Polarization Transfer Chamber; Horizontal Cross Section . . . . .	32
5. Deuteron Polarization Transfer Chamber; Vertical Cross Section . . . . .	33
6. Block Diagram of Electronics . . . . .	44
7. Vector Analyzing Power for $D(\vec{p}, d)H$ . . . . .	55
8. Analyzing Powers for $H(\vec{d}, p)D$ at 7.98 MeV . . . . .	63
9. Analyzing Powers for $H(\vec{d}, p)D$ at 10.00 MeV . . . . .	64
10. Analyzing Powers for $H(\vec{d}, p)D$ at 12.00 MeV . . . . .	65
11. Analyzing Powers for $H(\vec{d}, p)D$ at 14.00 MeV . . . . .	66
12. Experimental Arrangement for ${}^3\text{He}(\vec{d}, p){}^4\text{He}$ Calibration . . . . .	81
13. Excitation Function for ${}^3\text{He}(\vec{d}, p){}^4\text{He}$ Calibration . . . . .	92
14. Average Deuteron Interaction Energy as a Function of Machine Energy . . . . .	94
15. Deuteron Energy Distributions Entering the ${}^3\text{He}$ Cell . . . . .	95
16. Corrected ${}^3\text{He}(\vec{d}, p){}^4\text{He}$ Analyzing Powers . . . . .	101

FIGURE	Page
17. Ratios of Observed Analyzing Powers to Values Which would Obtain if the Reaction Proceeded Completely through a $j = 3/2^+$ Compound State . . .	102
18. Experimental Arrangement for $D(\vec{p}, \vec{d})H$ Polarization Transfer . . . . .	105
19. Typical Excitation Function for $D(\vec{p}, \vec{d})H$ Polarization Transfer . . . . .	110
20. Typical Mass and Energy Spectra for Unpolarized Run in $D(p, \vec{d})H$ at 8.09 MeV . . . . .	113
21. Detector Orientation with Beam going into the Plane of the Page . . . . .	114

## ABSTRACT

Vector-to-tensor polarization transfer coefficients in proton-deuteron elastic scattering have been measured at outgoing deuteron laboratory angles of  $0^\circ$ ,  $22.5^\circ$ , and  $45^\circ$  in the energy range  $4.1 \text{ MeV} \leq E_p \leq 9.1 \text{ MeV}$ . The various vector-to-tensor polarization transfer coefficients are consistent with zero, in view of the errors, but effects of the order of  $\sim 0.05$  cannot be ruled out. The  ${}^3\text{He}(\vec{d}, p){}^4\text{He}$  reaction near the 430 keV resonance was used as the deuteron tensor polarization analyzer.

Before the polarization transfer measurements could be completed, the following had to be determined: (1) the vector analyzing power for the reaction  $D(\vec{p}, d)H$ , (2) deuteron polarization resulting from an unpolarized incident proton beam, and (3) the analyzing properties of the  ${}^3\text{He}(\vec{d}, p){}^4\text{He}$  reaction near the resonance.

With respect to (1), angular distributions of the vector analyzing power for the reaction  $D(\vec{p}, d)H$  were measured at 4.00 MeV, 6.00 MeV, and 8.00 MeV. With respect to (2), angular distributions of deuteron polarization functions  $P^{y'}(\theta)$ ,  $P^{x'z'}(\theta)$ ,  $1/2(P^{x'x'}(\theta) - P^{y'y'}(\theta))$ , and  $P^{z'z'}(\theta)$  have been measured at proton energies of 3.99 MeV, 5.00 MeV, 6.00 MeV, and 7.00 MeV (corresponding to deuteron energies in the inverse reaction of 7.98 MeV, 10.00 MeV, 12.00 MeV,

and 14.00 MeV). These measurements were accomplished by measuring analyzing powers in the inverse reaction,  $H(\vec{d}, p)D$  and applying a generalization of the polarization-asymmetry equality theorem. The analyzing power measurements show considerable structure although the effects are small when compared to their maximum possible ranges of values.

With respect to (3),  $A_{xz}$  and  $1/2(A_{xx}-A_{yy})$  for the  ${}^3\text{He}(\vec{d}, p){}^4\text{He}$  reaction were measured in the vicinity of  $\theta_{\text{c.m.}} = 54.7^\circ$ .  $A_{zz}$  was measured at  $0^\circ$ . The measurements were made in thick geometry for average deuteron interaction energies in the range  $366 \text{ keV} \leq \bar{E}_d \leq 1090 \text{ keV}$ . Corrections made to the thick geometry measurements were typically 0.020 and in no case larger than 0.035. The measured values are indicative of the contribution of waves higher than S-waves in this energy region.

Finally, one vector-to-vector polarization transfer coefficient,  $K_x^{x'}$ , was measured at  $\theta_d^{\text{lab}} = 22.5^\circ$  at an incident proton energy of 9.08 MeV and found to be nonzero. The  ${}^3\text{He}(\vec{d}, p){}^4\text{He}$  reaction for deuteron energies near 5.6 MeV was used to analyze the outgoing deuteron vector polarization.

Recent calculations of nucleon and deuteron polarizations as well as cross sections for nucleon-deuteron scattering have been made by solving numerically the Faddeev-Lovelace three body integral equations (Fa 61, Lo 64) for a given set of potentials. Currently, the best qualitative agreement to nucleon-deuteron data for nucleon

energies  $2 \leq E_N \leq 77$  MeV has been obtained with a two-potential formula for separable S-, P-, and D-wave nucleon-nucleon forces with the inclusion of a  ${}^3S_1$ - ${}^3D_1$  tensor force (Pi 72b, Pi 73). The calculated vector-to-tensor polarization transfer coefficients agree well with the present measurements though there is some structure near a c.m. angle of  $120^\circ$  (corresponding to an outgoing deuteron laboratory angle of  $30^\circ$ ). This class of transfer measurements seems to be somewhat insensitive to changes in the scattering amplitudes. Calculations of vector-to-vector polarization transfer coefficients, on the other hand, are large and appear more sensitive to such changes--both in  $D(\vec{p}, \vec{p})D$  and  $D(\vec{p}, \vec{d})H$  elastic scattering. This then may be a more fruitful place in which to look. It is not yet known whether the two-standard-deviation disagreement with the single measurement of  $K_x^x$  is significant.

CHAPTER I  
INTRODUCTION

A. Description of Experiment

In an effort to better understand nuclear forces more and more experiments involving polarized nuclei are being performed. These experiments yield polarization and polarization related quantities which supplement differential cross section data and help provide information on the spin dependence of the nuclear interaction.

With the availability of polarized beams, first obtained by a scattering or reaction and more recently obtained with polarized ion sources, experiments and modeling efforts have become more and more sophisticated. This has resulted in the possibility of several classes of two-particle experiments:

1.  $A(B,C)D$  cross section experiments
2.  $A(\vec{B},C)D$  analyzing power experiments
3.  $A(B,\vec{C})D$  polarization experiments
4.  $\vec{A}(\vec{B},C)D$  and  
 $A(B,\vec{C})\vec{D}$  spin correlation experiments
5.  $A(\vec{B},\vec{C})D$  polarization transfer experiments

An arrow above a particle group indicates that its polarization is known or is measured. An experiment of type (1) involves a measurement of particle intensities. An experiment of type (2) involves the use of a polarized incident beam and the measurement of asymmetrical intensities

in the angular distribution of reaction products, such as a left-right asymmetry. Experiments of type (3) implies the use of some sort of device (a polarization analyzer) to measure the polarization of the outgoing particles; this is normally done in a further reaction or scattering of type (2) for which the analyzing properties have previously been measured or can be calculated. Spin correlation coefficients are obtained (1) by bombarding a polarized target with a polarized beam and measuring asymmetrical intensities for various combinations of beam and target polarization for the reaction products or (2) by bombarding an unpolarized target with an unpolarized beam and measuring the polarization of both of the reaction products.

Experiments of type (5) are similar to those of type (3) in that the polarization of outgoing particles are to be measured. The two types differ in that reactions of type (5) are initiated with polarized incident beams whereas those of type (3) are initiated with unpolarized incident beams. Experiments of type (5) are historically referred to as triple scattering experiments in deference to the manner in which the polarized beam was obtained; that is, the first reaction or scattering was used to produce the polarized beam, the second was the one under investigation, and the third was used to analyze the polarization of the particles emerging from the second. A polarized ion source replaces the first reaction thereby

reducing polarization transfer experiments to double scattering experiments although available beam intensities are less than can be obtained with unpolarized ion sources. Completion of polarization transfer experiments frequently requires that experiments of the second and third type also be performed.

Experiments involving the spins of three or more particle groups simultaneously might be considered to form an additional class of experiments (e.g.,  $\vec{A}(\vec{b}, \vec{c})D$  or  $A(\vec{b}, \vec{c})\vec{D}$ ). Such experiments would be extremely difficult. However, it is likely that experiments of this class will never be performed, for Simonius (Si 71) has shown that all scattering amplitudes can be determined by considering no more than two polarized particle groups at a time, i.e., that experiments of types (1-5) always suffice.

It should also be noted that the complexity of experiments within each class (except class (1)) is dependent upon the complexity of the spin structure of the particles involved. There are  $(2S+1)^2-1$  quantities required to describe the polarization of an ensemble of particles of spin  $S$ . For spin-1/2 particles, the three quantities form the components of a vector. For spin-1 particles, three of the eight quantities form the components of a vector while the remaining five form the components of a second-rank tensor. The number of observables in each class

of experiment increases as the spin structure becomes more complex. This will become more apparent in the next section of this chapter.

A very useful relation between the analyzing powers for reactions induced with polarized spin-1/2 particles and the polarization produced in the inverse reaction (Bl 52, Da 52, Wo 52), called the polarization-asymmetry equality (Be 58), has been generalized (Sa 58) to include spin polarization moments of higher order, provided time reversal invariance is satisfied. From an experimental point of view, this means that in principle an experiment of type (3) may be performed by doing the inverse reaction, one of type (2) (i.e.,  $A(B, \vec{C})D \leftrightarrow D(\vec{C}, B)A$ ). In practice, this is not always feasible as is the case where the polarized particles are neutrons or if the polarized beam,  $\vec{C}$ , is not available.

The purpose of this thesis was to design, build, and use a scattering chamber in which the second-rank (tensor) polarization moments of outgoing deuterons from reactions induced by polarized proton or deuteron beams could be measured at tandem accelerator energies. For incident polarized proton beams this would permit a determination of vector-to-tensor polarization transfer coefficients. For incident polarized deuteron beams both vector-to-tensor and tensor-to-tensor polarization transfer coefficients can be obtained.

Early design considerations were based on the reaction,  ${}^4\text{He}(\vec{d}, \vec{d}){}^4\text{He}$ . However, an engineering problem (to be discussed in Chapter II) prompted a change to the reaction  $\text{D}(\vec{p}, \vec{d})\text{H}$  for which there were also fewer observables. Although the engineering problem was later solved and the  ${}^4\text{He}(\vec{d}, \vec{d}){}^4\text{He}$  experiment resumed, those data will not be presented here.

Only recently have polarization transfer experiments become routinely feasible. However, previous experimenters have measured vector-to-vector polarization transfer coefficients; corresponding to the well known Wolfenstein (Wo 56) triple-scattering parameters (originally formulated for reactions of the type  $\text{A}(\vec{p}, \vec{p})\text{D}$  and later extended (Ga 70, Oh 72a) to reactions involving other spin combinations). An extensive review of polarization transfer and spin correlation experiments involving spin-1/2 and spin-1 particles has been written by Ohlsen (Oh 72b).

The experiment forming the subject of this thesis,  $\text{D}(\vec{p}, \vec{d})\text{H}$ , is the first experiment to measure polarization transfer coefficients of the vector-to-tensor type. In order to effect these measurements the following had to be done:

1. Design and build a scattering chamber.
2. Measure the vector analyzing power for the reaction  $\text{D}(\vec{p}, \vec{d})\text{H}$ .
3. Measure the deuteron tensor polarization components

which result from an unpolarized incident proton beam for the reaction  $D(p, \vec{d})H$ . This was accomplished by measuring the analyzing powers for the inverse reaction,  $H(\vec{d}, p)D$  and utilizing the polarization-asymmetry equality theorem.

4. Design, build, and calibrate a polarimeter to measure deuteron tensor polarization. The  ${}^3\text{He}(\vec{d}, p){}^4\text{He}$  reaction for  $E_d < 1$  MeV was chosen for this purpose.
5. Measure the deuteron tensor polarization components which result from a polarized incident proton beam for the reaction  $D(\vec{p}, \vec{d})H$  and extract the various polarization transfer coefficients.
6. Write various computer codes to analyze and correct the data for finite geometry and thick target effects.

Item (1) constitutes a large portion of Chapter II. Chapter III deals with items (2) and (3), and Chapter IV deals with item (4). Chapter V is reserved for the polarization transfer measurements. The finite geometry code is discussed in Appendix C.

## B. Formalism

### 1. Spin 1/2

It is the purpose of this section to outline briefly the formalism of polarization phenomena as it applies to p-d elastic scattering. The description given here is modeled after the formalism developed by Gammel

et al. (Ga 70), for which the reactions  $T(\vec{d}, \vec{n})^4\text{He}$  and  $^3\text{He}(\vec{d}, \vec{p})^4\text{He}$  are special cases, and Ohlsen et al. (Oh 72a) who in turn modeled their work after that of Wolfenstein (Wo 56).

A single spin-1/2 particle can be represented by a Pauli spinor  $\chi = \begin{pmatrix} a_1 \\ a_2 \end{pmatrix}$ . For such a particle there is a direction in which the projection of spin points. If this direction is chosen as the Z axis then  $\chi = \begin{pmatrix} 1 \\ 0 \end{pmatrix}$ . The expectation value of an observable corresponding to a Hermitian operator  $O$  is given by

$$\begin{aligned} \langle O \rangle &= \chi^\dagger O \chi = (a_1^* \ a_2^*) \begin{pmatrix} O_{11} & O_{12} \\ O_{21} & O_{22} \end{pmatrix} \begin{pmatrix} a_1 \\ a_2 \end{pmatrix} \\ &= |a_1|^2 O_{11} + a_1^* a_2 O_{12} + a_2^* a_1 O_{21} + |a_2|^2 O_{22} = \text{tr } \rho O, \end{aligned} \quad (1-1)$$

where  $\rho$ , the density matrix, has been defined as

$$\rho = \begin{pmatrix} |a_1|^2 & a_1 a_2^* \\ a_2 a_1^* & |a_2|^2 \end{pmatrix}. \quad (1-2)$$

For an ensemble of  $N$  particles, each element of the density matrix is replaced with the average value; e.g.,

$$\rho_{11} = \frac{1}{N} \sum_{n=1}^N |a_1^{(n)}|^2 \quad \text{and} \quad \rho_{12} = \frac{1}{N} \sum_{n=1}^N a_1^{(n)} a_2^{(n)*}.$$

The state of polarization of an ensemble of spin-1/2 particles is specified by the expectation values of the Pauli spin operators:

$$\begin{aligned}
p_x &= \langle \sigma_x \rangle = \text{tr } \rho \sigma_x \\
p_y &= \langle \sigma_y \rangle = \text{tr } \rho \sigma_y \\
p_z &= \langle \sigma_z \rangle = \text{tr } \rho \sigma_z \quad , \quad (1-3)
\end{aligned}$$

where

$$\begin{aligned}
\sigma_x &= \begin{pmatrix} 0 & 1 \\ 1 & 0 \end{pmatrix} \\
\sigma_y &= \begin{pmatrix} 0 & -i \\ i & 0 \end{pmatrix} \\
\sigma_z &= \begin{pmatrix} 1 & 0 \\ 0 & -1 \end{pmatrix} . \quad (1-4)
\end{aligned}$$

A polarized spin-1/2 beam produced in an ion source has an axis of symmetry referred to as the quantization axis. For such a beam having  $N_+$  particles with their spin projections aligned with the quantization axis and  $N_-$  particles with their spin projections aligned opposite to the quantization axis, the density matrix is given by

$\rho = \frac{1}{N_+ + N_-} \begin{pmatrix} N_+ & 0 \\ 0 & N_- \end{pmatrix}$ , where it has been assumed that the Z axis is along the axis of quantization. The beam polarization is then given by

$$p_z = \text{tr } \rho \sigma_z = \frac{N_+ - N_-}{N_+ + N_-} , \quad (1-5)$$

with  $p_x = p_y = 0$ . Each vector polarization component thus defined is bounded by the limits  $\pm 1$ . It should also be noted that the three Pauli operators and the 2x2 unit matrix are an orthogonal set in the sense that

$$\text{tr } \sigma_i \sigma_j = 2\delta_{ij} \quad . \quad (1-6)$$

Hence, any 2x2 matrix, M, may be expanded in terms of the basis set.

## 2. Spin 1

A spin-1 particle is characterized by a three-component spinor  $\chi = \begin{pmatrix} a_1 \\ a_2 \\ a_3 \end{pmatrix}$ . In this case there is a direction for which  $\chi = \begin{pmatrix} 1 \\ 0 \\ 0 \end{pmatrix}$  or  $\chi = \begin{pmatrix} 0 \\ 1 \\ 0 \end{pmatrix}$  if this direction is chosen as the quantization axis. The second case corresponds to the spin vector perpendicular to the quantization axis while precessing around it. This double possibility is what forces quantities more complicated than for the spin-1/2 case to be considered. A 3x3 density matrix may be defined in a manner similar to the 2x2 density matrix for the spin-1/2 case.

The basic spin-1 angular momentum operators are

$$\begin{aligned} S_x = \phi_x &= \frac{1}{\sqrt{2}} \begin{pmatrix} 0 & 1 & 0 \\ 1 & 0 & 1 \\ 0 & 1 & 0 \end{pmatrix} & S_y = \phi_y &= \frac{1}{\sqrt{2}} \begin{pmatrix} 0 & -i & 0 \\ i & 0 & -i \\ 0 & i & 0 \end{pmatrix} \\ S_z = \phi_z &= \begin{pmatrix} 1 & 0 & 0 \\ 0 & 0 & 0 \\ 0 & 0 & -1 \end{pmatrix} . \end{aligned} \quad (1-7)$$

These three vector polarization operators taken together with the 3x3 unit matrix comprise four Hermitian operators whereas nine are required to span the 3x3 space. It is desirable to construct the remaining operators in such a

way as to (1) have known rotational properties, and (2) have expectation values which vary between convenient limits, and (3) vanish for an unoriented ensemble. The set of tensor operators used here were first obtained by Goldfarb (Go 58) and are defined by

$$\rho_{ij} = \frac{3}{2}(\rho_i \rho_j + \rho_j \rho_i) - 2\delta_{ij}; \quad i, j = x, y, z. \quad (1-8)$$

Whereas five tensor operators were required, six have been defined thereby producing an overcomplete set. The dependence of the operators resulting from the overcompleteness condition is

$$\rho_{xx} + \rho_{yy} + \rho_{zz} = \begin{pmatrix} 0 & 0 & 0 \\ 0 & 0 & 0 \\ 0 & 0 & 0 \end{pmatrix}. \quad (1-9)$$

The set of spin-1 operators so defined are orthogonal in the sense that  $\text{tr} \rho_i \rho_j = 0$  for  $i \neq j$  and  $\text{tr} \rho_{ij} \rho_{kl} = 0$  for  $ij \neq kl$ , while  $\text{tr} \rho_i \rho_i = 2$ ,  $\text{tr} \rho_{ij} \rho_{ij} = 9/2$ , and  $\text{tr} \rho_{ii} \rho_{ii} = 6$ . As in the spin-1/2 case for 2x2 matrices, any 3x3 matrix may be expanded in terms of the overcomplete basis set.

The expectation values of the spin-1 vector operators form the components of a vector. Hence, if the components are known in one coordinate system, they may be obtained in another by a unitary transformation,  $\vec{p}' = \vec{U} \vec{p}$ . Expectation values of the second-rank operators form the elements of a 3x3 symmetrical second-rank tensor, (pp). The components of (pp) in a new system may be obtained by the transformation  $(pp)' = U(pp)\tilde{U}$ .

A polarized spin-1 beam produced in a polarized ion source may have  $N_+$  particles with spin projections aligned with,  $N_0$  with spin projections perpendicular to, and  $N_-$  with spin projections aligned opposite to the quantization axis. If the Z axis is chosen along the quantization axis then the density matrix is given by

$$\rho = \frac{1}{N_+ + N_0 + N_-} \begin{pmatrix} N_+ & 0 & 0 \\ 0 & N_0 & 0 \\ 0 & 0 & N_- \end{pmatrix}. \quad (1-10)$$

The nonzero polarization components are found to be, from the expression  $p_{ij} = \text{tr } \rho \phi_{ij}$ ,

$$p_Z = \frac{N_+ - N_-}{N_+ + N_0 + N_-} \quad p_{ZZ} = \frac{N_+ + N_- - 2N_0}{N_+ + N_0 + N_-}$$

$$p_{XX} = p_{YY} = -\frac{1}{2} p_{ZZ}. \quad (1-11)$$

The quantities  $p_Z$  and  $p_{ZZ}$  are referred to as the vector and tensor components, respectively, of the polarized beam. Note that  $p_{XX} + p_{YY} + p_{ZZ} = 0$  as do the sum of the respective operators. In general, the description of the state of polarization of a spin-1 beam lacking an axis of symmetry may require all three vector components and five independent tensor components.

Expectation values of the various operators are bounded by the limits  $\pm 1$  for vector polarization,  $\pm 3/2$  for  $p_{ij}$  quantities ( $i \neq j$ ), and  $+1$  to  $-2$  for  $p_{ii}$  quantities.

The differential cross section is given as  $\text{tr} \rho_f$  where  $\rho_f$  is the final density matrix given by

$$\rho_f = M \rho_i M^\dagger . \quad (1-12)$$

$\rho_i$  is the initial density matrix and M is a matrix which transforms the incoming spinor into an outgoing spinor (see Ref. (Oh 72a)). The elements of M are functions of both energy and scattering angle. In the present proton-deuteron case  $\rho_f$ ,  $\rho_i$ , and M are all 6x6 matrices. The initial density matrix may be expanded in terms of a direct product of appropriate spin-1 operators and spin-1/2 operators. The basis set obtained in this manner consists of 36 matrices, a typical example of which is

$$\rho_{x\sigma_x} = \frac{1}{\sqrt{2}} \left( \begin{array}{c|ccc} & 0 & 1 & 0 \\ & 1 & 0 & 1 \\ & 0 & 1 & 0 \\ \hline 0 & 1 & 0 & \\ 1 & 0 & 1 & 0 \\ 0 & 1 & 0 & \end{array} \right) . \quad (1-13)$$

When the suggested expansion is carried out with the aid of the normalization conditions (assuming an unpolarized deuteron target) and the expanded result substituted into

---

\*Some authors prefer to multiply the spin-1 operators by an appropriate constant such that  $\text{tr} \Omega_i \Omega_j = 3 \delta_{ij}$ , where  $\Omega_i = a_i \phi_{jk}$ , then expand in terms of the  $\Omega$  set.

Eq. (1-12), the resulting observables can be expressed compactly as

$$I(\theta, \varphi) = I_0(\theta) \left( 1 + \sum_{j=1}^3 p_j A_j(\theta) \right)$$

$$p_{\ell'} I(\theta, \varphi) = I_0(\theta) \left( P^{\ell'}(\theta) + \sum_{j=1}^3 p_j K_j^{\ell'}(\theta) \right)$$

$$p_{\ell'm'} I(\theta, \varphi) = I_0(\theta) \left( P^{\ell'm'}(\theta) + \sum_{j=1}^3 p_j K_j^{\ell'm'}(\theta) \right), \quad (1-14)$$

where

$$A_j(\theta) = \frac{\text{tr} M \sigma_j M^\dagger}{\text{tr} M M^\dagger} \quad \text{analyzing powers}$$

$$P^{\ell'}(\theta) = \frac{\text{tr} M M^\dagger \mathcal{P}^{\ell'}}{\text{tr} M M^\dagger} \quad \begin{array}{l} \text{outgoing polarization} \\ \text{(unpolarized incident} \\ \text{beam)} \end{array}$$

$$P^{\ell'm'}(\theta) = \frac{\text{tr} M M^\dagger \mathcal{P}^{\ell'm'}}{\text{tr} M M^\dagger} \quad \begin{array}{l} \text{outgoing polarization} \\ \text{(unpolarized incident} \\ \text{beam)} \end{array}$$

$$\left. \begin{array}{l} K_j^{\ell'}(\theta) = \frac{\text{tr} M \sigma_j M^\dagger \mathcal{P}^{\ell'}}{\text{tr} M M^\dagger} \\ K_j^{\ell'm'}(\theta) = \frac{\text{tr} M \sigma_j M^\dagger \mathcal{P}^{\ell'm'}}{\text{tr} M M^\dagger} \end{array} \right\} \quad \begin{array}{l} \text{polarization transfer} \\ \text{coefficients .} \end{array} \quad (1-15)$$

$I_0(\theta)$  and  $I(\theta, \varphi)$  are the unpolarized and polarized differential cross sections, respectively. The  $p_j$  (unprimed) refer to the vector polarization of the incident proton beam as described in the reaction initial coordinate system. The  $p_{\ell'}$  and  $p_{\ell'm'}$  refer to the vector and tensor

polarization, respectively, of the outgoing deuterons as described in the reaction final coordinate system (referred to as the outgoing laboratory helicity frame in Ref. (Oh 72b)). Both coordinate systems are illustrated in Fig. 18.

From an experimental point of view it is fortunate that parity conservation restricts the number of observables. This restriction requires that an observable vanish unless  $N_x + N_z$  is an even number where  $N_x$  is the number of times  $x$  appears and  $N_z$  is the number of times  $z$  appears. For example,  $K_x^{y'} z'$  would be allowed whereas  $K_y^{y'} z'$  would not be allowed. Rotational invariance requires that the observables be even or odd functions of the scattering angle,  $\theta$ , as  $N_x + N_y$  is even or odd.

When these rules are applied to Eq. (1-14), the following results:

$$\begin{aligned}
 I &= I_0(1 + p_y \underline{A_y}) \\
 p_x, I &= I_0(p_x \underline{K_x^{x'}} + p_z \underline{K_z^{x'}}) \\
 p_y, I &= I_0(\underline{p_y^{y'}} + p_y \underline{K_y^{y'}}) \\
 p_z, I &= I_0(p_x \underline{K_x^{z'}} + p_z \underline{K_z^{z'}}) \\
 p_{x', y'}, I &= I_0(p_x \underline{K_x^{x'} y'} + p_z \underline{K_z^{x'} y'}) \\
 p_{x', z'}, I &= I_0(\underline{p_{x'}^{x' z'}} + p_y \underline{K_y^{x' z'}})
 \end{aligned}$$

$$\begin{aligned}
p_{y',z',I} &= I_0(p_{x'}\underline{K_{x'}^{y'z'}} + p_{z'}\underline{K_{z'}^{y'z'}}) \\
p_{x',x',I} &= I_0(P^{x'x'} + p_{y'}\underline{K_{y'}^{x'x'}}) \\
p_{y',y',I} &= I_0(P^{y'y'} + p_{y'}\underline{K_{y'}^{y'y'}}) \\
p_{z',z',I} &= I_0(P^{z'z'} + p_{y'}\underline{K_{y'}^{z'z'}}) , \tag{1-16}
\end{aligned}$$

where odd functions of scattering angle have been underlined. Because of the overcompleteness of the operators, two of the last three equations of Eq. (1-16) may be rewritten in several ways as for example:

$$(p_{x',x'} - p_{y',y'})I = I_0 \left[ (P^{x'x'} - P^{y'y'}) + p_{y'}(\underline{K_{y'}^{x'x'}} - \underline{K_{y'}^{y'y'}}) \right] .$$

### C. Summary of Data to be Presented

Chapter III contains the results of analyzing power measurements made on p-d elastic scattering. In the reaction  $D(\vec{p}, d)H$ , angular distributions of  $A_y$  in the range  $21^\circ \leq \theta_{lab} \leq 60^\circ$  were made in  $3^\circ$  increments at proton target center energies of 4.00, 6.00, and 8.00 MeV. In the reaction  $H(\vec{d}, p)D$ ,  $A_y$ ,  $A_{yy}$ ,  $A_{xx}$ , and  $A_{xz}$  have been measured at deuteron energies of 7.98, 10.00, 12.00, and 14.00 MeV in the range  $21^\circ \leq \theta_{lab} \leq 60^\circ$ , again in  $3^\circ$  increments.  $A_{zz}$  and  $\frac{1}{2}(A_{xx} - A_{yy})$  have usually been quoted in the literature and so have been tabulated from  $A_{xx}$  and  $A_{yy}$  with the aid of the relation  $A_{xx} + A_{yy} + A_{zz} = 0$ .

In addition to the measured  $H(\vec{d}, p)D$  data, corresponding polarizations resulting in the inverse reaction,  $D(p, \vec{d})H$ , have been tabulated in the recoil deuteron laboratory helicity frame as these quantities were needed for the polarization transfer experiment.

Analyzing powers for the reaction  ${}^3\text{He}(\vec{d}, p){}^4\text{He}$  have been measured for average deuteron interaction energies in the range  $366 \leq \bar{E}_d \leq 1090$  keV.  $A_y$ ,  $A_{xz}$ , and  $\frac{1}{2}(A_{xx} - A_{yy})$  were measured near a center-of-mass scattering angle of  $54.7^\circ$ .  $A_{zz}$  was measured at  $0^\circ$ . Data have been tabulated in Chapter IV, both in thick geometry and with the geometry unfolded.

Chapter V contains results of the polarization transfer measurements for the reaction  $D(\vec{p}, \vec{d})H$ . All vector-to-tensor transfer coefficients have been measured for outgoing deuterons at laboratory angles of  $0^\circ$ ,  $22\frac{1}{2}^\circ$ , and  $45^\circ$ . Measurements were made in the energy range of 4.2 to 9.1 MeV. In addition to the vector-to-tensor transfer coefficients, one vector-to-vector transfer coefficient,  $K_x^{x'}$  (similar to the Wolfenstein R parameter), was measured at  $\theta_{\text{lab}} = 22\frac{1}{2}^\circ$  and at an incident proton energy of 9.08 MeV.

## CHAPTER II

### EXPERIMENTAL APPARATUS

#### A. Experimental Situation

The experiments described in this thesis were performed at the Los Alamos Van de Graaff accelerator facility. The facility consists of two Van de Graaff electrostatic accelerators, a vertical (one-stage) and a horizontal tandem (two-stage) which may be used separately or connected in series and used jointly. The tandem (High Voltage Engineering Corp., Model FN) was used exclusively for the experiments described here and was capable of accelerating ions to energies in the range of 1.5 MeV to 16 MeV. An overall view of the experimental setup used is illustrated in Fig. 1.

The Los Alamos Lamb-shift polarized ion source (La 69, Mc 71) was capable of producing hydrogen or deuterium polarized negative ion beams of approximately 90% and 80% polarization, respectively, with the quantization axis aligned (or antialigned) with the beam direction. Beam intensities produced by the source under operating conditions were typically 300 nA for both  $H^-$  and  $D^-$  ions as measured in the precessor "cup." Ions leaving the source were passed through the spin precessor which consisted of crossed electric and magnetic fields oriented in such a manner as to precess the spin quantization axis

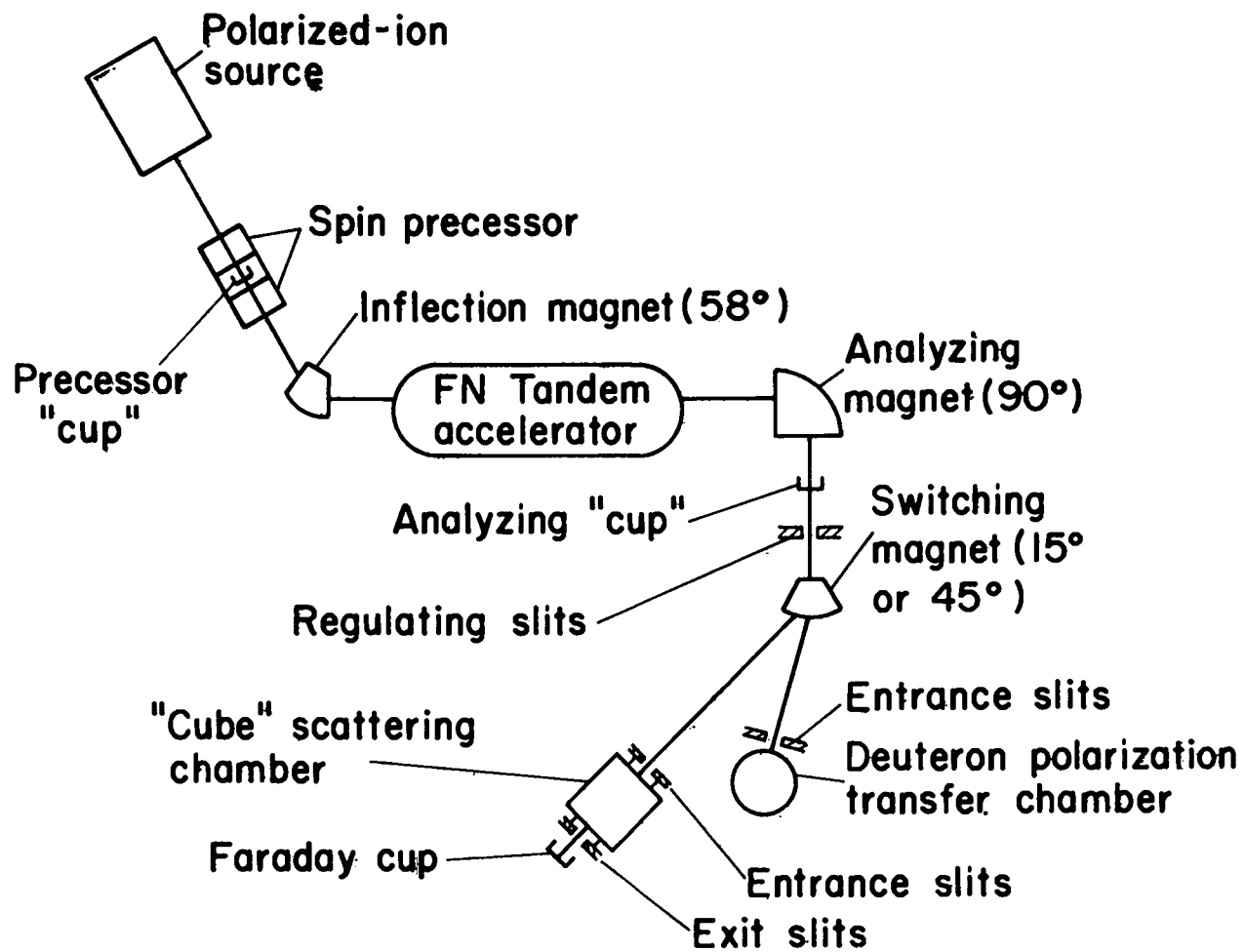


Fig. 1. Schematic of Experimental Facilities.

to the required initial direction which would give the desired final orientation at the target after having passed through the facility's system of bending magnets. Details of the precessing requirements are discussed elsewhere (Oh 70). After having passed through the spin precessor, the negative ions were injected into the tandem accelerator where they were accelerated electrostatically to half their terminal energy near the middle of the accelerator. The negative ions then passed through a thin carbon foil which removed the orbital electrons, thereby converting them to positive ions which acquired additional energy in traversing the remaining length of the accelerator tube. The beam was then energy analyzed with the  $90^\circ$  analyzing magnet used in conjunction with the regulating slits. A switching magnet was used to route the beam down the appropriate beam tube to one of the scattering chambers. The "cube" was used to measure analyzing powers for the reaction  $D(\vec{p}, d)H$  and  $H(\vec{d}, p)D$  (to be discussed in Chapter III). The deuteron polarization transfer chamber was used to calibrate the deuteron polarimeter ( ${}^3\text{He}(\vec{d}, p){}^4\text{He}$  reaction in the vicinity of the 430-keV resonance) and to measure recoil deuteron polarization for the reaction  $D(\vec{p}, \vec{d})H$  (to be discussed in Chapters IV and V, respectively). In all experiments, the polarization of the incident beam was measured by the quench ratio method (Oh 71a) at the analyzing "cup."

## B. "Cube" Scattering Chamber

The 12-in. cube was originally constructed by Starkovich (St 69) and later modified by Ohlsen, Keaton, and Armstrong of Los Alamos Scientific Laboratory (LASL) for the purpose of measuring analyzing powers. The modified version is illustrated in Fig. 2. For the experiments described here, a gas target cell was mounted in the center of the cube. The entrance foil was removed and the cube evacuated. Essential characteristics are:

- 1) provision for mounting either a gas or solid target;
- 2) four  $\Delta E$ -E detector telescopes, utilizing silicon surface barrier detectors, mounted in left (L), right (R), up (U), and down (D) azimuthal positions with variable polar angle;
- 3) provision for rotating the chamber about the beam axis so that any single detector telescope may occupy any of the four (L, R, U, D) azimuthal positions;
- 4) beam entrance and exit slits which are attached to the cube and rotate with it;
- 5) a Faraday cup beyond the exit slits which serves as a beam stop and beam intensity monitor.

The rotating feature of the cube and slit system is necessary in order to eliminate small differences in detector efficiencies, solid angle, and scattering angle, and also instrumental or false asymmetries.

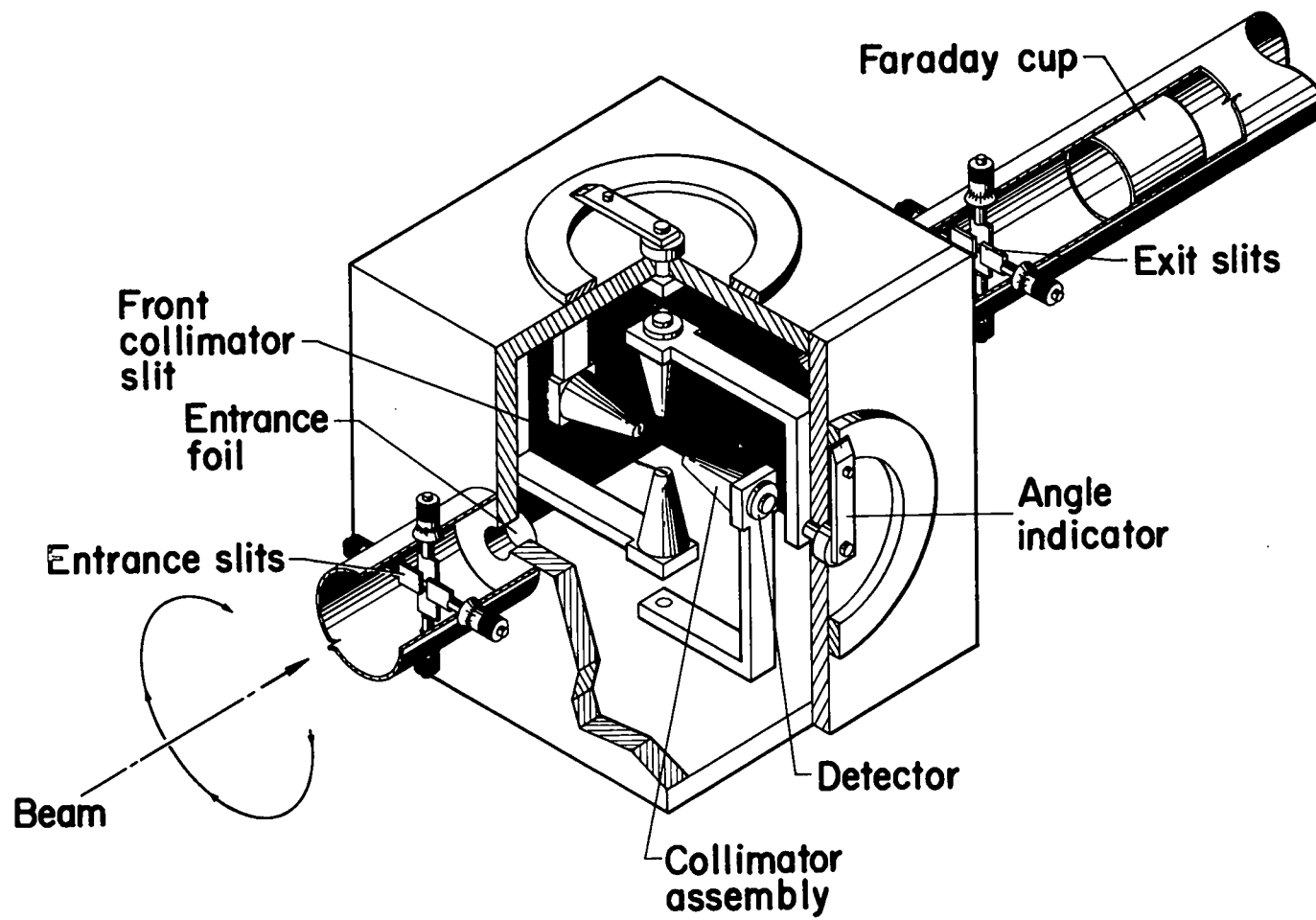


Fig. 2. "Cube" Scattering Chamber.

The four detector telescopes were mounted from the side surfaces of the cube in such a way as to permit selection of the polar angle ( $\theta$ ) for  $17^\circ \lesssim \theta \lesssim 163^\circ$ . Circular verniers on the outer surfaces of the chamber permitted the setting of  $\theta$  to an accuracy of  $\pm 0.1$  degree. Azimuthal rotation of the chamber was accomplished by means of a small electric motor used in conjunction with a series of microswitches and could either be operated manually or by computer control to an accuracy of about  $0.5^\circ$ .

Essential characteristics of the detector telescopes are illustrated in Fig. 3. The dimensions are:

$$R_0 = 9.210 \text{ cm}$$

$$h = 5.870 \text{ cm}$$

$$s_1 = 1.320 \text{ cm}$$

$$s_2 = 1.560 \text{ cm}$$

$$\text{Front slit width} = 0.102 \text{ cm}$$

$$\text{Front slit height} = 0.762 \text{ cm}$$

$$\text{Rear slit width} = 0.102 \text{ cm}$$

$$\text{Rear slit height} = 0.952 \text{ cm}$$

$$\text{Collimating slit thickness} = 0.052 \text{ cm}$$

$$\text{Anti-scatter slit width} = 0.436 \text{ cm}$$

$$\text{Anti-scatter slit height} = 0.834 \text{ cm}$$

$$\text{Anti-scatter slit thickness} = 0.158 \text{ cm}$$

The dimensions specified provide an angular resolution of  $1^\circ$  (FWHM). Ortec surface barrier detectors were

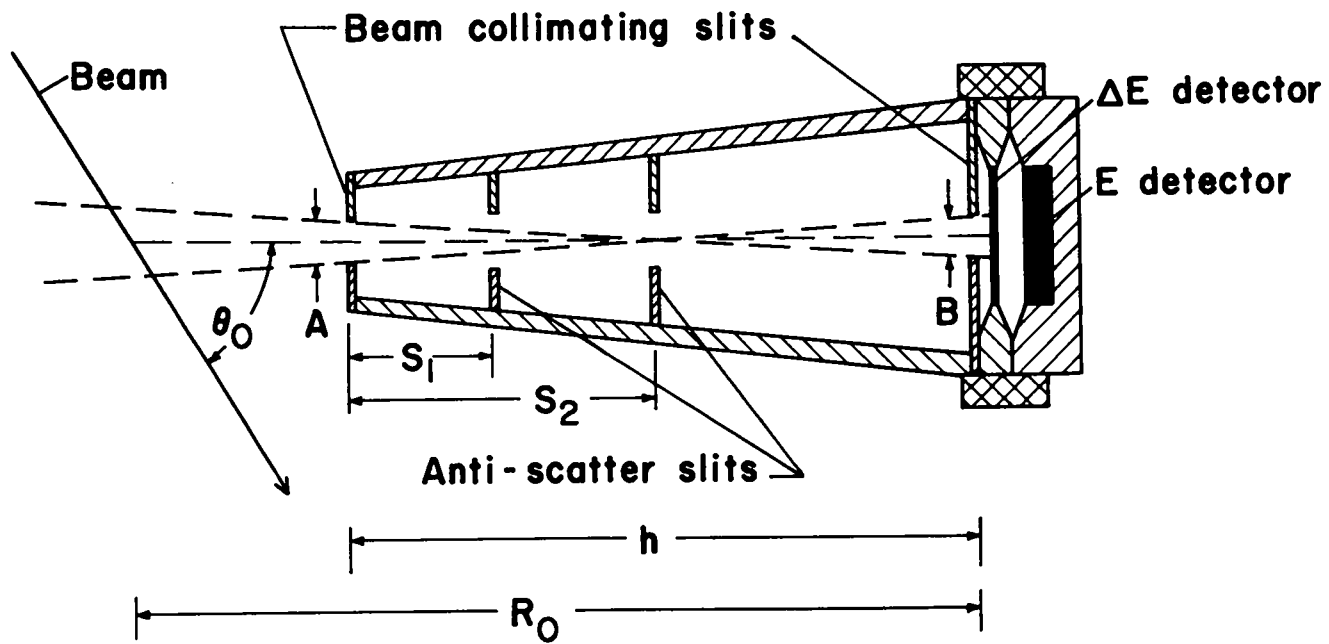


Fig. 3. "Cube" Detector Telescope Assembly.

positioned directly behind the rear collimating slit and were sufficiently large to intercept those particles emerging through the rear slit. The  $\Delta E$  detectors were totally depleted and of sufficient thickness (nominal value of 40  $\mu$ ) to give pulses large enough to trigger the associated electronics throughout the energy and angular ranges studied. The E detectors were partially depleted and of sufficient thickness (1000  $\mu$ ) to stop the charged particles.

The gas target was cylindrical in shape (3.810 cm diameter) and positioned at the center of the chamber by means of support struts. The struts were attached to the inner rear surface of the cube such that the cylindrical axis of the cell was parallel to a diagonal of the rear surface, thereby prohibiting the detector telescopes from viewing the cell frame. Entrance and exit windows of the gas cell were of 2.1 mg/cm<sup>2</sup> Havar\* foil and were attached to the cell frame by means of an epoxy resin.\*\*

Each slit of the chamber's front and rear slit systems was monitored separately and the currents on the four rear slits added (with the aid of a current summing unit) to the current of the Faraday cup for the

---

\*A high tensile strength cobalt alloy obtained from the Precision Metals Division of Hamilton Watch Company.

\*\*Type A-6 from Armstrong Products Company, Inc.

purpose of current integration. The front slits were generally set at 1.78 mm by 1.78 mm and the rear slits generally set at 2.03 mm by 2.03 mm.

### C. Deuteron Polarization Transfer Chamber and Polarimeter

#### 1. Early design considerations

Early design considerations were based on doing the experiment  ${}^4\text{He}(\vec{d}, \vec{d}){}^4\text{He}$  tensor polarization transfer at 12 MeV over as wide an angular range as possible. Although design considerations were based on doing a specific experiment, it was intended that the resulting design be flexible enough to accommodate a number of other polarization transfer experiments in which the second-rank polarization components of outgoing deuterons would be measured. Some of the additional experiments contemplated included:  $\text{D}(\vec{p}, \vec{d})\text{H}$  and  ${}^3\text{He}(\vec{d}, \vec{d}){}^3\text{He}$  elastic scattering.

There have been several experiments in which second-rank polarization components of outgoing deuterons in reactions induced by unpolarized incident beams have been measured by utilizing the analyzing properties of the reaction  ${}^3\text{He}(\vec{d}, \vec{p}){}^4\text{He}$  in the vicinity of the 430-keV resonance (Se 64, Mc 65, Yo 65, Iv 67). In those experiments, a system of four detectors (CsI scintillation crystals) was used, three of which were positioned at left, right, and up azimuthal positions and at a center-of-mass polar

angle near  $54.7^\circ$  or  $45^\circ$ . The fourth detector was positioned at a polar angle of  $0^\circ$ . This arrangement, to be compared to the five detector array of Fig. 18, was sufficient to measure the three second-rank Cartesian components  $p_{x'z'}$ ,  $\frac{1}{2}(p_{x'x'} - p_{y'y'})$ , and  $p_{z'z'}$  (corresponding to the spherical tensor moments of  $\langle T_{21} \rangle$ ,  $\langle T_{22} \rangle$ , and  $\langle T_{20} \rangle$ , respectively). These three tensor components are the only tensor components obtained with an unpolarized incident beam (as a consequence of conservation of parity). Polarized incident beams may produce the additional tensor components  $p_{y'z'}$  and  $p_{x'y'}$  (see Eq. (1-16)).

The tensor component  $p_{x'z'}$  can give rise to a left-right asymmetry (asymmetry in the  $x'z'$  plane) and is therefore sensed with the left-right detector pair.  $\frac{1}{2}(p_{x'x'} - p_{y'y'})$  may contribute equally to the yields in the left-right detector pair but can give rise to an asymmetry when yields in the vertical plane are compared to yields in the horizontal plane. This component is therefore sensed with one or more detectors in each of the two planes. The tensor component  $p_{z'z'}$  contributes to the yield of outgoing protons independently of azimuthal angle but dependent on the polar angle. It is therefore sensed by comparing proton yields at different polar angles (e.g., the yield in the  $0^\circ$  detector and the yield in one or more detectors at  $54.7^\circ$  or at  $45^\circ$ ) or by comparing yields in one detector for two runs of different

incident beam polarization. Hence, it was possible for earlier experimenters to make simultaneous measurements of these three tensors using a four-detector array.

The tensor component  $p_{y'z'}$  can give rise to an up-down asymmetry thus requiring either the addition of a "down" detector to the array or the ability to rotate the four-detector array.

There is a  $\sin\theta\cos\theta$  azimuthal angular dependence of the proton distribution on the tensor component  $p_{x'y'}$ . This component contributes equally to the proton yield in detectors located at azimuthal angles of  $45^\circ$  and  $225^\circ$  and equally to the yield in detectors located at azimuthal angles of  $135^\circ$  and  $315^\circ$ , while contributing differently for the two sets. That is,  $p_{x'y'}$  can provide its maximum contribution to an asymmetrical proton distribution in orthogonal planes (containing the  $z'$  axis) which are rotated  $45^\circ$  about the  $z'$  axis. Measurement of  $p_{x'y'}$  is then made with one or more detectors in each of the two rotated orthogonal planes.

To measure all five components simultaneously would require a minimum of seven detectors. Cleaner separation of polarization transfer coefficients obtain when the number of components required to describe the incident beam can be reduced. With the aid of the spin precessor (Fig. 1)  $p_x$ ,  $p_y$ , or  $p_z$  polarized incident proton beams could be selected. For any of these choices only four

of the five independent outgoing second-rank deuteron polarization components involve polarization transfer coefficients (see Eq. (1-16)). A similar situation obtains for the case of an incident polarized deuteron beam (e.g.,  ${}^4\text{He}(\vec{d}, \vec{d}){}^4\text{He}$ ) with judicious choices in quantization axis orientation. However, due to the larger number of experimental observables (resulting from a more complicated spin structure), separation of the transfer coefficients is not as clean as in the present proton-deuteron case.

Based on these considerations, a rotatable five-detector array was chosen. Solid state detectors were chosen because of compactness and the ability to discriminate against background radiation.

Because of the necessity of slowing the outgoing deuterons to energies near the 430-keV resonance of the analyzing reaction, it was thought to be desirable to have the degrading foils in air where they could be inserted and removed with ease. It was also desirable to have the degrading foils as near to the  ${}^3\text{He}$  cell as possible in order to minimize deuteron losses due to multiple scattering and deuteron depolarization due to electron pickup. Consequently, depolarization due to electron pickup has been neglected in view of

- 1) the continuous energy degradation once the slowup process had commenced. This prohibits appreciable numbers of deuterons from picking up electrons, and keeping

them, for times comparable to the Larmor angular precession period (Li 71); and

2) the relative cross sections of the various processes involved. That is, electron pickup becomes more important for deuteron energies  $\lesssim 200$  keV, while typical average interaction energies under operating conditions were  $\sim 500$  keV. Those deuterons with energies less than 200 keV contributed little to the total proton yield.

Since the measurement of outgoing polarization components produced in a reaction necessarily involves a second analyzing reaction, such experiments are difficult in view of the counting rates obtainable. This is especially true if the first reaction is initiated by an incident polarized beam for which currently available beam intensities at the target are about 5% of those usable in experiments utilizing unpolarized incident beams in this same low energy region. With this limitation in mind, it was hoped that a suitable chamber could be built that would give counting rates in the order of 100 counts/hour/detector for an incident polarized beam intensity of 80 nA. To achieve this goal it was necessary to relax requirements on energy and angular resolution, thereby obtaining thick geometry.

In order to prohibit the deuteron polarimeter from viewing deuterons scattered from the entrance and exit foils of the primary gas target, a collimator with

rectangular apertures was designed and built with the front and rear slits being of equal width in order to maximize the well known geometry factor (Si 59) (and hence the deuteron yield at the  $^3\text{He}$  cell entrance) subject to a given constant angular resolution. A 1.25-in. diameter cylindrical gas target cell capable of maintaining a pressure of 6 atm at LN temperature was built for the  $^4\text{He}(\vec{d}, \vec{d})^4\text{He}$  polarization transfer experiment. The resulting chamber and polarimeter were thus chosen in an attempt to maximize the outgoing deuteron yield while minimizing energy and angular spreading of the deuterons entering the  $^3\text{He}$  cell throughout the energy and angular ranges to be studied.

After a preliminary attempt on the  $^4\text{He}(\vec{d}, \vec{d})^4\text{He}$  polarization transfer problem, it became apparent that the neutron flux produced by the 12-MeV incident beam was higher than early calculations had indicated it would be. An upper limit on the machine energy of about 9.5 MeV was established for which radiation to the detectors was still at an acceptable level. In addition to the radiation problem, it was found that the yield in the zero degree detector was contaminated by protons produced by the reaction  $^{14}\text{N}(d, p)^{15}\text{N}$  ( $Q = +8.6$  MeV) in the primary gas target due to nitrogen outgassing from the walls of the target cell and that for some operating conditions the protons from the analyzing reaction could not be

distinguished from those produced by the nitrogen. This problem was common to the experiments of McIntyre (Mc 65) and Young (Yo 65) who chose to use an annular detector at zero degrees to avoid the problem. These difficulties prompted the change to the  $D(\vec{p}, \vec{d})H$  tensor polarization transfer problem for which the form of the observables is also simpler. Although data for the  ${}^4\text{He}(\vec{d}, \vec{d}){}^4\text{He}$  problem have since been obtained for deuteron energies less than the upper limit established, and after having solved the nitrogen problem by modifying the primary cell to include activated zeolite at LN temperature as an adsorbent, that data will not be reported as part of this thesis.

## 2. Polarization transfer chamber

Shown in Figs. 4 and 5 are top and side views of the deuteron polarization transfer chamber and polarimeter. In each figure two detector telescopes have been omitted in order to show the zero degree telescope. Both figures illustrate the apparatus as used for the  ${}^3\text{He}(\vec{d}, p){}^4\text{He}$  calibration experiment.

Polarized beam was directed against the solid (or gaseous) target and the outgoing deuterons were permitted to enter the  ${}^3\text{He}$  cell after having passed through the chamber's 5-mg/cm<sup>2</sup> Havar exit foil, about 5 mm of air, an aluminum degrading foil of appropriate thickness to give an average deuteron interaction energy of about

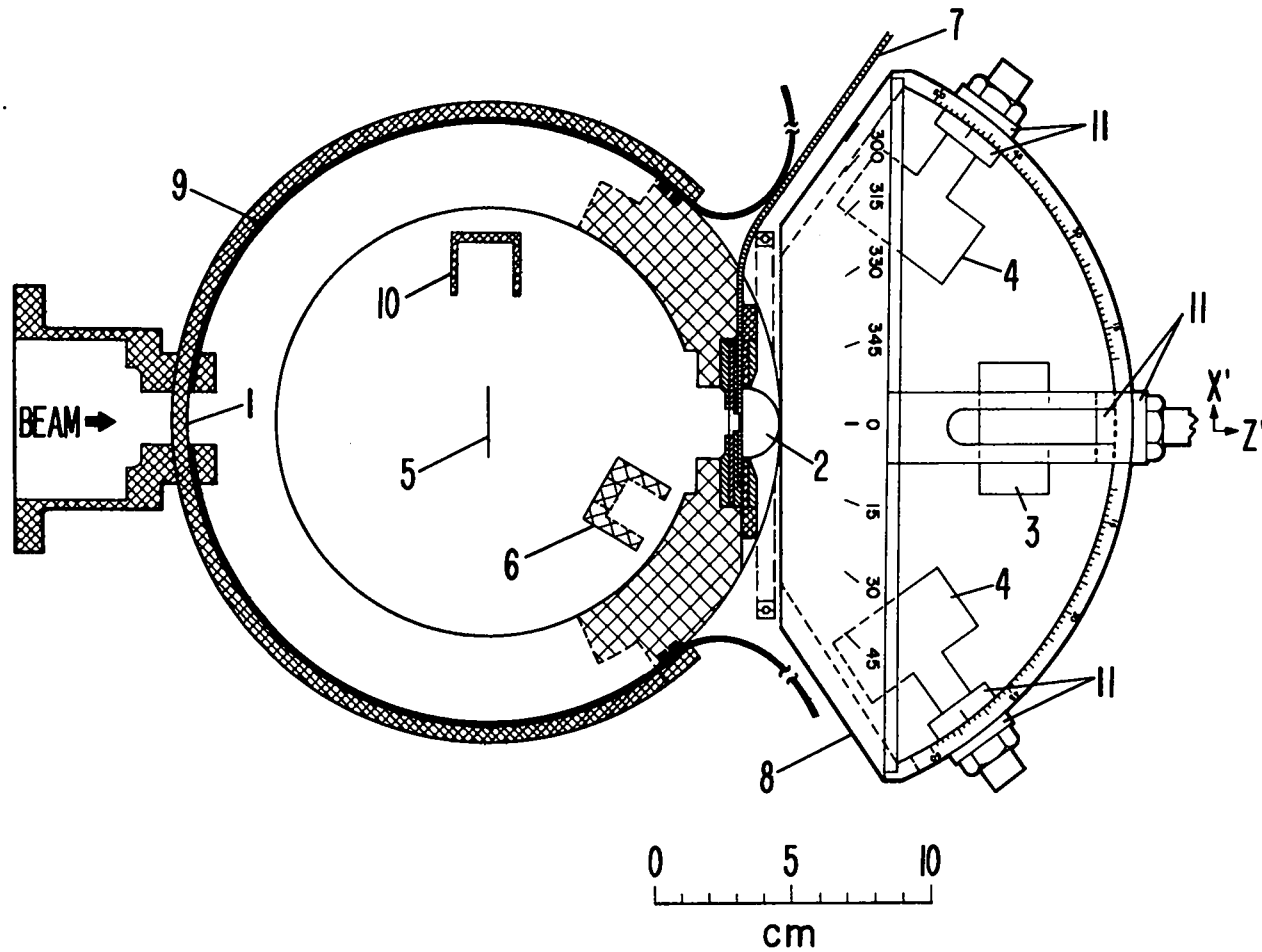


Fig. 4. Deuteron Polarization Transfer Chamber; Horizontal Cross Section. (1) beam entrance, (2)  $^3\text{He}$  cell, (3)  $0^0$  detector, (4) left-right detectors ( $\theta_{2c.m.} = 54.7^\circ$ ), (5) thin gold foil, (6) E- $\Delta$ E beam intensity monitor, (7) phenolic foil holder, (8) detector holding apparatus, (9) sliding steel band, (10) Faraday cup, (11) aligning lugs.

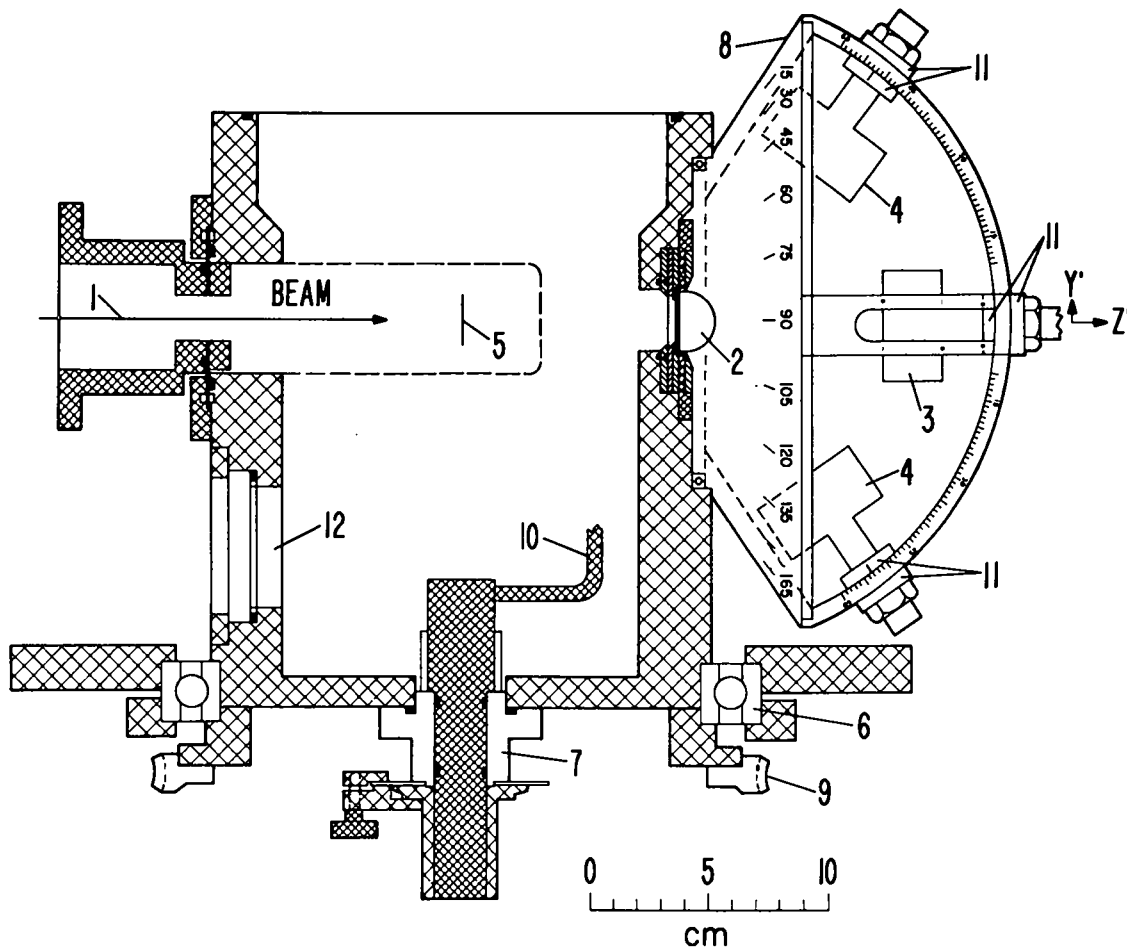


Fig. 5. Deuteron Polarization Transfer Chamber; Vertical Cross Section. (1) beam entrance, (2)  $^3\text{He}$  cell, (3)  $0^\circ$  detector, (4) up-down detectors ( $\theta_{2\text{c.m.}} = 54.7^\circ$ ), (5) thin gold foil, (6) support bearing, (7) teflon insulator, (8) detector holding apparatus, (9) worm gear, (10) Faraday cup support, (11) aligning lugs, (12) pyrex viewing port.

500 keV, and the 5-mg/cm<sup>2</sup> Havar <sup>3</sup>He cell entrance foil. The deuterons then initiated the reaction <sup>3</sup>He( $\vec{d}$ ,p)<sup>4</sup>He (Q = +18.35 MeV) and the high energy protons were detected in the various detector telescopes of the array. By using algebraic techniques (to be discussed in Chapters IV and V) and the number of counts in each telescope, the polarization components of the deuterons entering the <sup>3</sup>He cell could be determined. In the <sup>3</sup>He( $\vec{d}$ ,p)<sup>4</sup>He calibration experiment, an incident beam of deuterons of known polarization permitted a determination of the analyzing powers for the <sup>3</sup>He( $\vec{d}$ ,p)<sup>4</sup>He reaction near the 430-keV resonance.

The 15-cm (i.d.) aluminum chamber was mounted on a bearing which permitted continuous rotation of the chamber about its cylindrical axis to an angle in the range of -110° to 110°, to an accuracy of about 0.3°, without having to break vacuum. The sliding seal consisted of a 0.30-mm thick spring steel band bolted to the end of the beam tube which was permitted to slide on teflon bearings during the chamber rotation while maintaining vacuum with viton "O" rings. The thickness of the band was somewhat critical in that it had to be thick enough to withstand the force of the atmosphere when the chamber was evacuated and thin enough to bend away from the detector array in the available space. A rigid support was attached to the end of the beam tube near the chamber

to eliminate flexing of the band, and subsequent loss of vacuum, during rotation, as this had been a problem on an earlier scattering chamber utilizing this type of sliding seal. The rotation was accomplished with a small electric motor mated to a worm gear attached to the bottom of the chamber. The  $^3\text{He}$  cell and the detector array assembly were attached to the chamber. The center of the chamber was located near the focal point of the beam tube's quadrupole focusing magnet. An insulated set of beam defining slits was located about 31.8 cm upstream from the center of the chamber and was typically set at a width of 1.27 mm and a height of 2.54 mm during collection of polarization transfer data.

Because of the rather large magnification of small outgoing deuteron energy differences during the slowing process, and the high degree of sensitivity of the proton yield in the  $^3\text{He}$  cell on the entering deuteron energy distribution, it was necessary to monitor the current balance on the left-right slit pair during data acquisition. Such energy differences can arise from small angular changes of the outgoing deuterons which result from beam steering. That is,  $\Delta E_d/E_d = -2\tan\theta\Delta\theta$  where  $E_d$  is the outgoing deuteron energy and  $\theta$  is the scattering angle. Both beam translation and beam entrance angle variations contribute to this effect. The importance of beam position monitoring became apparent as a nonreproducibility

in the "excitation function" part of the data collection routine (to be discussed in Chapter V) when such monitoring was not used.

A diffusion pump was located 40 cm in front of the chamber; this produced a typical pressure of  $2 \times 10^{-7}$  Torr at the pump inlet.

The Faraday cup and beam stop was supported from a rotatable shaft through the center of the bottom of the chamber and was insulated from the chamber with teflon. Electron suppression was handled magnetically with a 75 gauss field produced by a pair of permanent magnets clamped to the Faraday cup. Originally, tantalum had been chosen as the material for the beam stop. However, when it became apparent that neutron fluxes produced were somewhat larger than had previously been estimated, gold was substituted for the tantalum. This change was based on the findings of Allen et al. (Al 51) that 15-MeV deuterons in stopping produce about  $2/3$  as high a neutron flux in gold as in tantalum. A carbon beam stop was tried but the resulting high gamma ray flux made this impractical.

3. Accessory lid for the  ${}^3\text{He}(\vec{d},p){}^4\text{He}$  calibration

For the  ${}^3\text{He}(\vec{d},p){}^4\text{He}$  calibration experiment an accessory lid was made for the scattering chamber from which metal foils could be suspended and with provision for mounting an E- $\Delta$ E detector telescope within the chamber. The E- $\Delta$ E detector telescope was used as a substitute current intensity monitor by counting deuterons Coulomb scattered at  $30^\circ$  from a 24.5-mg/cm<sup>2</sup> gold foil. The monitor was necessary for this experiment in view of the need of the ability to deliver the same amount of charge to the  ${}^3\text{He}$  cell in each of two or three runs with the chamber in the zero degree position. The detector telescope consisted of a 50- $\mu$   $\Delta$ E and a 300- $\mu$  E surface barrier detector pair positioned behind a 0.74-mm diameter collimator located 5.4 cm from the gold foil. Because this experiment was a single scattering experiment (high count rate), the beam defining slits were cut to 0.50 mm by 0.50 mm and the beam was cut to  $\sim 1/2$  nanoampere.

4. Cryostat and primary gas target

For polarization transfer experiments utilizing gas targets, a liquid nitrogen cryostat was built from which the gas target could be suspended. The cryostat had a 3.3- $\ell$  reservoir and, although it was usually filled after each 6-8 hours of operation, it was capable of lasting 12 hours. This cryostat was a scaled down version

of an earlier model for which gas targets could be bolted directly in contact with the liquid nitrogen reservoir, the seal being made by an indium "O" ring. The gas cell used in the  $D(\vec{p}, \vec{d})H$  polarization transfer experiment was 1.27 cm in diameter with 2.1-mg/cm<sup>2</sup> Havar entrance and exit windows attached to the cell frame by epoxy resin. The cell was filled through a stainless steel filling lead which extended up through the cryostat reservoir and was operated at a pressure of 6.2 atm (~ 95% of its upper limit). During operation the cell was left open to a pressure gauge.

The polarization transfer data collected at  $\theta_{lab} = 0^\circ$  posed a particular problem in that the Faraday cup had to be rotated to a position out of the beam path. In order to give the machine operator something to monitor during data collection, the cryostat and gas target were insulated from the chamber, and secondary electron emission from the target was used in lieu of the Faraday cup. Insulation of the cryostat and gas target was accomplished with the aid of a teflon spacer between the chamber and cryostat and a kovar filling lead seal soldered in the gas target filling line. (The method of polarization transfer data processing made accurate current integration unnecessary.)

## 5. Deuteron polarimeter

The deuteron polarimeter consisted of the energy degrading foil, the  $^3\text{He}$  cell, and the five detector telescope array, all of which were located in air. An assortment of aluminum degrading foils ranging in thickness from  $6.69 \text{ mg/cm}^2$  to  $40.38 \text{ mg/cm}^2$  were made by mounting various foils in phenolic slides which were flexible enough to permit insertion into a slot machined into the side of the chamber (see Fig. 4).

The  $^3\text{He}$  cell was quite similar to the one used by Young (Yo 65) in his experiment on  $\text{D}(\text{p}, \vec{\text{d}})\text{H}$ . It was a 2.54-cm diameter aluminum hemispherical "hat," 125  $\mu$  thick, mounted in a three piece frame which bolted together. The gas seal was accomplished by sandwiching thin latex rubber washers between the central brass frame piece and each of the two stainless steel retaining pieces--one for the "hat" and one for the cell's entrance foil. This was done in order to (1) make the assembly thin enough so as not to obstruct the region of proton production from the view of the detector array, and (2) make the assembly as a unit which could be removed from the chamber without depressurizing the cell. By making the  $^3\text{He}$  cell, the detector array, and the chamber's exit foil assembly removable, it was possible for other experimenters (with the aid of an adapter) to pass beam through the chamber and perform experiments "downstream" without having to

remove the chamber and thus destroy the alignment.

Although the rubber washer seals did permit slow leakage of  $^3\text{He}$  from the cell ( $\sim 100$  Torr/month), the leakage rate was not sufficient to warrant the use of an epoxy resin.

Filling of the cell was accomplished through a small hole drilled along a radius through the central frame piece via a small stainless steel hypodermic filling lead soldered into place. The cell was left open to a pressure gauge and was repressurized to 55 psig (4.5 atm) at room temperature prior to the start of each run. This pressure was sufficient to stop 800-keV deuterons. The entrance of the cell was a rectangular aperture 1.90 cm high and 0.64 cm wide located 9.327 cm from the center of the scattering chamber.

The collimator (and gas target) that had been built for the  $^4\text{He}(\vec{d}, \vec{d})^4\text{He}$  polarization transfer experiment was not needed for the  $\text{D}(\vec{p}, \vec{d})\text{H}$  polarization transfer experiment as protons scattered from the deuterium cell's entrance and exit windows were not energetic enough to get through all the foils and be detected in the zero degree detector. The apparatus as used had an angular resolution of  $7.8^\circ$  (FWHM).

The detector array consisted of five E- $\Delta$ E silicon detector telescopes mounted in an aluminum frame which could be rotated about the z' axis and set to an accuracy of  $\pm 0.5^\circ$ . The rotation feature was accomplished by

attaching the frame to a bearing which fit snugly into a counterbore machined into the side of the scattering chamber. The assembly was then secured to the side of the chamber with a plastic hold-down ring. With the array positioned in the  $0^\circ$  azimuthal position as shown, the outgoing deuteron polarization tensors  $p_{x'z'}$ ,  $p_{y'z'}$ , and  $\frac{1}{2}(p_{x'x'} - p_{y'y'})$  could be sensed. Rotation of the array by  $45^\circ$  permitted a sensing of the polarization tensors  $p_{x'z'}$ ,  $p_{y'z'}$ ,  $p_{z'z'}$ , and  $p_{x'y'}$ . The essential difference in the two positions is the trade-off of  $\frac{1}{2}(p_{x'x'} - p_{y'y'})$  in the  $0^\circ$  position for  $p_{x'y'}$  in the  $45^\circ$  position; the other three tensors were sensed with equal efficiency in both positions.

The four detector telescopes were mounted in brass holders in such a way as to permit variable polar angle in the range of about  $15^\circ$  to  $60^\circ$  (to an accuracy of  $\pm 1/4$  degree) with each telescope viewing a point along the  $z'$  axis near the effective center of the  $^3\text{He}$  cell. The final choice in polar angle was one which gave an average interaction center-of-mass angle near  $54.7^\circ$ . At this angle, and in this geometry, the analyzing power,  $A_{zz}$ , for the  $^3\text{He}(\vec{d}, p)^4\text{He}$  reaction is approximately zero. Hence the four detectors are insensitive to the outgoing deuteron polarization component  $p_{z'z'}$ , and, to first order (neglecting detector efficiency, solid angle, and the like), the sum of the yields in the four detectors

is polarization independent. In principle it is the sum of the yields in the four detectors that should be used in the "excitation function" part of the data collecting procedure. However, in view of the small outgoing deuteron polarizations involved in the  $D(\vec{p}, \vec{d})H$  reaction and the large dependence of the proton yield on deuteron energy, the zero degree detector was mounted in a teflon holder so that it could be moved in close to the  ${}^3\text{He}$  cell, thereby substantially reducing the time required for the excitation function part of the data collecting procedure.

Alignment of each telescope was accomplished by threading the detector holder shank and using two aligning lugs (the inner one of which was threaded with surfaces machined to mate the frame of the detector holder assembly).

Each detector telescope consisted of a 2.1-cm diameter circular collimator located 7.9 cm from the effective center of the  ${}^3\text{He}$  cell and two 500- $\mu$  thick silicon surface barrier detectors of area 450  $\text{mm}^2$  (Ortec;  $\Delta E$  detectors totally depleted, some E detectors totally depleted and some partially depleted). There was 200  $\mu$  of aluminum separating the two detectors and sufficient aluminum in front of the first detector to ensure stoppage of the high energy protons in the second detector.

The aluminum separating foil was used for the purpose of eliminating as much as possible of the "cross talk" between the detectors due to neutron induced reactions in the silicon.

D. Associated Electronics

A block diagram of the electronics used in the experiments described here is shown in Fig. 6. Pulses from each detector were amplified before entering the mixer coder. The mixer coder was a device designed and built by J. Gallagher of LASL for Ohlsen, Keaton, and Armstrong. Its function was to: (1) discriminate against those pulses which were too small ( $\lesssim 300$  mV), (2) require coincidence between an E pulse and its respective  $\Delta E$  pulse, (3) generate a gate pulse in the event that the coincidence requirement was met, and (4) generate binary coded output pulses to tell the computer which E- $\Delta E$  pair was in coincidence. The resolving time of the mixer coder was approximately  $2.5 \mu\text{sec}$ . The mixed E pulses and the mixed  $\Delta E$  pulses were then routed to two analog-to-digital converters (ADC's) which accepted only those pulses for which there was a gate pulse. During the time interval in which the ADC's were busy a logic pulse was sent to the mixer coder which routed those gates produced in the mixer coder during that time interval to the "lost counts" scaler. This permitted dead time

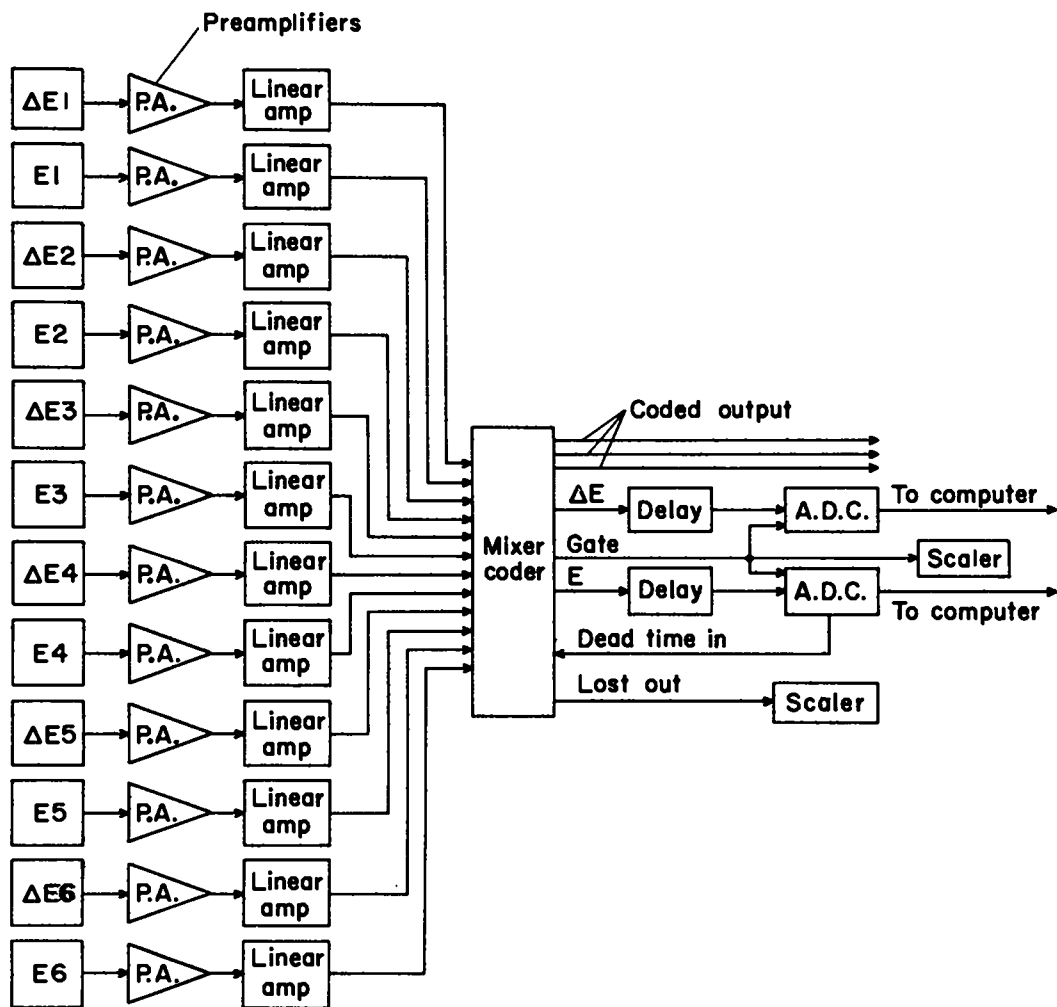


Fig. 6. Block Diagram of Electronics.

corrections to be made to those data where dead time losses were significant. (There were up to ~ 5% dead time corrections in the analyzing power measurements described in Chapter III.)

An on-line Xerox Data Systems computer (XDS-930) served partly as a multi-channel analyzer for each of the detector pairs with particle selectivity based on mass and energy discrimination (Ar 69). Each detector pair was allotted 256 channels for the accumulation of mass or energy spectra. In "mass mode" operation, mass spectra were computed by the algorithm  $(E+\Delta E)^{1.73} - E^{1.73}$ , stored in a designated section of memory, and displayed on an oscilloscope where upper and lower bounds (gates) could be specified for the desired particle group by the use of a light pen. In "energy mode," energy spectra were computed  $(E+\Delta E)$  for those events satisfying the mass criterion and were displayed on the oscilloscope where again upper and lower bounds could be specified. Because of the length of time required ( $0.5 \text{ hour} \lesssim t \lesssim 3 \text{ hour}$ ) for each run of the  $D(\overset{\rightarrow}{p}, \overset{\rightarrow}{d})H$  experiment and the possible neutron background, it was desirable to have available at the end of each run both mass and energy spectra for inspection (see Fig. 20 for typical spectra) even though mass gates still had to be set before energy spectra could be computed. This feature was not needed for the

analyzing power measurements made in the cube where run times were typically a few minutes.

The computer was also used to perform some of the mechanical duties (rotate the cube, measure beam polarization, read various scalars and sensing switches, etc.), and to reduce the raw analyzing power data collected in the cube.

Polarization transfer coefficients for the reaction  $D(\vec{p}, \vec{d})H$  could not be obtained on line without prior knowledge of the analyzing power for the reaction  $D(\vec{p}, \vec{d})H$  (for the ratio of the polarized cross section to the unpolarized cross section;  $I/I_0$  in Eq. (1-16)), and the deuteron polarization components resulting from an unpolarized incident proton beam in the reaction  $D(\vec{p}, \vec{d})H$  at the appropriate energy and angle. However, it was desirable to do enough preliminary raw data reduction on line to insure that no gross errors were being made. This was especially important for this experiment because of the large amount of time required for each run. An on-line program called ANA was written for this purpose. ANA calculated the second-rank outgoing deuteron polarization components and their corresponding statistical errors for the data collected by the polarized/unpolarized incident beam method (discussed in Chapter V), given effective analyzing powers and the relevant polarization functions.

## CHAPTER III

### MEASUREMENT OF PROTON-DEUTERON ANALYZING POWERS

#### A. Experimental Procedure

The experiments described in this chapter were undertaken with a view to obtaining  $I/I_0$  and the various deuteron polarization components resulting from an unpolarized incident proton beam (see Eq. (1-16)). In general, both these quantities must be known before polarization transfer coefficients can be determined.

#### 1. $D(\vec{p}, d)H$

For the reaction  $D(\vec{p}, d)H$ , polarized protons having a vertical quantization axis were directed at a 3.8-cm diameter cell filled with deuterium to a pressure of 560 Torr at room temperature. Measurements were made in the cube scattering chamber (Chapter II). Detection of the recoil deuterons was of interest although some data were obtained by detecting protons and converting that data to correspond to deuteron data.

For reactions induced by a beam of polarized spin-1/2 particles the differential cross section can be written (Oh 72b)

$$I(\theta, \varphi) = I_0(\theta)(1 + p \cdot n A(\theta)) , \quad (3-1)$$

where  $I_0(\theta)$  is the cross section for scattering an

unpolarized beam into the scattering angle,  $\theta$ ,  $\vec{p}$  is the vector polarization of the incident beam,  $\hat{n}$  is a unit vector normal to the reaction plane ( $\hat{n} = (\vec{k}_{in} \times \vec{k}_{out}) / |\vec{k}_{in} \times \vec{k}_{out}|$ ), and  $A(\theta)$  is the analyzing power of the reaction.

For the usual choice of coordinates ( $\hat{z}$  along  $\vec{k}_{in}$ ,  $\hat{y} = \hat{n}$ , and  $\hat{x}$  to make a right-handed system) the cross section may be written as  $I(\theta, \varphi) = I_0(\theta)(1 + p_y A_y)$ . If  $\hat{y}$  is used to define "up" then scattering left (L) or right (R) corresponds to  $\varphi = 0^\circ$  or  $180^\circ$ , respectively.

The measurements described here were made with a left-right detector pair utilizing a fourfold sequence. This sequence consisted of positioning the cube in each of two azimuthal positions ( $0^\circ$  and  $180^\circ$ ) with the quantization axis normal and reversed (spin up, spin down). Spin reversal was accomplished by reversing a magnetic field in the polarized ion source. Detector efficiencies, current integration, target parameters, and solid angle factors may be eliminated by either a rotation of the cube (effecting an interchange of the left-right detector pair) or by reversal of the quantization axis direction (spin flip). However, when the possibility of misalignments is considered, the rotation or spin flip must be made in a particular way if false asymmetries are to be minimized (Ke 71). The desired results can be obtained by flipping the spin of the incident polarized

beam while leaving the beam position unchanged or by rotating the analyzer in such a way that the beam passes through in the same position relative to the detectors. These considerations prompted Keaton et al. (Ke 71) to install beam defining slits fore and aft of the cube which rotate with it. To ensure that the beam passed through the cube the same way each time, a front and rear slit balance was maintained for each leg of the sequence. Asymmetry in an up-down detector pair was also monitored as a nonzero asymmetry would have been indicative of spin misalignment or undesirable beam steering effects.

Writing expressions for the yield in the left and right detector pair for each combination, one obtains:

$$\begin{aligned}
 L_{\uparrow} &= n_1 N \Omega_L \epsilon_L I_0 [1 + p A_y] & L_{\downarrow} &= n_3 N \Omega_L \epsilon_L I_0 [1 - p A_y] \\
 R_{\uparrow} &= n_1 N \Omega_R \epsilon_R I_0 [1 - p A_y] & R_{\downarrow} &= n_3 N \Omega_R \epsilon_R I_0 [1 + p A_y] \\
 L'_{\uparrow} &= n_2 N \Omega'_L \epsilon'_L I_0 [1 - p A_y] & L'_{\downarrow} &= n_4 N \Omega'_L \epsilon'_L I_0 [1 + p A_y] \\
 R'_{\uparrow} &= n_2 N \Omega'_R \epsilon'_R I_0 [1 + p A_y] & R'_{\downarrow} &= n_4 N \Omega'_R \epsilon'_R I_0 [1 - p A_y] , \quad (3-2)
 \end{aligned}$$

where  $n$  is the number of incident projectiles,  $N$  is the target density ( $\#/cm^2$ ),  $\Omega$  is the solid angle subtended by the detector,  $\epsilon$  is the efficiency of the detector, and where  $I_0$ ,  $p$ , and  $A_y$  mean the same as before. The prime denotes the cube in its rotated position and the arrow denotes spin up or spin down. If one defines

$$\mathcal{L} \equiv (L_{\uparrow} R'_{\uparrow} R_{\downarrow} L'_{\downarrow})^{\dagger}$$

$$\mathcal{R} \equiv (R_{\uparrow} L'_{\uparrow} L_{\downarrow} R'_{\downarrow})^{\dagger}, \quad (3-3)$$

then  $A_y = \frac{1}{p} \frac{I - \beta}{I + \beta}$ , where geometrical, target, and detector parameters have canceled. The fourfold sequence typically took a few minutes to complete with data reduction being done on line.

## 2. $H(\vec{d}, p)D$

For the measurement of spin-1 analyzing powers several experimental methods have evolved at LASL utilizing the flexibility of the polarized ion source and spin precessor combination. The various methods are considered supplemental and arise as a result of selection of various combinations of magnetic substates and quantization axis direction.

The "Rapid Method," as it has come to be known, is documented elsewhere (La 71). It features

- 1) an  $m_I = 1$  beam with  $\beta = 54.7^\circ$  for simultaneous measurements of  $A_y$ ,  $A_{xz}$ , and  $\frac{1}{2}(A_{xx} - A_{yy})$ , and
- 2) two separate runs of  $m_I = 1$  and 0, respectively, with  $\beta = 0^\circ$  for measurement of  $A_{zz}$ .

Measurement of  $A_y$ ,  $A_{xz}$ , and  $\frac{1}{2}(A_{xx} - A_{yy})$  is independent of current integration though good knowledge and control of the quantization axis direction is required. Measurement of  $A_{zz}$ , on the other hand, depends on good

current integration but is rather insensitive to small  $\beta$  misalignments.

A second method, which has come to be known as the "Ratio Method," is described in Appendix A. It features

- 1) two runs with  $m_I = 1, 0$  with  $\beta = 90^\circ$  for measurement of  $A_y$ ,  $A_{yy}$ , and  $A_{xx}$ , and
- 2) an  $m_I = 0$  run with  $\beta = 45^\circ$  for measurement of  $A_{xz}$  with additional determinations of  $A_y$ ,  $A_{xx}$ , and  $A_{yy}$  being possible though all four are not independent.

The advantage of this method is that there are no first order errors due to  $\beta$  (spin axis) and  $\varphi$  (azimuthal) misalignments (Oh 71). Disadvantage lies in the need for good current integration for the measurements in part one of this method.

Both methods utilize the cube rotation technique as illustrated in Sec. A.1 to eliminate detector efficiency and the like. Some early data were obtained using the second method exclusively while later data were obtained using the first part of method two and the second part of method one ( $\beta = 54.7^\circ$ ). This was believed to be more desirable in our case as  $A_{xz}$  was obtained with nearly the same efficiency as in the  $\beta = 45^\circ$  case while the use of  $\beta = 54.7^\circ$  gave the redundant measurement of  $\frac{1}{2}(A_{xx} - A_{yy})$  to serve as a check on that obtained from the independent

determinations of  $A_{xx}$  and  $A_{yy}$  in part one of the second method.

For this experiment the target cell was pressurized to a pressure of about 540 Torr of deuterium at room temperature. Incident beam currents were limited to a few nanoamperes at small scattering angles, and to about 60 nA at the larger scattering angles, in order to keep dead time corrections below approximately 10%. Again, runs typically took a few minutes.

## B. Results

### 1. $D(\vec{p}, \vec{d})H$

Values of the analyzing power measurements for the reaction  $D(\vec{p}, \vec{d})H$  are presented in Table 1. They are given in a coordinate system for which the deuterons are the detected particles; that is,  $\hat{z}$  along  $\vec{k}_{in}$  (protons),  $\hat{y}$  along  $\vec{k}_{in}$  (protons)  $\times$   $\vec{k}_{out}$  (deuterons), and  $\hat{x}$  chosen to make a right-handed system. The data are presented in this manner rather than the more conventional form  $[D(\vec{p}, \vec{p})D, \text{ where } \hat{y} \text{ is along } \vec{k}_{in} \text{ (protons)} \times \vec{k}_{out} \text{ (protons)}]$  because of their relationship to the polarization transfer experiment,  $D(\vec{p}, \vec{d})H$ . To convert to the more conventional form, change the sign of  $A_y$  and record the data at  $\theta_p(\text{c.m.}) = \pi - \theta_d(\text{c.m.})$ . The errors given in the table are purely statistical.

TABLE 1

Measured Analyzing Powers ( $A_y$ ) for theReaction  $D(\vec{p}, d)H$ 

$\theta_{\text{lab}}$ (deg)	$\theta_d$ (cm) (deg)	$E_p = 4.00$ (MeV)	$E_p = 6.00$ (MeV)	$E_p = 8.00$ (MeV)
21	42	-0.022±0.003	-0.048±0.004	-0.072±0.004
24	48	-0.040±0.003	-0.071±0.006	-0.102±0.004
27	54	-0.049±0.004	-0.074±0.005	-0.121±0.003
30	60	-0.057±0.003	-0.088±0.006	-0.123±0.004
33	66	-0.064±0.004	-0.103±0.005	-0.118±0.006
36	72	-0.063±0.003	-0.099±0.005	-0.098±0.006
39	78	-0.062±0.005	-0.072±0.004	-0.076±0.005
42	84	-0.044±0.009	-0.066±0.007	-0.062±0.005
45	90		-0.052±0.012	-0.058±0.005
48	96			-0.069±0.010
51	102			-0.057±0.008
*21	148.6	-0.009±0.003	-0.023±0.003	-0.034±0.003
*24	144.2	-0.019±0.003	-0.023±0.005	-0.031±0.003
*27	139.8	-0.018±0.003	-0.023±0.003	-0.026±0.002
*30	135.5	-0.026±0.003	-0.031±0.004	-0.029±0.003
*33	131.1	-0.024±0.003	-0.029±0.003	-0.030±0.004
*36	126.8	-0.027±0.002	-0.029±0.004	-0.032±0.004
*39	122.6	-0.029±0.003	-0.035±0.003	-0.028±0.004
*42	118.4	-0.026±0.004	-0.030±0.003	-0.040±0.005
*45	114.2	-0.024±0.004	-0.036±0.003	-0.047±0.005
*48	110.1		-0.038±0.005	-0.037±0.005
*51	106.0	-0.022±0.005	-0.041±0.005	-0.039±0.004
*54	102.0		-0.036±0.005	-0.046±0.006
*57	98.1	-0.024±0.005	-0.044±0.006	-0.039±0.007
*60	94.3	-0.041±0.006	-0.048±0.007	

\*Protons were detected and data converted. Energies are at target center. Errors are purely statistical. Systematic errors are estimated to be less than 0.005.

Shown in Fig. 7 is a plot of the data in Table 1. Small dots represent data obtained by detecting deuterons and large dots represent data obtained by detecting protons. The smooth curves were drawn through the data points simply to serve as a guide to the eye. Also illustrated is the data of Clegg and Haeberli (Cl 67) (triangles) and Gruebler et al. (Gr 66) (squares). Agreement is good for the 6.00 and 8.00 MeV angular distributions though our values at 4.00 MeV are consistently somewhat smaller in magnitude in the angular range where we and Clegg et al. both detected recoil deuterons. The values of  $A_y$  obtained here are to be compared to the maximum range of this observable of  $\pm 1$ .

$I/I_0$  in Eq. (1-16), for various polarization transfer runs having polarization along the y axis ( $p_y$  beams), was then determined from the relation  $I/I_0 = 1 + p_y A_y$  (Eq. (3-1)). For those runs having polarization along the x axis or along the z axis ( $p_x$  beams or  $p_z$  beams, respectively) and for unpolarized runs,  $I/I_0 = 1$ .

## 2. $H(d,p)D$

Results of the analyzing power measurements for the reaction  $H(d,p)D$  are tabulated in Tables 2-5, inclusive, in a coordinate system in which  $\hat{y}$  is along  $\vec{k}_{in}(d) \times \vec{k}_{out}(p)$ . To convert to the more conventional form  $[H(d,d)H$  where  $\hat{y}$  is along  $\vec{k}_{in}(d) \times \vec{k}_{out}(d)]$ , change

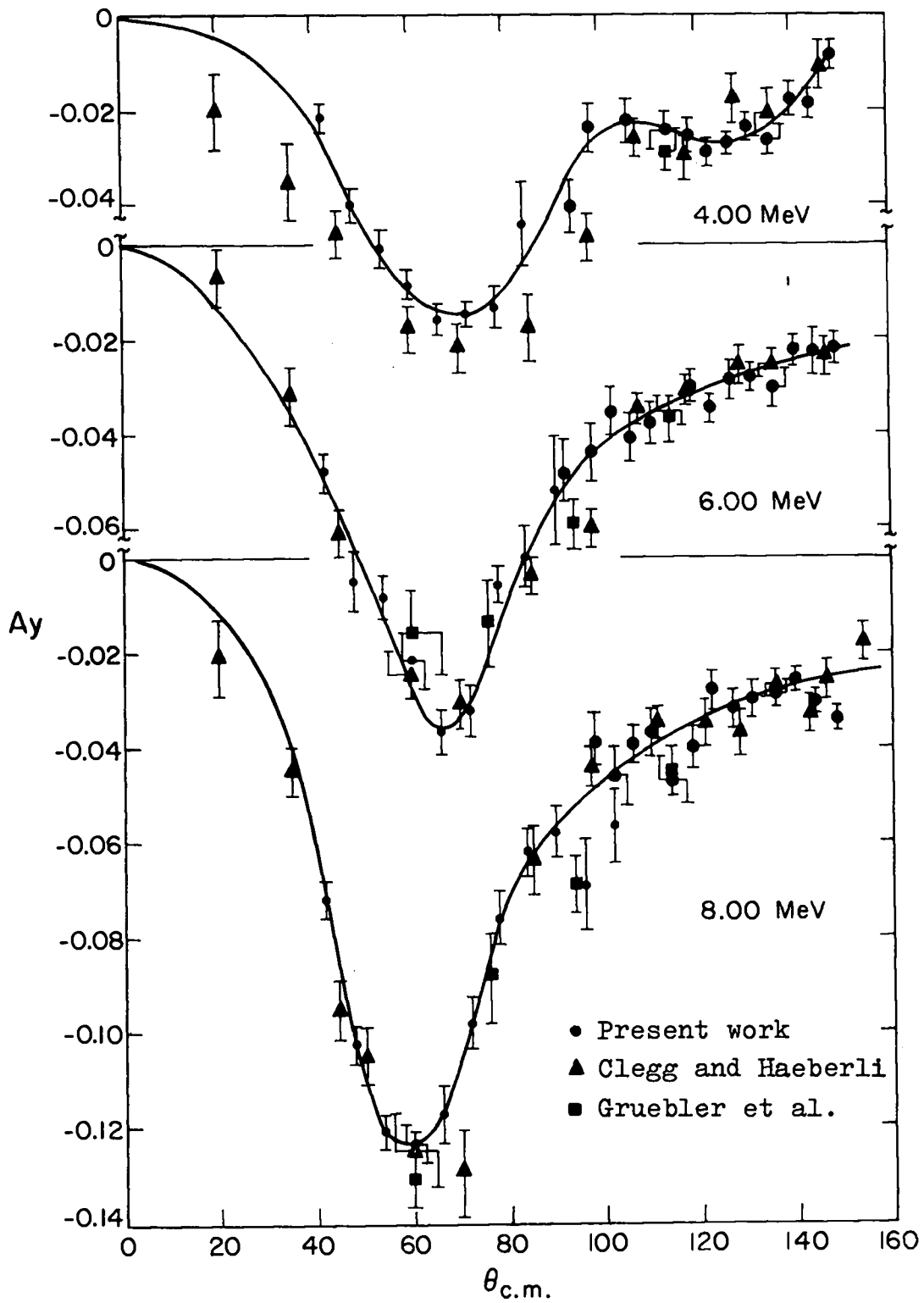


Fig. 7. Vector Analyzing Power for  $D(\vec{p},d)H$  ( $\hat{y}$  along  $\vec{k}_{in}(p) \times \vec{k}_{out}(d)$ ).

TABLE 2

Measured Analyzing Powers for  $H(\vec{d},p)D$  at 7.98 MeV.

$\theta_{lab}$ (P) (deg)	$\theta_{cm}$ (P) (deg)	$A_y$	$A_{yy}$	$A_{xx}$	$A_{xz}$ <sup>a)</sup>	$A_{zz}$	$\frac{1}{2}(A_{xx} - A_{yy})$
21	42.1	-0.020±0.003	0.022±0.005	-0.063±0.005		0.040±0.007	-0.042±0.004
24	48.1	-0.035±0.004	0.029±0.006	-0.075±0.006	0.032±0.007	0.046±0.009	-0.052±0.005
27	54.1	-0.029±0.004	0.055±0.007	-0.080±0.007	0.047±0.008	0.026±0.010	-0.068±0.005
30	60.1	-0.039±0.005	0.064±0.008	-0.067±0.008	0.051±0.009	0.003±0.012	-0.065±0.006
33	66.1	-0.039±0.003	0.082±0.005	-0.061±0.005	0.050±0.005	-0.021±0.008	-0.072±0.004
36	72.1	-0.040±0.003	0.070±0.005	-0.053±0.006	0.043±0.006	-0.017±0.008	-0.061±0.004
39	78.1	-0.031±0.003	0.066±0.004	-0.039±0.004	0.021±0.006	-0.026±0.006	-0.052±0.003
42	84.1	-0.025±0.003	0.061±0.004	-0.037±0.004	0.016±0.004	-0.024±0.006	-0.049±0.003
45	90.1	-0.020±0.003	0.059±0.004	-0.037±0.004	0.008±0.004	-0.023±0.006	-0.048±0.003
48	96.1	-0.017±0.003	0.057±0.004	-0.036±0.004	0.006±0.004	-0.020±0.006	-0.047±0.003
51	102.1	-0.011±0.003	0.051±0.005	-0.028±0.005	0.000±0.004	-0.022±0.007	-0.039±0.004
54	108.1	-0.016±0.004	0.040±0.007	-0.030±0.007	0.014±0.005	-0.009±0.010	-0.035±0.005
57	114.1	-0.015±0.003	0.038±0.004	-0.036±0.004	0.046±0.011	-0.002±0.006	-0.037±0.003

a)  $A_{xz}$  was determined by the Rapid Method.

TABLE 3

Measured Analyzing Powers for  $H(\vec{d},p)D$  at 10.00 MeV.

$\theta_{\text{lab}}$ (P) (deg)	$\theta_{\text{cm}}$ (P) (deg)	$A_y$	$A_{yy}$	$A_{xx}$	$A_{xz}$ <sup>a)</sup>	$A_{zz}$	$\frac{1}{2}(A_{xx} - A_{yy})$
21	42.1	-0.020±0.003	0.035±0.004	-0.085±0.004	0.042±0.003	0.050±0.006	-0.060±0.003
24	48.1	-0.037±0.004	0.058±0.005	-0.090±0.005	0.050±0.007	0.032±0.007	-0.074±0.004
27	54.1	-0.048±0.003	0.066±0.004	-0.099±0.004		0.032±0.006	-0.083±0.003
30	60.1	-0.044±0.004	0.081±0.005	-0.077±0.005	0.063±0.010	-0.004±0.007	-0.079±0.004
33	66.1	-0.046±0.002	0.089±0.003	-0.066±0.003	0.052±0.004	-0.024±0.004	-0.077±0.002
36	72.1	-0.040±0.002	0.085±0.003	-0.051±0.003	0.033±0.005	-0.034±0.004	-0.068±0.002
39	78.1	-0.032±0.002	0.084±0.003	-0.040±0.003	0.015±0.005	-0.044±0.004	-0.062±0.002
42	84.1	-0.025±0.002	0.074±0.003	-0.041±0.003	0.004±0.005	-0.033±0.004	-0.057±0.002
45	90.1	-0.018±0.004	0.067±0.005	-0.036±0.006	0.000±0.004	-0.031±0.008	-0.052±0.004
48	96.1	-0.016±0.002	0.053±0.003	-0.041±0.003	-0.011±0.004	-0.012±0.004	-0.047±0.002
51	102.1	-0.008±0.002	0.052±0.003	-0.043±0.003	-0.007±0.004	-0.009±0.004	-0.047±0.002
54	108.1	-0.007±0.002	0.042±0.003	-0.043±0.003	-0.006±0.004	-0.001±0.004	-0.042±0.002
57	114.1	-0.006±0.002	0.041±0.003	-0.040±0.003	-0.007±0.005	0.000±0.004	-0.041±0.002

a)  $A_{xz}$  was determined by the Rapid Method.

TABLE 4

Measured Analyzing Powers for  $H(\vec{d},p)D$  at 12.00 MeV.

$\theta_{\text{lab}}$ (P) (deg)	$\theta_{\text{cm}}$ (P) (deg)	$A_y$	$A_{yy}$	$A_{xx}$	$A_{xz}$ <sup>a)</sup>	$A_{zz}$	$\frac{1}{2}(A_{xx} - A_{yy})$
21	42.1	-0.037±0.003	0.046±0.004	-0.107±0.004	0.025±0.007	0.061±0.006	-0.077±0.003
24	48.1	-0.046±0.004	0.069±0.005	-0.116±0.005	0.056±0.008	0.048±0.008	-0.092±0.004
27	54.1	-0.055±0.005	0.090±0.006	-0.116±0.006	0.068±0.009	0.026±0.009	-0.103±0.004
30	60.1	-0.063±0.004	0.104±0.005	-0.082±0.006	0.062±0.011	-0.022±0.008	-0.093±0.004
33	66.2	-0.051±0.003	0.108±0.003	-0.069±0.004	0.060±0.011	-0.039±0.005	-0.089±0.003
36	72.2	-0.042±0.003	0.098±0.003	-0.047±0.003	0.018±0.008	-0.051±0.005	-0.073±0.002
39	78.2	-0.029±0.002	0.095±0.003	-0.043±0.003	-0.003±0.008	-0.052±0.005	-0.069±0.002
42	84.2	-0.025±0.002	0.084±0.003	-0.043±0.003	-0.031±0.008	-0.041±0.004	-0.063±0.002
45	90.2	-0.014±0.002	0.074±0.003	-0.040±0.003	-0.026±0.008	-0.034±0.004	-0.057±0.002
48	96.2	-0.014±0.002	0.062±0.003	-0.046±0.003	-0.034±0.008	-0.016±0.004	-0.054±0.002
51	102.2	-0.007±0.002	0.056±0.003	-0.050±0.003	-0.020±0.008	-0.006±0.004	-0.053±0.002
54	108.2	-0.005±0.002	0.046±0.003	-0.055±0.003	-0.018±0.007	0.008±0.004	-0.050±0.002
57	114.2	-0.007±0.002	0.040±0.003	-0.054±0.003	-0.004±0.007	0.013±0.004	-0.047±0.002

a)  $A_{xz}$  was determined by the Ratio Method.

TABLE 5

Measured Analyzing Powers for  $H(\vec{d},p)D$  at 14.00 MeV.

$\theta_{\text{lab}}$ (P) (deg)	$\theta_{\text{cm}}$ (P) (deg)	$A_y$	$A_{yy}$	$A_{xx}$	$A_{xz}^{\text{a)}$	$A_{zz}$	$\frac{1}{2}(A_{xx} - A_{yy})$
21	42.1	-0.047±0.004	0.062±0.005	-0.099±0.005	0.017±0.006	0.037±0.007	-0.081±0.004
27	54.1	-0.060±0.003	0.091±0.005	-0.105±0.005	0.075±0.012	0.014±0.007	-0.098±0.003
30	60.2	-0.062±0.004	0.117±0.005	-0.092±0.006	0.044±0.006	-0.025±0.008	-0.104±0.004
33	66.2	-0.041±0.003	0.128±0.004	-0.059±0.004	0.032±0.006	-0.070±0.006	-0.094±0.003
36	72.2	-0.035±0.003	0.115±0.004	-0.042±0.004	-0.018±0.006	-0.073±0.006	-0.079±0.003
39	78.2	-0.024±0.003	0.114±0.004	-0.034±0.004	-0.043±0.006	-0.080±0.005	-0.074±0.003
42	84.2	-0.013±0.003	0.096±0.004	-0.041±0.004	-0.050±0.006	-0.055±0.005	-0.068±0.003
45	90.2	-0.009±0.002	0.082±0.002	-0.049±0.002	-0.053±0.005	-0.033±0.003	-0.065±0.002
48	96.2	-0.009±0.002	0.067±0.002	-0.056±0.002	-0.048±0.005	-0.011±0.003	-0.061±0.002
51	102.2	-0.006±0.002	0.063±0.002	-0.060±0.002	-0.035±0.005	-0.003±0.003	-0.061±0.002
54	108.2	-0.005±0.002	0.059±0.002	-0.056±0.002	-0.035±0.005	-0.003±0.003	-0.057±0.002
57	114.2	-0.006±0.002	0.048±0.003	-0.054±0.003	-0.014±0.005	0.006±0.005	-0.051±0.002

a)  $A_{xz}$  was determined by the Rapid Method.

the sign of  $A_y$  and  $A_{xz}$  and record the data at  $\theta_{c.m.}(d) = \pi - \theta_{c.m.}(p)$ . At each energy,  $\frac{1}{2}(A_{xx} - A_{yy})$  and  $A_{zz}$  were determined from the measured values of  $A_{xx}$  and  $A_{yy}$ , the latter from the relation  $A_{xx} + A_{yy} + A_{zz} = 0$ . Errors listed in the tables are purely statistical. In addition to the statistical errors,  $A_y$ ,  $A_{yy}$ , and  $A_{xx}$  are estimated to have errors less than 0.005, 0.010, and 0.010, respectively. These estimates are based on a 2% uncertainty in beam polarization and a 1% uncertainty in current integration between runs of different magnetic substate. Additional error in  $A_{xz}$  is estimated to be less than 0.005 based on the 2% uncertainty in beam polarization and a  $1^\circ$  misalignment in  $\beta$  and in  $\varphi$ .

Additional analyzing power measurements were later made by Mitchell, Gruebler, Ohlsen, Simon, and Salzman with the apparatus described in Chapter II. These measurements increase the energy range and are tabulated in Tables 6 and 7 for the sake of completeness. Systematic errors should be comparable to those already quoted.

Plotted in Figs. 8-11 are the data tabulated in Tables 2-5. Again, the errors shown are purely statistical. The observables show a considerable amount of structure even though they are small when compared to their maximum possible range of values:  $\pm 1$  for  $A_y$ ,  $\pm 3/2$  for  $A_{xz}$  and  $\frac{1}{2}(A_{xx} - A_{yy})$ , and  $+1$  to  $-2$  for  $A_{xx}$ ,  $A_{yy}$ , and  $A_{zz}$ .

TABLE 6

Measured Analyzing Powers for  $H(\vec{d},p)D$  at 16.0 MeV

$\theta_{\text{lab}}$ (P) (deg)	$\theta_{\text{cm}}$ (P) (deg)	$A_y$	$A_{yy}$	$A_{xx}$	$A_{xz}$	$A_{zz}$	$\frac{1}{2}(A_{xx} - A_{yy})$
21	42.2	-0.054±0.006	0.056±0.008	-0.151±0.009	0.034±0.010	0.094±0.012	-0.104±0.006
24	48.2	-0.069±0.008	0.094±0.011	-0.161±0.012	0.085±0.013	0.067±0.016	-0.127±0.008
27	54.2	-0.072±0.007	0.144±0.009	-0.137±0.010	0.083±0.015	-0.008±0.013	-0.140±0.007
30	60.2	-0.060±0.009	0.102±0.012	-0.067±0.012	0.028±0.013	-0.035±0.017	-0.084±0.008
33	66.2	-0.055±0.004	0.149±0.006	-0.052±0.006	0.029±0.010	-0.097±0.009	-0.101±0.004
36	72.2	-0.038±0.004	0.134±0.005	-0.027±0.005	-0.021±0.007	-0.107±0.007	-0.080±0.003
39	78.2	-0.015±0.006	0.110±0.009	-0.023±0.009	-0.046±0.007	-0.087±0.013	-0.067±0.006
42	84.2	-0.017±0.006	0.097±0.008	-0.020±0.009	-0.077±0.007	-0.077±0.012	-0.058±0.006
45	90.2	-0.012±0.006	0.096±0.008	-0.061±0.008	-0.067±0.006	-0.034±0.011	-0.079±0.006
48	96.2	0.001±0.006	0.081±0.008	-0.052±0.008	-0.060±0.006	-0.028±0.011	-0.067±0.005
51	102.2	0.001±0.005	0.054±0.007	-0.067±0.008	-0.048±0.006	0.013±0.011	-0.060±0.005
54	108.2	-0.013±0.005	0.069±0.007	-0.073±0.007	-0.034±0.006	0.004±0.010	-0.071±0.005
57	114.2	-0.014±0.005	0.052±0.007	-0.065±0.007	-0.019±0.006	0.013±0.010	-0.058±0.005
60	120.2	-0.015±0.005	0.048±0.007	-0.052±0.007	-0.008±0.006	0.004±0.010	-0.050±0.005
63	126.2	-0.008±0.005	0.028±0.007	-0.043±0.008	-0.015±0.006	0.014±0.010	-0.036±0.005
66	132.2	-0.016±0.004	0.047±0.005	-0.035±0.005	-0.011±0.011	-0.012±0.008	-0.041±0.004

a)  $A_{xz}$  was determined by the Ratio Method.

TABLE 7

Measured Values of  $A_{xz}$  for  $H(\vec{d},p)D$  at 17.0 MeV

$\theta_{lab}$ (P) (deg)	$\theta_{cm}$ (P) (deg)	$A_{xz}$ a)
27	54.2	0.065±0.009
30	60.2	0.023±0.008
33	66.2	0.010±0.010
36	72.2	-0.051±0.010
39	78.2	-0.077±0.009
42	84.2	-0.076±0.009
45	90.2	-0.075±0.009
48	96.2	-0.086±0.009
51	102.2	-0.063±0.008
54	108.2	-0.042±0.008
57	114.2	-0.047±0.008
60	120.2	-0.018±0.008
63	126.2	-0.010±0.008

a) In order to determine  $A_{xz}$  it was necessary to assume the values for  $A_{xx}$  and  $A_{zz}$  to be the same as those obtained at 16 MeV. The fractional error,  $\Delta A_{xz}/A_{xz}$ , introduced by this procedure is  $p_{zz}(1/3\Delta A_{xx} + 1/6\Delta A_{zz})$  where  $\Delta A_{xx}$  and  $\Delta A_{zz}$  are the differences between the relevant analyzing powers at 16 and 17 MeV. Crude extrapolation of the data indicates that the uncertainty introduced by this assumption is much less than the quoted statistical errors.

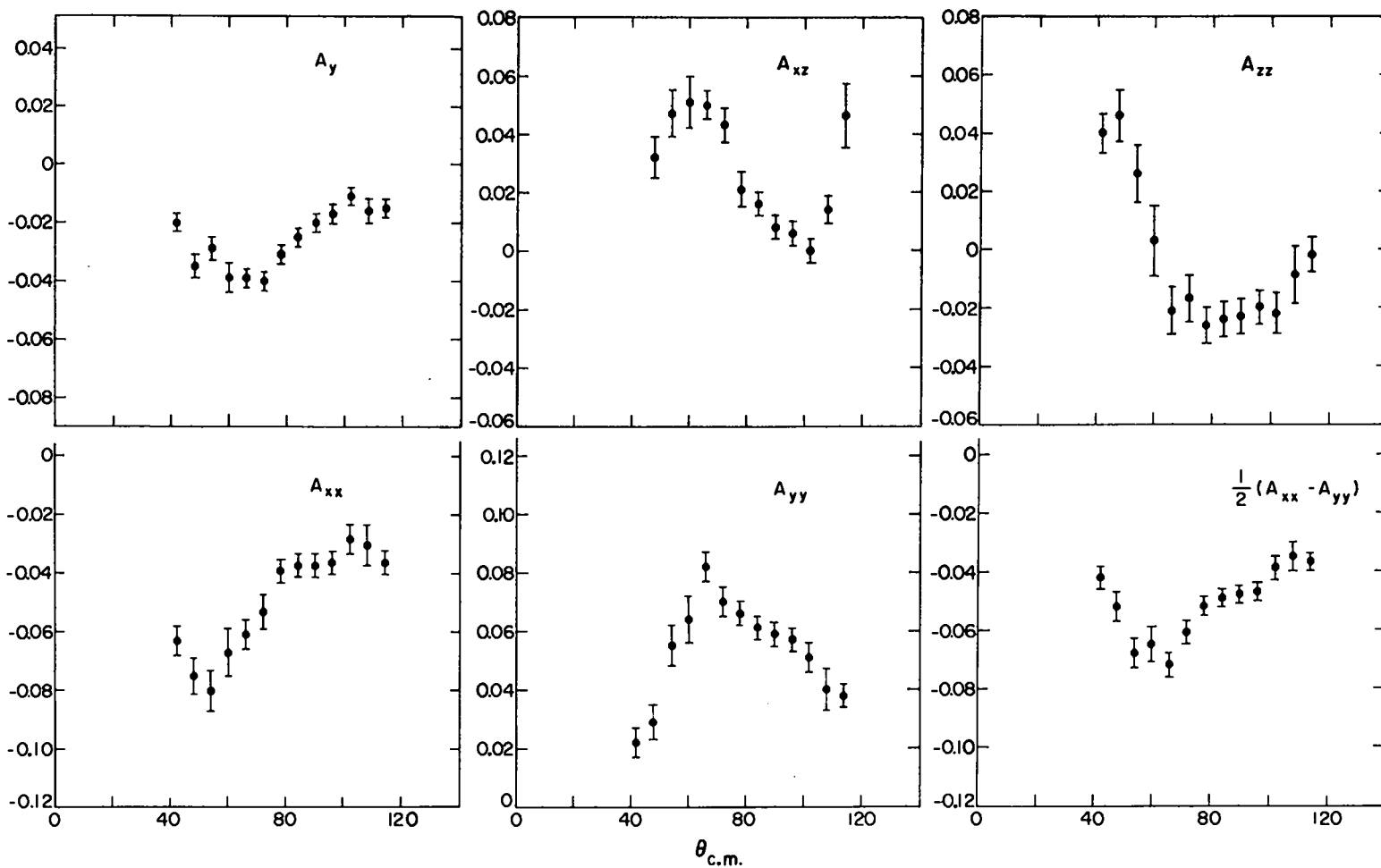


Fig. 8. Analyzing Powers for  $H(\vec{d}, p)D$  at 7.98 MeV ( $\hat{y}$  along  $\vec{k}_{in}(d) \times \vec{k}_{out}(p)$ ).

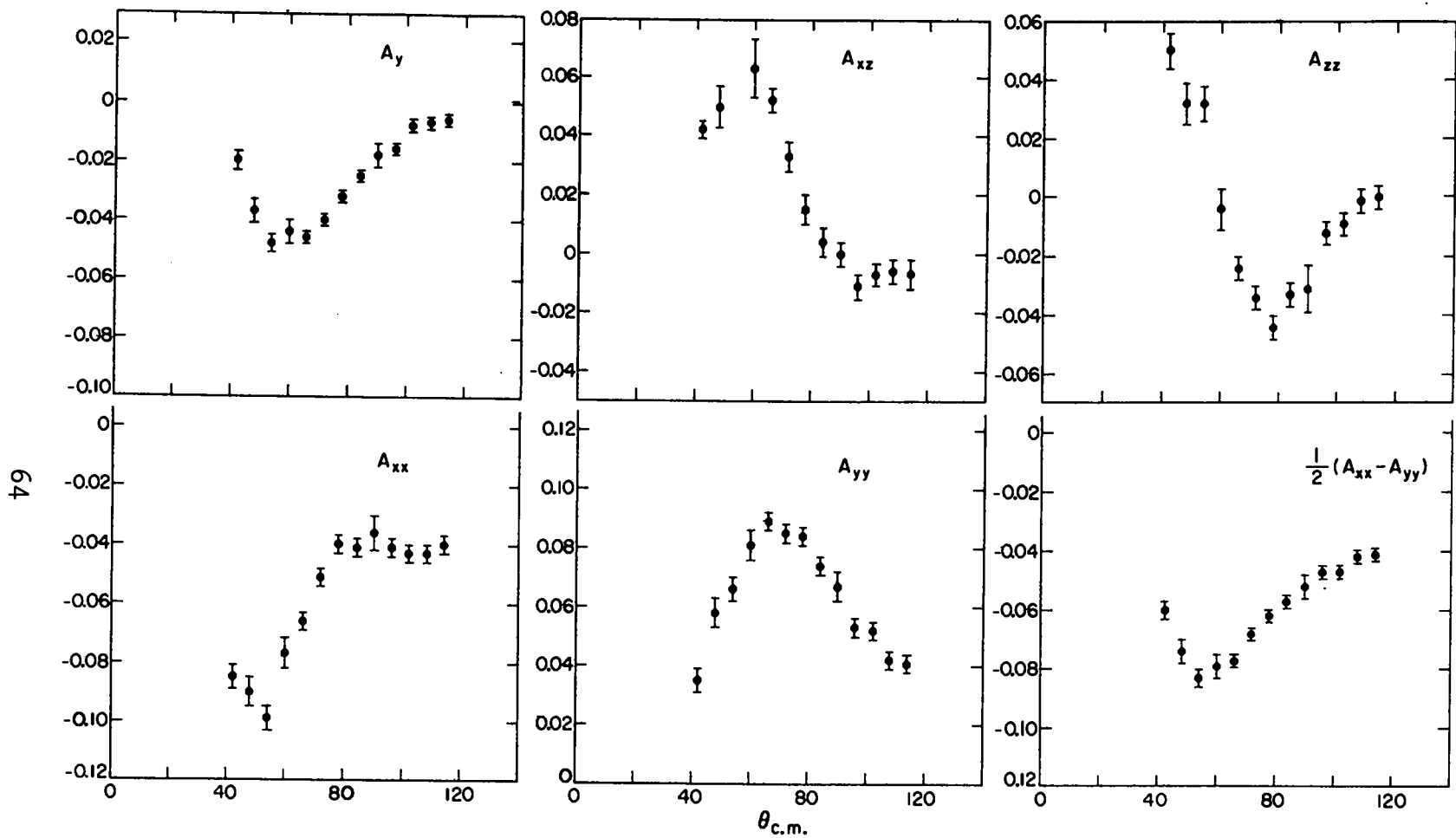


Fig. 9. Analyzing Powers for  $H(\vec{d}, p)D$  at 10.00 MeV ( $\hat{y}$  along  $\vec{k}_{in}(d)\vec{k}_{out}(p)$ ).

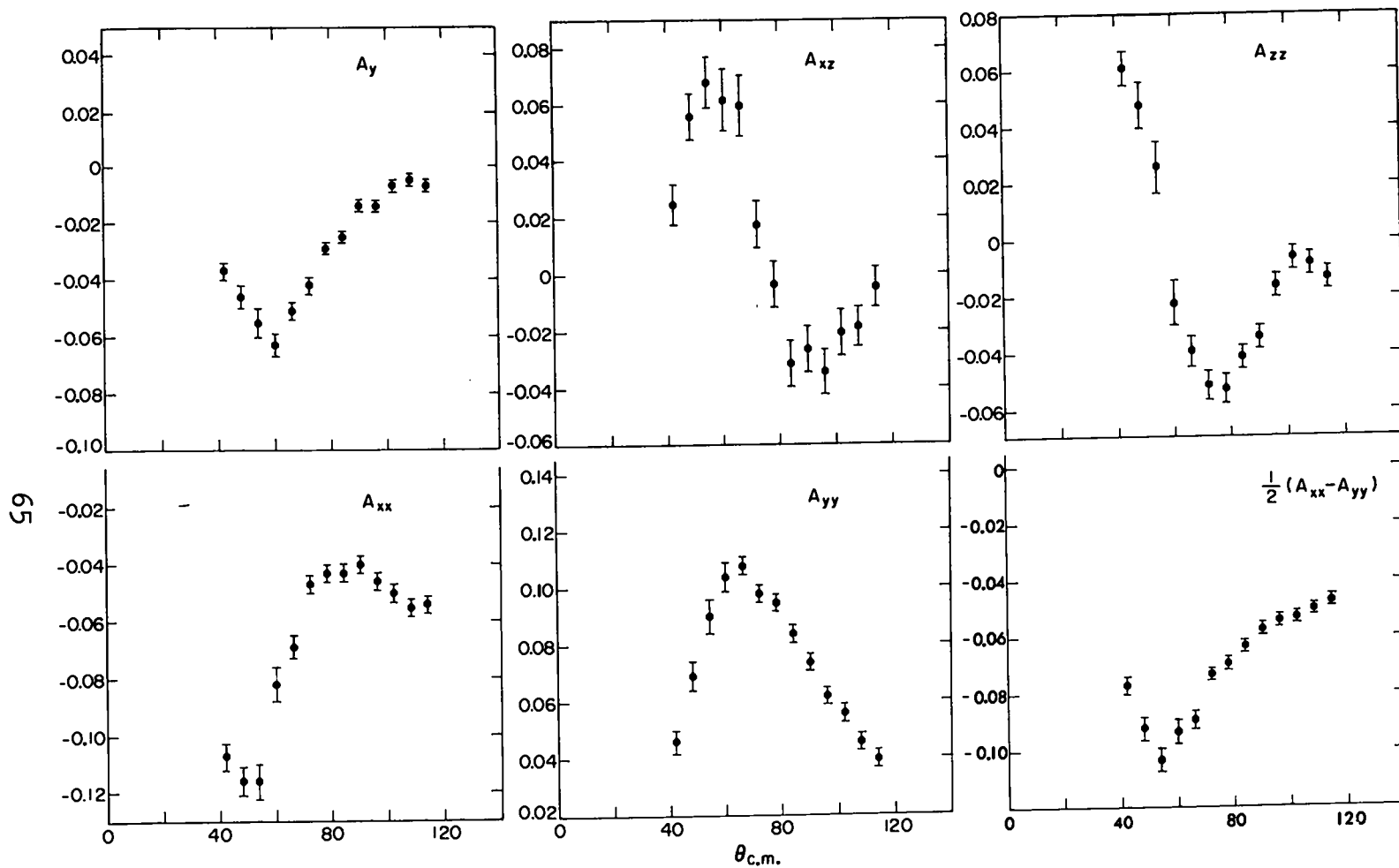


Fig. 10. Analyzing Powers for  $H(\vec{d}, p)D$  at 12.00 MeV ( $\hat{y}$  along  $\vec{k}_{in}(d)\vec{x}_{out}(p)$ ).

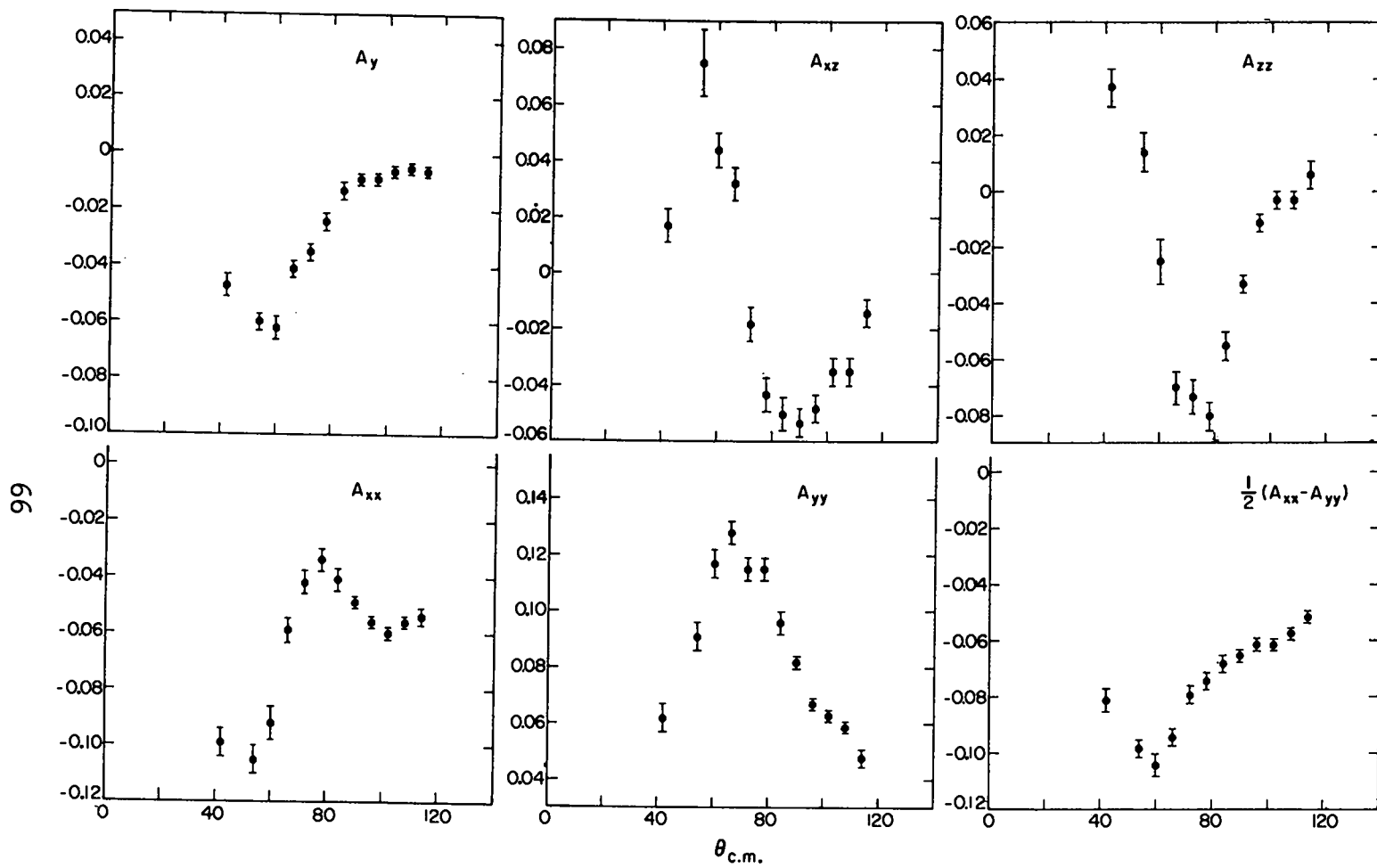


Fig. 11. Analyzing Powers for  $H(\vec{d}, p)D$  at 14.00 MeV ( $\hat{y}$  along  $\vec{k}_{in}(d)\vec{x}\vec{k}_{out}(p)$ ).

The most comprehensive set of data with which to compare the present results consists of measurements made by White et al. (Wh 72) of  $iT_{11}$ ,  $T_{20}$ ,  $T_{21}$ , and  $T_{22}$  (corresponding to  $A_y$ ,  $A_{zz}$ ,  $A_{xz}$ , and  $\frac{1}{2}(A_{xx}-A_{yy})$ , respectively) at deuteron energies of 6, 8, 10, and 11.5 MeV. Agreement is generally quite good. Their data have been omitted from the figures for the sake of clarity.

### 3. $D(p,d)H$

For elastic scattering in the center-of-mass system, polarizations resulting in the inverse reaction,  $D(p,d)H$ , are equal to the analyzing powers for the reaction,  $H(d,p)D$ , except for a sign change of  $A_{xz}$ . Hence, in order to obtain the outgoing polarization components resulting from an unpolarized incident beam appropriate for use in Eq. (1-16) in the laboratory frame, the analyzing powers had to be related to their respective polarizations through the c.m. system and the polarization quantities thus obtained rotated through an angle  $\psi$  about the y axis. The sense of  $\psi$  is such that  $\psi = \theta_{c.m.} - \theta_{lab}$ , a positive number. The unitary matrix required to effect this transformation is given by

$$U = \begin{pmatrix} \cos\psi & 0 & \sin\psi \\ 0 & 1 & 0 \\ -\sin\psi & 0 & \cos\psi \end{pmatrix} .$$

Outgoing vector and tensor polarization components given in a laboratory frame [ $\hat{z}'$  along  $\vec{k}_{\text{out}}(\text{lab})$ ] may then be expressed in terms of the polarizations given in the c.m. frame [ $\hat{z}'$  along  $\vec{k}_{\text{out}}(\text{c.m.})$ ]:

$$\vec{P}_{\text{lab}} = U \vec{P}_{\text{c.m.}}$$

and

$$(PP)_{\text{lab}} = U(PP)_{\text{c.m.}} \tilde{U} .$$

For the present application, the polarization components of interest for the reaction,  $D(p,d)H$ , expressed in terms of the analyzing powers for the inverse reaction,  $H(d,p)D$ , are

$$P^{Y'}(\text{lab}) = P^{Y'}(\text{c.m.}) = A_y$$

$$\begin{aligned} P^{X'X'}(\text{lab}) &= P^{X'X'}(\text{c.m.}) \cos^2 \psi + P^{Z'Z'}(\text{c.m.}) \sin^2 \psi \\ &\quad + 2P^{X'Z'}(\text{c.m.}) \sin \psi \cos \psi \\ &= A_{xx} (\cos^2 \psi - \sin^2 \psi) - A_{yy} \sin^2 \psi - 2A_{xz} \sin \psi \cos \psi \end{aligned}$$

$$P^{Y'Y'}(\text{lab}) = P^{Y'Y'}(\text{c.m.}) = A_{yy}$$

$$\begin{aligned} P^{Z'Z'}(\text{lab}) &= P^{X'X'}(\text{c.m.}) \sin^2 \psi + P^{Z'Z'}(\text{c.m.}) \cos^2 \psi \\ &\quad - 2P^{X'Z'}(\text{c.m.}) \sin \psi \cos \psi \\ &= A_{xx} (\sin^2 \psi - \cos^2 \psi) - A_{yy} \cos^2 \psi + 2A_{xz} \sin \psi \cos \psi \end{aligned}$$

$$\begin{aligned}
P^{x'z'}(\text{lab}) &= -P^{x'x'}(\text{c.m.})\sin\psi\cos\psi + P^{z'z'}(\text{c.m.})\sin\psi\cos\psi \\
&\quad + P^{x'z'}(\text{c.m.})x(\cos^2\psi - \sin^2\psi) \\
&= -2A_{xx}\sin\psi\cos\psi - A_{yy}\sin\psi\cos\psi - A_{xz}(\cos^2\psi - \sin^2\psi),
\end{aligned}$$

where use of the relation  $A_{xx} + A_{yy} + A_{zz} = 0$  has been used to express the desired polarizations in terms of the independently measured quantities. For nonrelativistic p-d elastic scattering  $\psi = \theta_{\text{lab}}$ .

Data resulting from the above transformation are presented in Tables 8-11 inclusive. The errors given in the tables were rotated through the angle  $\psi$  and are again purely statistical.

TABLE 8

Polarization of Deuterons from p-d Elastic Scattering at 3.99 MeV.

$\theta_{\text{lab}}$ (d) (deg)	$P_{y'}$	$P_{y'y'}$	$P_{x'x'}$	$P_{x'z'}$	$P_{z'z'}$	$\frac{1}{2}(P_{x'x'} - P_{y'y'})$
21	-0.020±0.003	0.022±0.005				
24	-0.035±0.004	0.029±0.006	-0.078±0.007	0.024±0.005	0.050±0.008	-0.054±0.005
27	-0.029±0.004	0.055±0.007	-0.096±0.008	0.015±0.007	0.041±0.010	-0.076±0.006
30	-0.039±0.005	0.064±0.008	-0.093±0.009	0.005±0.008	0.029±0.011	-0.079±0.007
33	-0.039±0.003	0.082±0.005	-0.095±0.006	-0.002±0.006	0.012±0.006	-0.088±0.004
36	-0.040±0.003	0.070±0.005	-0.081±0.006	0.004±0.006	0.011±0.007	-0.076±0.005
39	-0.031±0.003	0.066±0.004	-0.055±0.006	0.002±0.005	-0.011±0.006	-0.060±0.004
42	-0.025±0.003	0.061±0.004	-0.046±0.005	0.005±0.005	-0.014±0.005	-0.054±0.004
45	-0.020±0.003	0.059±0.004	-0.037±0.005	0.007±0.005	-0.022±0.005	-0.048±0.004
48	-0.017±0.003	0.057±0.004	-0.034±0.005	0.009±0.005	-0.023±0.005	-0.046±0.004
51	-0.011±0.003	0.051±0.005	-0.025±0.005	0.003±0.006	-0.026±0.005	-0.038±0.004
54	-0.016±0.004	0.040±0.007	-0.030±0.007	0.014±0.008	-0.010±0.006	-0.035±0.006
57	-0.015±0.003	0.038±0.004	-0.054±0.010	0.034±0.004	0.016±0.010	-0.046±0.006

TABLE 9

Polarization of Deuterons from p-d Elastic Scattering at 5.00 MeV.

$\theta_{\text{lab}}$ (d) (deg)	$P_{y'}$	$P_{y'y'}$	$P_{x'x'}$	$P_{x'z'}$	$P_{z'z'}$	$\frac{1}{2}(P_{x'x'} - P_{y'y'})$
21	-0.023±0.003	0.036±0.004	-0.097±0.003	0.015±0.003	0.061±0.004	-0.067±0.003
24	-0.040±0.003	0.056±0.004	-0.106±0.006	0.012±0.003	0.050±0.007	-0.081±0.004
27	-0.048±0.003	0.066±0.004		0.000±0.005	0.032±0.010	-0.097±0.006
30	-0.044±0.004	0.081±0.005	-0.113±0.009	-0.002±0.003	0.011±0.005	-0.094±0.003
33	-0.046±0.002	0.089±0.003	-0.101±0.004	-0.003±0.003	-0.009±0.005	-0.081±0.003
36	-0.040±0.002	0.085±0.003	-0.077±0.005	-0.005±0.003	-0.028±0.005	-0.070±0.003
39	-0.032±0.002	0.084±0.003	-0.056±0.005	0.003±0.003	-0.032±0.005	-0.058±0.003
42	-0.025±0.002	0.074±0.003	-0.042±0.005	0.003±0.006	-0.034±0.005	-0.050±0.005
45	-0.018±0.004	0.067±0.005	-0.033±0.005	0.013±0.003	-0.039±0.005	-0.033±0.003
48	-0.016±0.002	0.052±0.003	-0.014±0.005	0.015±0.003	-0.037±0.004	-0.034±0.003
51	-0.008±0.002	0.052±0.003	-0.015±0.005	0.019±0.003	-0.033±0.004	-0.025±0.003
54	-0.007±0.002	0.042±0.003	-0.008±0.005	0.015±0.003	-0.035±0.005	-0.023±0.003
54	-0.006±0.002	0.041±0.003	-0.005±0.005			

TABLE 10

Polarization of Deuterons from p-d Elastic Scattering at 6.00 MeV.

$\theta_{\text{lab}}$ (d) (deg)	$P_{y'}$	$P_{y'y'}$	$P_{x'x'}$	$P_{x'z'}$	$P_{z'z'}$	$\frac{1}{2}(P_{x'x'} - P_{y'y'})$
21	-0.037±0.003	0.047±0.004	-0.103±0.006	0.038±0.003	0.056±0.007	-0.074±0.004
24	-0.046±0.004	0.069±0.005	-0.131±0.007	0.023±0.005	0.062±0.008	-0.100±0.005
27	-0.055±0.005	0.090±0.006	-0.142±0.009	0.018±0.006	0.052±0.010	-0.116±0.006
30	-0.063±0.004	0.104±0.005	-0.121±0.010	-0.005±0.005	0.017±0.011	-0.112±0.006
33	-0.051±0.003	0.108±0.003	-0.115±0.011	-0.011±0.004	0.007±0.011	-0.112±0.006
36	-0.042±0.003	0.098±0.003	-0.065±0.008	-0.007±0.004	-0.033±0.008	-0.082±0.005
39	-0.029±0.002	0.095±0.003	-0.044±0.008	-0.004±0.004	-0.051±0.008	-0.070±0.005
42	-0.025±0.002	0.084±0.003	-0.011±0.008	0.004±0.004	-0.073±0.008	-0.047±0.005
45	-0.014±0.002	0.074±0.003	-0.011±0.008	0.003±0.003	-0.063±0.008	-0.042±0.005
48	-0.014±0.002	0.062±0.003	0.005±0.008	0.012±0.003	-0.067±0.008	-0.028±0.004
51	-0.005±0.002	0.046±0.003	0.004±0.007	0.024±0.003	-0.050±0.007	-0.021±0.004
57	-0.007±0.002	0.041±0.003	-0.003±0.007	0.029±0.003	-0.037±0.007	-0.022±0.004

TABLE 11

Polarization of Deuterons from p-d Elastic Scattering at 7.00 MeV.

$\theta_{\text{lab}}$ (d) (deg)	$P_{y'}$	$P_{y'y'}$	$P_{x'x'}$	$P_{x'z'}$	$P_{z'z'}$	$\frac{1}{2}(P_{x'x'} - P_{y'y'})$
21	-0.047±0.004	0.062±0.005	-0.093±0.006	0.033±0.004	0.031±0.007	-0.077±0.004
27	-0.060±0.003	0.091±0.005	-0.141±0.010	0.004±0.004	0.050±0.011	-0.116±0.006
30	-0.062±0.004	0.117±0.005	-0.114±0.006	0.007±0.006	-0.003±0.007	-0.115±0.005
33	-0.041±0.003	0.128±0.004	-0.091±0.006	-0.018±0.004	-0.037±0.006	-0.110±0.004
36	-0.035±0.003	0.115±0.004	-0.035±0.006	-0.009±0.004	-0.080±0.006	-0.075±0.004
39	-0.024±0.003	0.114±0.004	-0.010±0.006	-0.014±0.004	-0.104±0.006	-0.062±0.004
42	-0.013±0.003	0.096±0.004	0.002±0.006	-0.002±0.004	-0.098±0.006	-0.047±0.004
45	-0.009±0.002	0.082±0.002	0.012±0.006	0.008±0.002	-0.094±0.006	-0.035±0.003
48	-0.009±0.002	0.067±0.002	0.016±0.005	0.018±0.002	-0.083±0.005	-0.025±0.003
51	-0.006±0.002	0.063±0.002	0.008±0.005	0.020±0.002	-0.071±0.005	-0.027±0.003
54	-0.005±0.002	0.059±0.002	0.012±0.005	0.014±0.002	-0.071±0.005	-0.023±0.003
57	-0.006±0.002	0.048±0.003	0.001±0.005	0.022±0.004	-0.049±0.005	-0.024±0.004

## CHAPTER IV

### CALIBRATION OF THE DEUTERON POLARIMETER

#### A. Introduction

In order to measure the polarization components of a beam of particles, a reaction or scattering which has known analyzing properties is required. For the measurement of deuteron tensor polarization, the reactions  ${}^3\text{He}(\vec{d}, p){}^4\text{He}$  and  $T(\vec{d}, n){}^4\text{He}$  were first suggested by Galonsky et al. (Ga 59) and by Goldfarb (Go 59). These reactions have pronounced resonances near 430 keV and 107 keV, respectively, for which early resonance parameter fits indicated that the reactions proceeded via s-wave deuteron absorption consisting of a large  $j = 3/2^+$  and a small  $j = 1/2^+$  contribution. Assuming the presence of only these two channels, the analyzing powers in the center-of-mass system are

$$\begin{aligned}
 A_y &= 0 & \frac{1}{2}(A_{xx} - A_{yy}) &= -\frac{3}{4} \kappa \sin^2\theta \\
 A_{xz} &= -\frac{3}{2} \kappa \sin\theta \cos\theta & A_{zz} &= -\frac{1}{2} \kappa (3\cos^2\theta - 1) .
 \end{aligned}
 \tag{4-1}$$

If the reaction proceeds purely through the  $j = 3/2^+$  channel,  $\kappa = 1$ . Hence, a value of  $\kappa$  other than 1 is indicative of the  $j = 1/2^+$  contribution.

Zero vector analyzing power is a very desirable property for an analyzing reaction which is to be used

to detect tensor polarization. This is because vector and tensor polarization effects could, if  $A_y \neq 0$ , each give rise to an asymmetry in the same plane. The use of an analyzer with nonzero vector analyzing power would therefore require an additional experiment in order to separate vector polarization from tensor polarization effects. The reaction  ${}^3\text{He}(\vec{d}, p){}^4\text{He}$  was chosen over the reaction  $\text{T}(\vec{d}, n){}^4\text{He}$  (or equivalently  $\text{T}(\vec{d}, \alpha)n$ ) in view of: (1) the radiation hazards associated with the use of tritium; (2) the considerable greater ease in detecting protons than neutrons or low energy alpha particles; and (3) the availability of reasonably reliable energy, range, and straggle tables for proton energies only above 100 keV (corresponding to tables for deuteron energies above 200 keV). This is well above the resonance for the  $\text{T}(d, \alpha)n$  reaction but sufficiently below the  ${}^3\text{He}(d, p){}^4\text{He}$  resonance for the necessary finite target calculations to be made; i.e., the ratio of the cross section at 200 keV to the ratio of the cross section at the  ${}^3\text{He}(d, p){}^4\text{He}$  resonance is only about 0.2. Hence, only a crude knowledge of the energy distribution of deuterons entering the  ${}^3\text{He}$  cell is necessary for deuteron energies less than 200 keV, as such particles contribute very little to the overall yield (see Fig. 15 for various distributions used in the calibration). This would not be the case for the  $\text{T}(d, n){}^4\text{He}$  reaction.

Based on the experimental work of Brown et al., (Br 66), McIntyre and Haeberli (Mc 67) suggested that  $\kappa$  is  $0.88 \pm 0.05$  for the  ${}^3\text{He}(\vec{d}, p){}^4\text{He}$  reaction. However, at a deuteron energy of 430 keV, Leemann et al. (Le 71) observed substantial values of  $A_y$  as well as slight deviations of the angular distributions of  $A_{xz}$ ,  $\frac{1}{2}(A_{xx} - A_{yy})$ , and  $A_{zz}$  from the form of Eq. (4-1), thereby demonstrating the presence of partial waves other than s waves.

The calibration experiment to be described here was undertaken to provide more accurate values for the effective analyzing power to be used for the polarization transfer experiment. The procedure was as follows. First, various asymmetries were measured using a polarized beam directly from the ion source. Finite geometry and finite energy distribution effects were then unfolded from the raw analyzing power results. This resulted in a knowledge of the analyzing powers which would be observed with perfect geometry and a sharply defined energy. This information, together with appropriate estimates of the intensity and energy distributions which prevailed in each polarization transfer measurement, could then be used (with a computer code) to calculate the average deuteron interaction energy, the location of the centroid of proton production, and the effective analyzing powers in the  ${}^3\text{He}$  cell for each of the energies and angles at which polarization transfer data were taken. It was also

intended that the computer code be capable, if necessary, of correcting the polarization transfer coefficients for variations in angle due to the large angular acceptance of the  $^3\text{He}$  cell. However, in view of the smallness of the outgoing deuteron polarizations and consequently the polarization transfer coefficients, an accurate knowledge of the effective analyzing powers was not needed and the corrections were not made.

The differential cross section for parity conserving reactions induced by polarized deuterons may be written in the notation of Gammel et al. (Ga 71),

$$I(\theta, \varphi) = I_0(\theta) \left( 1 + \frac{3}{2} p_y A_y + \frac{2}{3} p_{xz} A_{xz} + \frac{1}{6} (p_{xx} - p_{yy}) (A_{xx} - A_{yy}) + \frac{1}{2} p_{zz} A_{zz} \right) . \quad (4-2)$$

$I_0(\theta)$  is the differential cross section at the scattering angle  $\theta$  for reactions induced by an unpolarized incident spin-1 beam. The p's represent the incident beam polarization quantities referred to a right-handed Cartesian coordinate system (called the reaction initial coordinate system or projectile helicity frame) with z along  $\vec{k}_{in}$  and y along  $\vec{k}_{in} \times \vec{k}_{out}$ . The A's are analyzing powers and are a measure of the extent to which their respective polarization components contribute to the cross section.

Polarized beams produced by any polarized ion source possess an axis of symmetry (called the quantization axis,  $\hat{S}$ ) which is defined by a magnetic field within the

source. If the quantization axis is rotated (e.g., by a spin precessor and system of bending magnets), the various beam polarization quantities at the target, expressed in the projectile helicity frame, may be found by applying a rotation matrix to the vector and tensor quantities expressed in the source coordinate system (Z along  $\vec{k}_{in}$ , Y chosen arbitrarily, X chosen to make a right-handed system). The result of the rotation is (Ga 70)

$$\begin{aligned}
 p_x &= p_Z \sin\beta \sin\varphi & p_{xz} &= -\frac{3}{2} p_{ZZ} \sin\beta \cos\beta \sin\varphi \\
 p_y &= p_Z \sin\beta \cos\varphi & p_{yz} &= \frac{3}{2} p_{ZZ} \sin\beta \cos\beta \cos\varphi \\
 p_z &= p_Z \cos\beta & \frac{1}{2}(p_{xx} - p_{yy}) &= -\frac{3}{4} p_{ZZ} \sin^2\beta \cos 2\varphi \\
 p_{xy} &= -\frac{3}{2} p_{ZZ} \sin^2\beta \sin\varphi \cos\varphi & p_{zz} &= \frac{1}{2} p_{ZZ} (3\cos^2\beta - 1),
 \end{aligned}
 \tag{4-3}$$

where  $\beta$  is the angle between  $\hat{S}$  and  $\vec{k}_{in}$  and  $\varphi$  is the angle between  $\hat{S} \times \vec{k}_{in}$  and the x axis. The vector and tensor polarization,  $p_Z$  and  $p_{ZZ}$ , respectively, are as defined in Chapter I. If "up" is defined by the half plane containing  $\hat{S}$  and  $\vec{k}_{in}$  and "left" defined by the half plane containing  $\hat{S} \times \vec{k}_{in}$  and  $\vec{k}_{in}$ , then scattering left, right, up, and down correspond to the use of  $\varphi = 0^\circ, 180^\circ, 270^\circ,$  and  $90^\circ$ , respectively.

In principle, a 100% polarized beam of deuterons in the  $m_I = 1$  magnetic substate would have  $p_Z = p_{ZZ} = 1$  ( $n_+ = 1, n_- = n_0 = 0$ , where  $n_+, n_-$ , and  $n_0$  are the fractional populations of the respective magnetic substates). In the  $m_I = 0$  substate the beam would have  $p_Z = 0, p_{ZZ} = -2$ , and in the  $m_I = -1$  substate the beam would have  $p_Z = -1, p_{ZZ} = 1$ . Production of pure  $m_I = 0$  and  $-1$  substates would require an infinite magnetic field in the source. In practice, one obtains, for these states, values of  $p_Z$  and  $p_{ZZ}$ , slightly lower than for the ideal case (Mc 71). For the fields generally used in the LASL source, the polarizations are:

$\frac{m_I}{}$	$\frac{p_Z}{}$	$\frac{p_{ZZ}}{}$
1	1	1
0	0.012	-1.966
-1	-0.984	0.952

Actual values of  $p_Z$  and  $p_{ZZ}$  are obtained by multiplying these values by the quenchable fractional value (Oh 70),  $p_Q$  (i.e.,  $p_Q \sim 0.8$  for deuterons). It is more desirable to reverse the direction of the quantization axis defining field with the  $m_I = 1$  substate when the  $m_I = -1$  substate is wanted than it is to use the  $m_I = -1$  substate in view of the somewhat less than ideal operating conditions for the latter state. Hence, when reference to an  $m_I = -1$  beam is made, an  $m_I = 1$  beam with reversed quantization

axis will be implied. It should also be noted that an unpolarized spin-1 beam is one for which  $n_+ = n_- = n_0$ . Hence, an unpolarized beam may be considered to consist of the sum of three polarized beams, each of which consists of particles in only one of the three magnetic substates. This enables one to construct an "unpolarized" run from three separate polarized runs.

### B. Experimental Procedure

The experimental arrangement is shown schematically in Fig. 12. The beam passed through a 24.5-mg/cm<sup>2</sup> gold foil, and the particles which scattered at  $\theta_1 = 30^\circ$  (Coulomb scattering) served to monitor the beam intensity. The degrader foils, the <sup>3</sup>He cell, and the five detectors are in air. The beam passed through a 5-mg/cm<sup>2</sup> Havar vacuum window and through a 28.5-mg/cm<sup>2</sup> aluminum energy degrading foil before entering the <sup>3</sup>He cell. The <sup>3</sup>He cell is a 2.5-cm diameter hemisphere of 125- $\mu$  thick aluminum with a 5-mg/cm<sup>2</sup> Havar entrance window. It is operated at room temperature at a pressure of 4.5 atm. Protons from the <sup>3</sup>He( $\vec{d}, p$ )<sup>4</sup>He reaction have about 17 MeV of energy and are therefore relatively easy to distinguish from background radiation. The five counter telescopes are placed 7.9 cm from the effective center of the <sup>3</sup>He cell. Each E- $\Delta$ E telescope consists of a 2.1-cm diameter circular collimator, two surface barrier detectors of

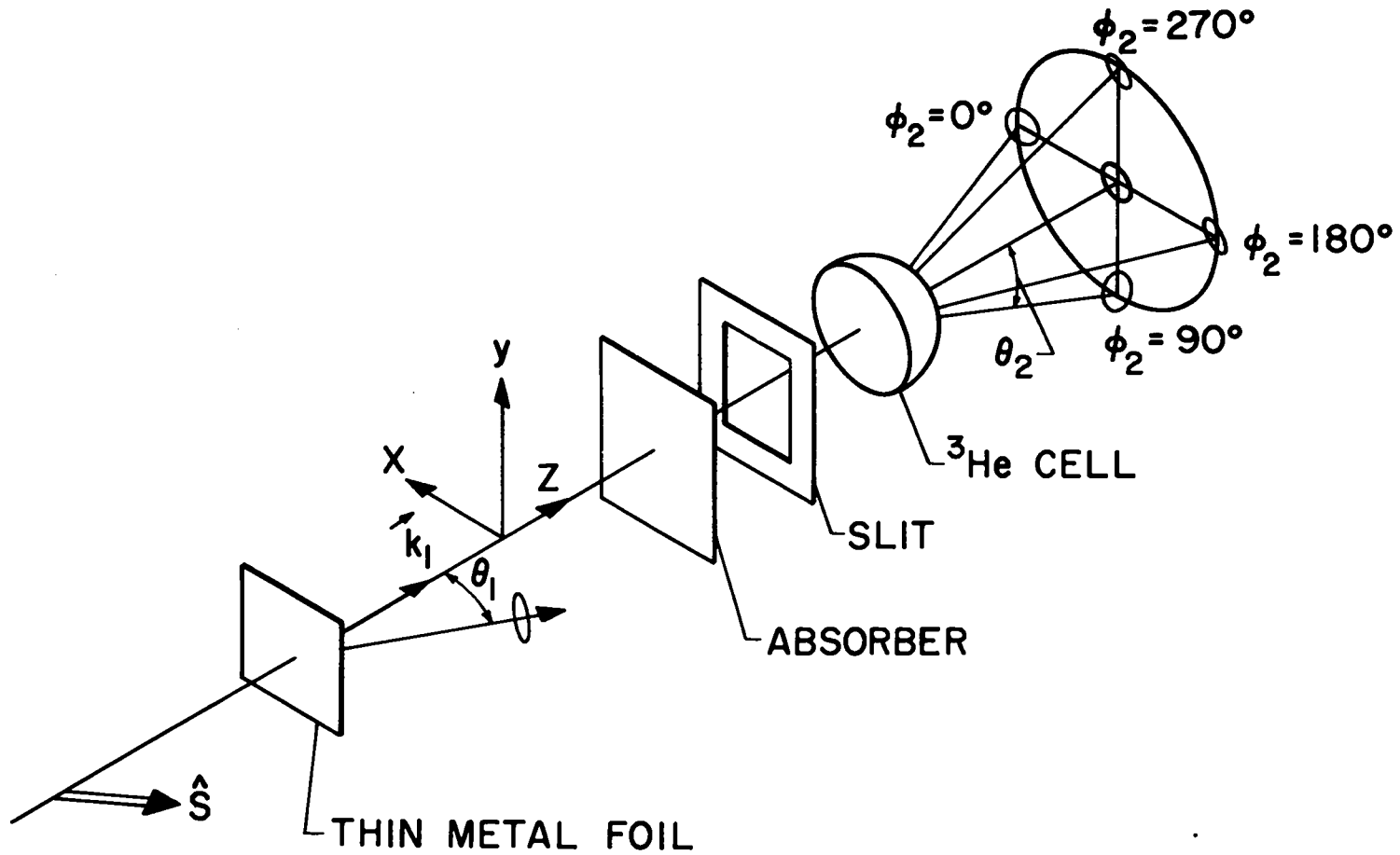


Fig. 12. Experimental Arrangement for  ${}^3\text{He}(d,p){}^4\text{He}$  Calibration.

area  $450 \text{ mm}^2$  and thickness  $500 \mu$ , and appropriate aluminum foils in front of and between the two detectors. The foils serve to enhance particle selectivity. Additional details of the scattering chamber are discussed in Chapter II.

The beam energy was varied between 6.10 and 6.50 MeV; this resulted in average interaction energies of the deuterons in the  $^3\text{He}$  cell between 366 and 1090 keV. The rather high beam energy was selected because the accuracy of the quench ratio method (Oh 70) for determining the beam polarization is at present uncertain at very low beam energies. The previously mentioned finite geometry computer code was modified to unfold the energy dependence of the analyzing powers from the thick geometry and wide energy distributions.

Experimental data were collected in two phases. The first phase consisted of measuring the analyzing powers for the four detectors located near the center-of-mass scattering angle of  $54.7^\circ$  for which the effective analyzing power,  $A_{zz}$ , is approximately 0. For this phase, the quantization axis,  $\hat{S}$ , was placed at an angle ( $\beta$ ) of  $54.7^\circ$  with respect to  $\vec{k}_{in}$  (for which  $p_{zz} = 0$ ). Hence, even with thick geometry and possible small  $\beta$  misalignment,  $p_{zz}A_{zz}$  was considered small enough to be omitted from the cross section expression. At each incident deuteron bombarding energy, three runs were taken ( $m_I = 1$ ,

0, and -1), thereby generating fifteen numbers. Because the zero degree detector yield is independent of all of the analyzing tensors except  $A_{zz}$ , and since  $p_{zz}$  was chosen to be zero, the three yields obtained for this detector were polarization independent. This served as a check on the accuracy of the monitor detector. The indication was that the monitor detector was good to within 1% for the data as a whole. Also, as was pointed out in Chapter II, the sum of the yields in the four  $54.7^\circ$  detectors is nearly polarization independent (neglecting small differences in solid angle, detector efficiencies, and the like). As will be discussed in Chapter V, this feature is, in principle, important during the excitation function part of the polarization transfer data collection procedure.

For the operating conditions described above, one can write expressions for the yield in each detector for each of the three runs, in terms of the quenched fractions,  $p_i$  ( $i = 1, 0, -1$ ):

$$Y_{L,1} = n_1 N t \epsilon_L \Omega_L I_0 \left[ 1 + \sqrt{\frac{3}{2}} p_1 A_y - \frac{1}{6} p_1 (A_{xx} - A_{yy}) \right]$$

$$Y_{L,0} = n_0 N t \epsilon_L \Omega_L I_0 \left[ 1 + 0.012 \sqrt{\frac{3}{2}} p_0 A_y + (1.966) \left(\frac{1}{6}\right) p_0 (A_{xx} - A_{yy}) \right]$$

$$Y_{L,-1} = n_{-1} N t \epsilon_L \Omega_L I_0 \left[ 1 - \sqrt{\frac{3}{2}} p_{-1} A_y - \frac{1}{6} p_{-1} (A_{xx} - A_{yy}) \right]$$

$$Y_{R,1} = n_1 N t \epsilon_R \Omega_R I_0 \left[ 1 - \sqrt{\frac{3}{2}} p_1 A_y - \frac{1}{6} p_1 (A_{xx} - A_{yy}) \right]$$

$$\begin{aligned}
Y_{R,0} &= n_0 N t \epsilon_R \Omega_R I_0 \left[ 1 - 0.012 \sqrt{\frac{3}{2}} p_0 A_y + (1.966) \left(\frac{1}{6}\right) p_0 (A_{xx} - A_{yy}) \right] \\
Y_{R,-1} &= n_{-1} N t \epsilon_R \Omega_R I_0 \left[ 1 + \sqrt{\frac{3}{2}} p_{-1} A_y - \frac{1}{6} p_{-1} (A_{xx} - A_{yy}) \right] \\
Y_{U,1} &= n_1 N t \epsilon_U \Omega_U I_0 \left[ 1 - \frac{\sqrt{2}}{3} p_1 A_{xz} + \frac{1}{6} p_1 (A_{xx} - A_{yy}) \right] \\
Y_{U,0} &= n_0 N t \epsilon_U \Omega_U I_0 \left[ 1 - (1.966) \left(\frac{\sqrt{2}}{3}\right) p_0 A_{xz} \right. \\
&\quad \left. - (1.966) \left(\frac{1}{6}\right) (A_{xx} - A_{yy}) \right] \\
Y_{U,-1} &= n_{-1} N t \epsilon_U \Omega_U I_0 \left[ 1 + \frac{\sqrt{2}}{3} p_{-1} A_{xz} + \frac{1}{6} p_{-1} (A_{xx} - A_{yy}) \right] \\
Y_{D,1} &= n_1 N t \epsilon_D \Omega_D I_0 \left[ 1 - \frac{\sqrt{2}}{3} p_1 A_{xz} + \frac{1}{6} p_1 (A_{xx} - A_{yy}) \right] \\
Y_{D,0} &= n_0 N t \epsilon_D \Omega_D I_0 \left[ 1 + 1.966 \frac{\sqrt{2}}{3} p_0 A_{xz} - (1.966) \left(\frac{1}{6}\right) p_0 (A_{xx} - A_{yy}) \right] \\
Y_{D,-1} &= n_{-1} N t \epsilon_D \Omega_D I_0 \left[ 1 - \frac{\sqrt{2}}{3} p_{-1} A_{xz} + \frac{1}{6} p_{-1} (A_{xx} - A_{yy}) \right] \\
Y_{O,1} &= n_1 N t \epsilon_O \Omega_O I_0 \\
Y_{O,0} &= n_0 N t \epsilon_O \Omega_O I_0 \\
Y_{O,-1} &= n_{-1} N t \epsilon_O \Omega_O I_0 .
\end{aligned} \tag{4-4}$$

The quantities  $n_i$  are proportional to the amount of charge delivered in each of the three runs. The product  $Nt$  characterizes the density and effective thickness of the  ${}^3\text{He}$  cell.  $\epsilon_j$  is the efficiency of the  $j^{\text{th}}$  telescope and is dependent on the setting of mass and energy windows as discussed in Chapter II, while  $\Omega_j$  is the solid angle subtended by the  $j^{\text{th}}$  telescope.  $I_0$  is the unpolarized

differential cross section. L, R, U, D, and O refer to the left, right, up, down, and  $O^0$  detectors, respectively. Allowance has been made for variations in the quenchable fraction from run to run. Note that the quantity  $0.012 \times p_0 \sqrt{3/2} A_y$  is quite small for the present application ( $A_y \sim 0.01$  and  $p_0 \sim 0.8$ ) and so can be deleted from the  $m_{\perp} = 0$  yield expressions for the left and right detectors.

Given the various yields in the detectors, the problem was to extract the effective analyzing powers in such a way as to be independent of solid angle, detector efficiencies, and the like, while making other possible errors (e.g., current integration, beam steering, etc.) self-compensating as much as possible. To do this, each of the three yield expressions for a given detector was multiplied by an appropriate factor, such that when the three were summed, the result was independent of analyzing power effects (assuming  $n_{\perp} = n_0 = n_{-\perp}$ ). An unpolarized run was thus "constructed" from the three polarized runs for each detector thereby generating five "unpolarized" yields. Each polarized yield was then divided by the "unpolarized" yield for that detector, thereby generating fifteen ratios independent of solid angle, detector efficiency, unpolarized cross sections, and target parameters. The fifteen ratios obtained are given by Eq. (4-5).

$$\begin{aligned}
R_{L,1} &= 1 + \sqrt{\frac{3}{2}} p_1 A_y - \frac{1}{6} p_1 (A_{xx} - A_{yy}) \\
R_{L,0} &= 1 + (1.966) \left(\frac{1}{6}\right) p_0 (A_{xx} - A_{yy}) \\
R_{L,-1} &= 1 - \sqrt{\frac{3}{2}} p_{-1} A_y - \frac{1}{6} p_{-1} (A_{xx} - A_{yy}) \\
R_{R,1} &= 1 - \sqrt{\frac{3}{2}} p_1 A_y - \frac{1}{6} p_1 (A_{xx} - A_{yy}) \\
R_{R,0} &= 1 + (1.966) \left(\frac{1}{6}\right) p_0 (A_{xx} - A_{yy}) \\
R_{R,-1} &= 1 + \sqrt{\frac{3}{2}} p_{-1} A_y - \frac{1}{6} p_{-1} (A_{xx} - A_{yy}) \\
R_{U,1} &= 1 + \frac{\sqrt{2}}{3} p_1 A_{xz} + \frac{1}{6} p_1 (A_{xx} - A_{yy}) \\
R_{U,0} &= 1 - (1.966) \left(\frac{\sqrt{2}}{3}\right) p_0 A_{xz} - (1.966) \left(\frac{1}{6}\right) p_0 (A_{xx} - A_{yy}) \\
R_{U,-1} &= 1 + \frac{\sqrt{2}}{3} p_{-1} A_{xz} + \frac{1}{6} p_{-1} (A_{xx} - A_{yy}) \\
R_{D,1} &= 1 - \frac{\sqrt{2}}{3} p_1 A_{xz} + \frac{1}{6} p_1 (A_{xx} - A_{yy}) \\
R_{D,0} &= 1 + (1.966) \left(\frac{\sqrt{2}}{3}\right) p_0 A_{xz} - (1.966) \left(\frac{1}{6}\right) p_0 (A_{xx} - A_{yy}) \\
R_{D,-1} &= 1 - \frac{\sqrt{2}}{3} p_{-1} A_{xz} + \frac{1}{6} p_{-1} (A_{xx} - A_{yy}) \\
R_{O,1} &= R_{O,0} = R_{O,-1} = 1 .
\end{aligned} \tag{4-5}$$

It was these ratios (in terms of actual yields and quenchable fraction values) that were considered to be the experimentally observed quantities; that is, it was these ratios that the finite geometry code was required to reproduce. Appropriate linear combinations of these ratios were then sufficient to determine the effective

analyzing powers. A computer code, ANALYZ, was written to calculate the ratios and their errors, and to extract the analyzing powers. Dead time corrections were not needed as both the intensity monitor detector and the detectors in the array were "dead" simultaneously because both utilized the same electronics system (see Chapter II for details). The statistical errors were calculated numerically by the code.

The second phase of data collection consisted of measuring the analyzing power,  $A_{ZZ}$ , for the zero degree detector. For this phase, the quantization axis,  $\hat{S}$ , was placed along  $\vec{k}_{in}$  ( $\beta = 0^\circ$ ). In this configuration the cross section expression given by Eq. (4-2) reduces to

$$I(0^\circ) = I_0(0^\circ) \left(1 + \frac{1}{2} p_{ZZ} A_{ZZ}(0^\circ)\right) .$$

At each incident deuteron energy, two runs were taken ( $m_I = 1$  and  $m_I = 0$ ). In terms of the quenchable fractions,  $p_i$  ( $i = 1, 0$ ), expressions for the two yields in the zero degree detector can be written:

$$\begin{aligned} Y_1 &= n_1 N t \epsilon \Omega I_0 \left[1 + \frac{1}{2} p_1 A_{ZZ}\right] \\ Y_0 &= n_0 N t \epsilon \Omega I_0 \left[1 - (1.966) \left(\frac{1}{2}\right) p_0 A_{ZZ}\right] , \end{aligned} \quad (4-7)$$

where the quantities  $n$ ,  $N$ ,  $t$ ,  $\epsilon$ ,  $\Omega$ , and  $I_0$  are the same as in Eq. (4-4) with the detector-identifying subscript having been dropped. If one defines the ratio,  $R = Y_1/Y_0$

and again assumes  $n_1 = n_0$ , then

$$A_{zz} = \frac{2(R-1)}{p_1 + 1.966Rp_0} .$$

A computer code, AZZA, was written to calculate the ratio and its error, and extract  $A_{zz}$ .

### C. Determination of Average Deuteron Interaction Energy

In order to obtain the energy dependence of the analyzing powers it was necessary to determine the average deuteron interaction energy at each bombarding energy. This required a knowledge of the shape of the various energy distributions of deuterons entering the  ${}^3\text{He}$  cell for each incident deuteron machine energy, the shape of the unpolarized cross section function  $[\sigma(E)$  for  ${}^3\text{He}(d,p){}^4\text{He}]$ , the specific energy loss of deuterons in helium, and the details of the target and detector assembly. One version of the finite geometry code, YIELD, then utilized this information to calculate the average interaction energies.

The shape of the unpolarized cross section function was obtained from the  $86^\circ$  data of Yarnell (Ya 53). Specific energy loss data for deuterons in helium were obtained from Whaling (Wh 58). The first attempt at obtaining deuteron energy distributions by repeated use of a LASL code, STRAGGL, which was designed for small

energy losses ( $\Delta E \lesssim 0.2E$ ), did not prove satisfactory, presumably because of the large energy losses prevailing. Satisfactory estimates of the deuteron energy distributions at the  $^3\text{He}$  cell entrance for each incident energy were obtained from the proton range, energy, and straggle tables of Janni (Ja 66) by first converting the tables to correspond to deuterons, and then using a residual range look-up scheme utilizing numerical techniques.

The tables were converted under the following assumptions:

- 1) The range of a deuteron of energy  $E$  is twice the range of a proton of energy  $E/2$  (Se 65).
- 2) The specific energy loss of a deuteron of energy  $E$  is equal to the specific energy loss of a proton of half the energy (Se 65).
- 3) The standard deviation of range straggling for deuterons of energy  $E$  is equal to the standard deviation of range straggling for protons of half the energy (Se 65).
- 4) The stopping power of a compound (in this case Havar which is composed of nine elements) is the weighted sum of the stopping powers of the individual constituents acting independently (Th 52, Re 53).

That is

$$\frac{dE}{dx}|_{\text{Havar}} = \sum_{i=1}^9 W_i \left(\frac{dE}{dx}\right)_i .$$

Using  $\left(\frac{dE}{dx}\right)_i = \frac{k_i}{E} \ln \alpha E$  (Se 65), it follows that

$$\frac{1}{\text{Range}_{\text{Havar}}} = \sum_{i=1}^9 \frac{W_i}{\text{Range}_i} ,$$

where  $k_i$  and  $\alpha$  are constants and where  $W_i$  is the weight fraction of the stopping material which is composed of the element  $i$ .

Also,  $\sigma_{\text{Havar}} = \left(\sum_{i=1}^9 W_i \sigma_i^2\right)^{\frac{1}{2}}$  (Ja 66), where  $\sigma$  represents the standard deviation of the energy distribution (assumed to be gaussian for our purposes). YIELD then used these energy distributions to calculate the proton yield in the zero degree detector for various incident deuteron energies. The characteristics of the "excitation" curve thus obtained are:

- 1) Zero yield for machine energies below some threshold required to penetrate the degrading foils.
- 2) Rapidly increasing yield with increasing machine energy as more and more deuterons enter the  $^3\text{He}$  cell with sufficient energy so as to pass through the 430-keV resonance within the cell.
- 3) A peak yield at a machine energy which produces the most deuterons within the  $^3\text{He}$  cell which pass through the resonance.

- 4) A decrease in yield for higher machine energies due to an increasing number of deuterons penetrating the  $^3\text{He}$  cell without having slowed through the resonance.

YIELD was written in terms of particle rays (polarized or unpolarized) entering the  $^3\text{He}$  cell and slowing within the cell until stoppage or penetration resulted. Each incremental path length within the  $^3\text{He}$  cell contributed to the proton yield in the detector. Incremental path lengths were determined on the basis of equal energy loss increments. Energy increments of 25 keV were finally chosen as larger increments produced a nonsmooth yield curve for machine energies above that corresponding to the peak yield. The code integrated numerically over (1) the incident deuteron energy distribution, (2) the irradiated volume of the  $^3\text{He}$  cell, and (3) the area of the detector. Although a capability for integrating over the area of the  $^3\text{He}$  cell entrance was provided in the code, that capability was not needed in this case. It was necessary to convert the c.m. cross section at each energy and angle to the corresponding laboratory cross section.

The "excitation function" thus obtained (normalized to the peak yield) is plotted in Fig. 13 as the solid curve. The points are the experimentally observed "unpolarized" yields in the zero degree detector. (This curve is corrected for the (Coulomb) energy dependence of the monitor detector which was used in lieu of a current

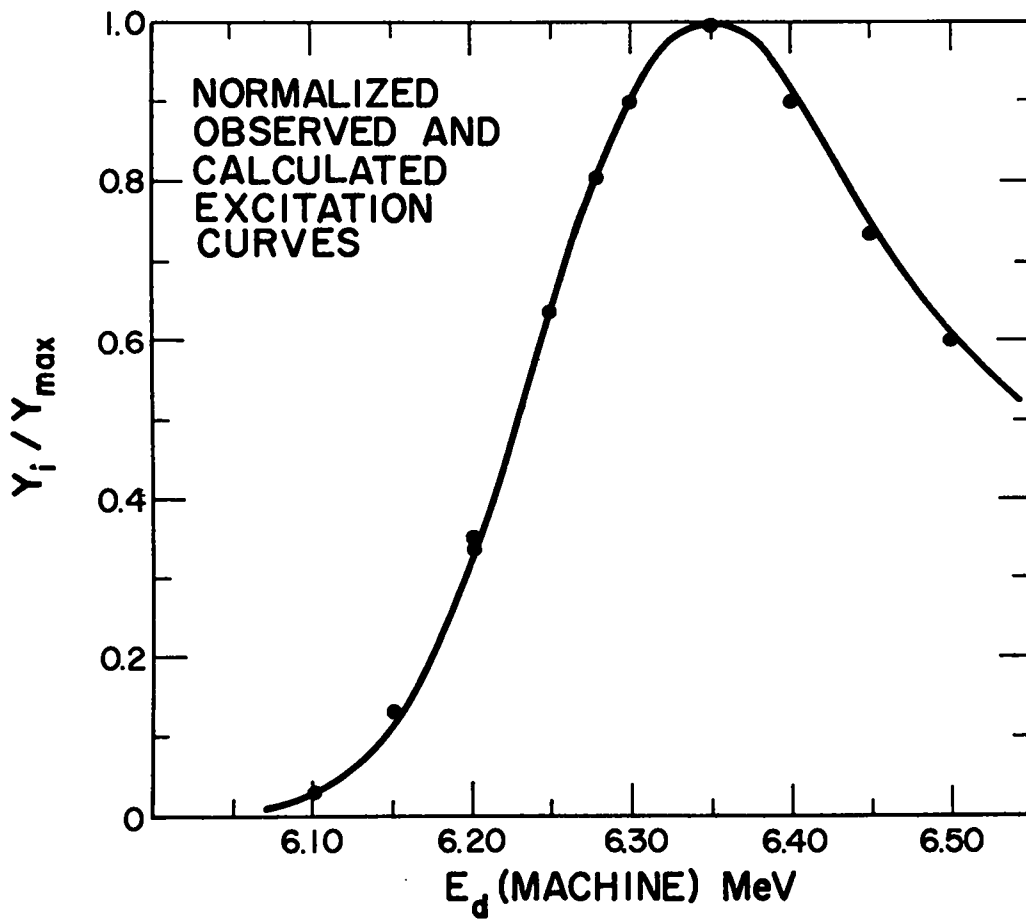


Fig. 13. Excitation Function for  ${}^3\text{He}(\vec{d}, p){}^4\text{He}$  Calibration.

integrator.) Again, the experimental points have been normalized to their peak yield. A shift of the calculated curve by 210 keV toward lower energies was required for best agreement between the experimental excitation function and the calculated excitation function, as illustrated in Fig. 13. This overall shift was considered acceptable in view of a lack of accurate knowledge of the degrading foil thickness and possible inaccuracies in the straggling parameter proton-to-deuteron data mapping function at the low energies involved. After having made the 210-keV shift it was noted that no single experimental point was farther than 10 keV from the calculated curve. This gave us confidence in the calculated average interaction energies for each incident energy. Figure 14 is a plot of average interaction energy vs machine energy and can be used to give estimates of the uncertainty in the average interaction energy which results from lack of a precise fit of the observed to the calculated excitation functions. That is, a small uncertainty in machine energy (e.g., 10 keV) about some initial energy projects an uncertainty in average deuteron interaction energy which depends on the initial machine energy. Figure 15 shows some of the deuteron energy distributions obtained from the residual range lookup scheme after having allowed for the required 210-keV shift in machine energy. The

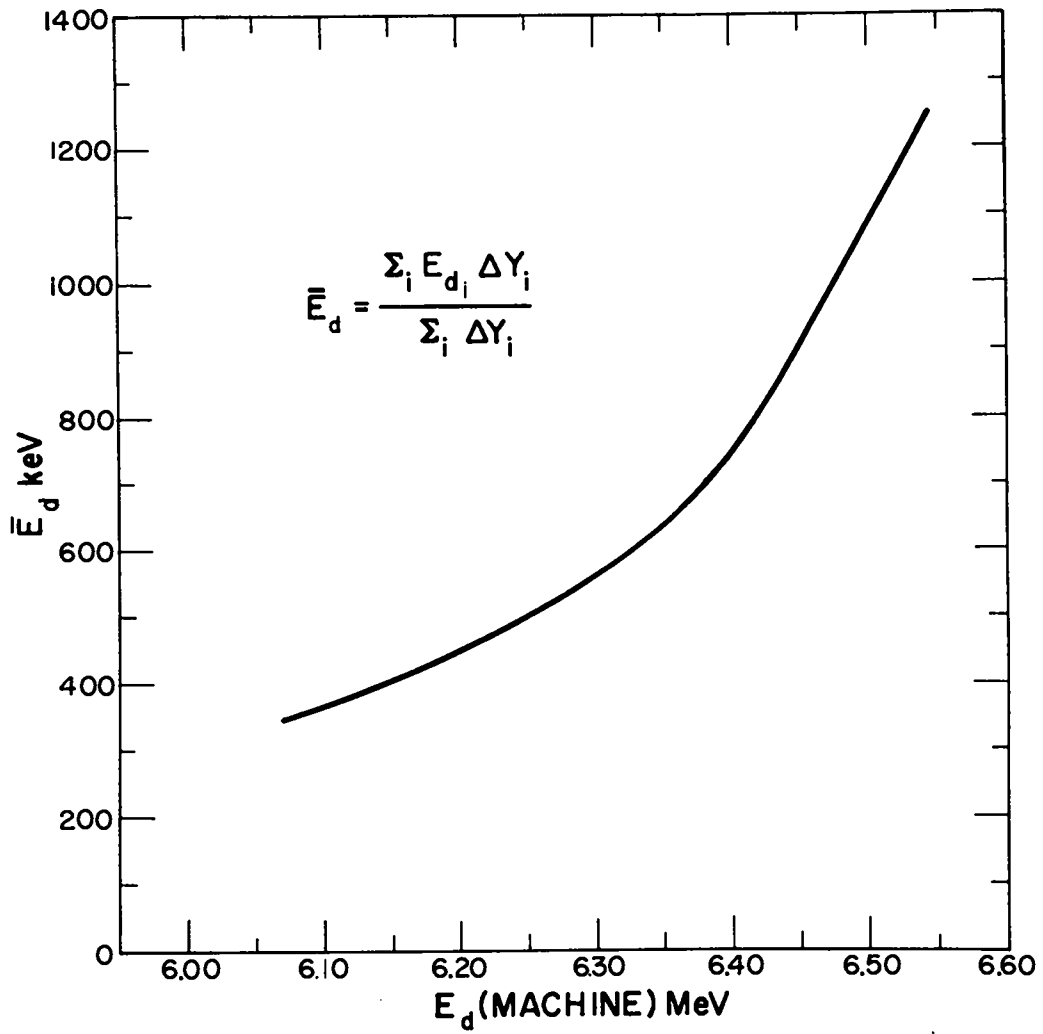


Fig. 14. Average Deuteron Interaction Energy as a Function of Machine Energy.

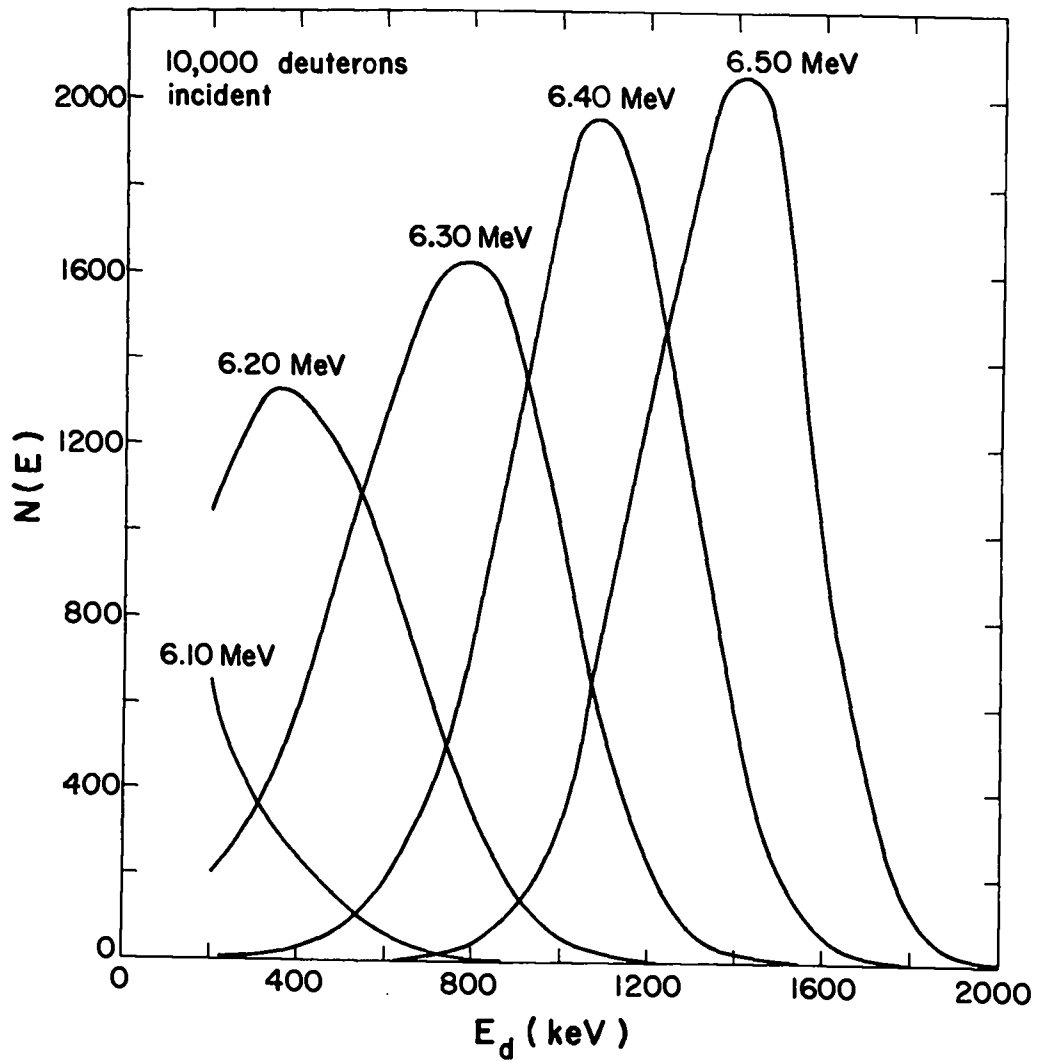


Fig. 15. Deuteron Energy Distributions Entering the  $^3\text{He}$  Cell at the Respective Machine Energy.

energy dependence of the analyzing powers for thick geometry was thus established.

#### D. Unfolding Analyzing Powers from Thick Geometry

The (uncorrected) thick geometry analyzing powers showed that  $\kappa$  in Eq. (4-1) is different for each of the three tensor analyzing powers. Thus, for the unfolding process, a generalization of Eq. (4-1) with  $\kappa$  a different function of energy for each of the analyzing tensors was assumed to hold; that is,  $A_{ij} = \kappa_{ij}(E)F(\theta)$ .  $\kappa_{ij}(E)$  was represented by a third-order power series. It should be noted that the only assumption made in this procedure is that the angular dependence of the analyzing powers in the regions near  $54.7^\circ$  and near  $0^\circ$  are given correctly by Eq. (4-1).

The procedure involved an iterative process in which the  $\kappa_{ij}(E)$  obtained from the thick geometry analyzing powers were fitted by the power series. An appropriate version of YIELD was then used to (1) calculate the various detector yields (i.e., simulated runs for  $m_I = 1, 0, -1$ ), (2) calculate ratios corresponding to those in Eq. (4-5), and (3) on the basis of the difference between the calculated and experimental ratios, determine new  $\kappa_{ij}(E_\ell)$  for the  $\ell$  data points. The new  $\kappa_{ij}(E_\ell)$  thus obtained were again fitted by the power series and the process repeated until no further improvement in fit

was noted. One version of YIELD was used for the 54.7° data. A similar version was used to unfold  $A_{zz}$  at 0°. An important feature of the code, which helped to reduce the amount of computation time required, was the use of vector dot and cross products to determine the required sines and cosines of the angles which are involved in the computation of the incremental yields for a polarized beam. A later version of YIELD is listed in Appendix C.

#### E. Results

Analyzing powers measured in thick geometry are presented in Table 12. The errors shown are purely statistical. Estimates of average interaction energy uncertainties range from 5% at 366 keV up to 7% at 1090 keV. These estimates are based on (1) the previous mentioned failure to calculate exactly the observed excitation function (see Fig. 13), and (2) a 10-keV shift in the peak of the excitation function resulting from a 2-psi uncertainty in the  $^3\text{He}$  cell pressure and a 3% uncertainty in the stopping cross section data for deuterons in helium.

Table 13 shows the analyzing powers obtained through the unfolding process. Third-order fits to the  $\kappa$ 's are given by  $\kappa_{ij} = a_0 + a_1 E + a_2 E^2 + a_3 E^3$ , where the expansion coefficients are

TABLE 12

Measured  ${}^3\text{He}(\vec{d},p){}^4\text{He}$  Analyzing Powers in Thick Geometry

(errors are statistical only)

$E_d$ (machine) (MeV)	$\bar{E}_d$ (keV)	$\bar{A}_y$	$\bar{A}_{xz}$	$\frac{1}{2}(A_{xx} - A_{yy})$	$\bar{A}_{zz} (0^\circ)$
6.10	366	0.010±0.020	-0.640±0.032	-0.484±0.030	
6.15	404	-0.005±0.007	-0.645±0.011	-0.456±0.010	-0.925±0.012
6.20	445	-0.001±0.004	-0.639±0.007	-0.438±0.006	-0.920±0.008
6.25	493	0.013±0.003	-0.617±0.005	-0.434±0.005	-0.900±0.006
6.28	527	0.007±0.003	-0.601±0.004	-0.432±0.004	-0.883±0.007
6.30	554	0.008±0.003	-0.602±0.004	-0.410±0.004	-0.882±0.007
6.35	636	0.014±0.002	-0.588±0.004	-0.403±0.004	-0.840±0.006
6.40	752	0.018±0.002	-0.548±0.004	-0.353±0.004	-0.802±0.006
6.45	915	0.020±0.003	-0.537±0.004	-0.292±0.004	-0.778±0.008
6.50	1090	0.038±0.003	-0.508±0.005	-0.220±0.005	-0.736±0.008

TABLE 13 .

Finite Geometry Corrected  ${}^3\text{He}(\vec{d},p){}^4\text{He}$  Analyzing Powers (errors include counting statistics, errors due to current integration, and errors due to beam polarization).

$E_d$ (Machine) (MeV)	$E_d$ (keV)	$A_y(54.7^\circ)$	$A_{xz}(54.7^\circ)$	$\frac{1}{2}(A_{xx} - A_{yy})$	$A_{zz}(0^\circ)$
6.10	366	0.004±0.020	-0.641±0.035	-0.472±0.032	
6.15	404	0.004±0.007	-0.637±0.017	-0.464±0.014	-0.933±0.024
6.20	445	0.005±0.004	-0.633±0.015	-0.455±0.011	-0.924±0.022
6.25	493	0.006±0.003	-0.628±0.014	-0.442±0.010	-0.912±0.021
6.28	527	0.006±0.003	-0.625±0.013	-0.433±0.010	-0.903±0.021
6.30	554	0.007±0.003	-0.622±0.013	-0.425±0.009	-0.896±0.021
6.35	636	0.008±0.002	-0.613±0.013	-0.397±0.009	-0.871±0.020
6.40	752	0.012±0.002	-0.598±0.012	-0.353±0.008	-0.833±0.019
6.45	915	0.019±0.003	-0.574±0.012	-0.284±0.007	-0.778±0.019
6.50	1090	0.031±0.003	-0.543±0.012	-0.204±0.007	-0.724±0.018

	$a_0$	$a_1$	$a_2$	$a_3$
$\kappa_y$	$-1.3410 \times 10^{-5}$	$2.5735 \times 10^{-5}$	$-4.5149 \times 10^{-8}$	$4.2892 \times 10^{-11}$
$\kappa_{xz}$	0.9520	$-1.2583 \times 10^{-4}$	$2.0619 \times 10^{-8}$	$-5.4884 \times 10^{-11}$
$\kappa_{xx} - \kappa_{yy}$	0.9522	$3.6262 \times 10^{-4}$	$-1.1962 \times 10^{-6}$	$3.7247 \times 10^{-10}$
$\kappa_{zz}$	0.9523	$1.5935 \times 10^{-4}$	$-6.1191 \times 10^{-7}$	$2.5120 \times 10^{-10}$

with E in keV. The analyzing powers given in the table were thus calculated by first calculating the appropriate  $\kappa$  to be used in Eq. (4-1). The errors listed include statistical errors, errors due to a 1% fluctuation in current integration from run to run, and errors due to a 2% (G. G. Ohlsen, private communication) uncertainty in beam polarization for the operating conditions used, combined in quadrature. Corrections were generally less than 0.02 and in no case greater than 0.035. A plot of the finite geometry corrected analyzing powers (before final fit) is shown in Fig. 16 (dots). Also shown in Fig. 16 are the measurements of Leemann et al. (Le 71) (triangles) and of Forssmann et al. (Fo 71) (squares). Agreement is good except for the  $A_{xz}$  measurement of Leemann et al.

The experimental results in terms of the ratios of the s wave,  $j = 3/2^+$  predictions are summarized in Fig. 17. Values of  $\kappa$  other than 1 is indicative of a  $j = 1/2^+$  contribution while the rapid decrease of  $\kappa_{xx} - \kappa_{yy}$  relative

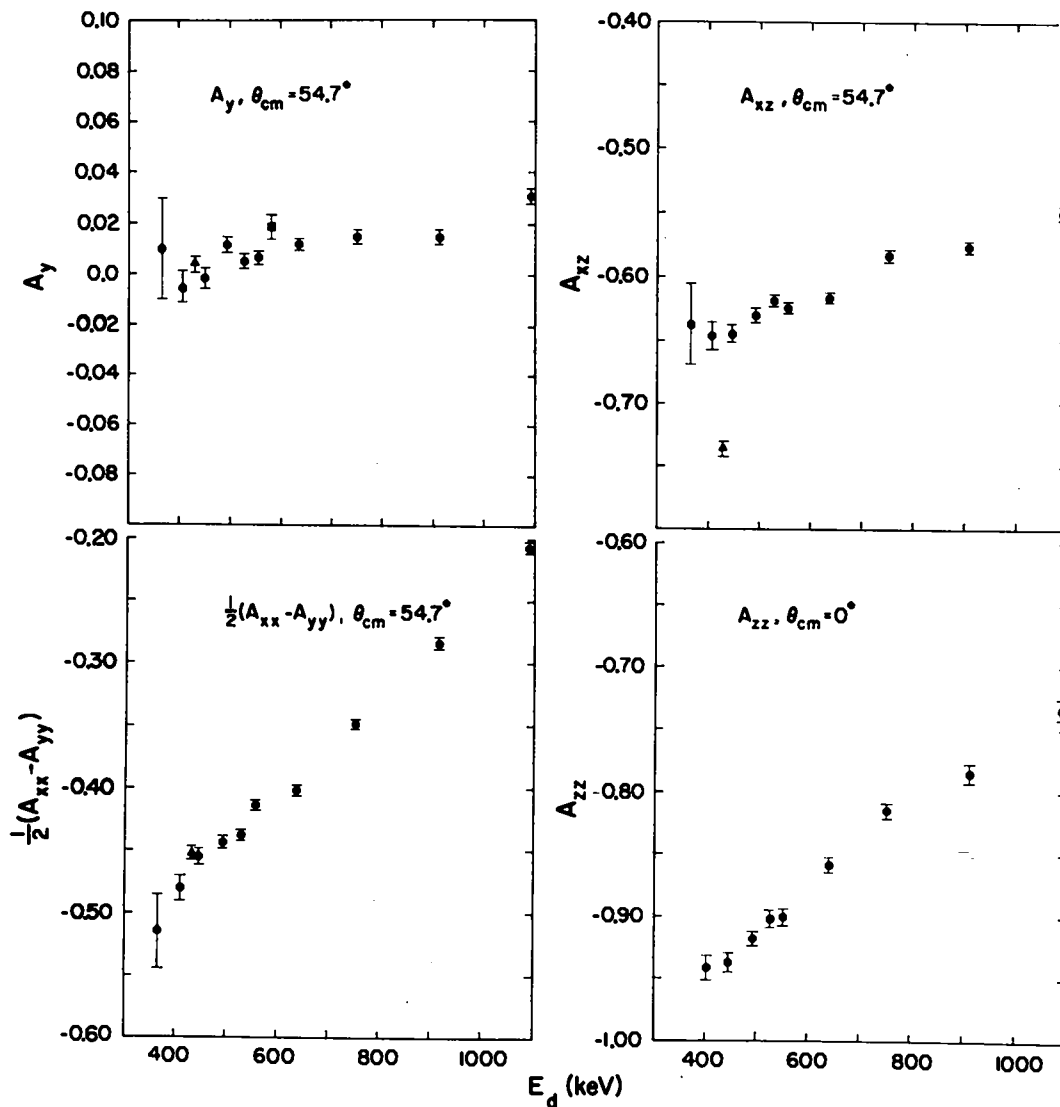


Fig. 16. Corrected  ${}^3\text{He}(\vec{d}, p){}^4\text{He}$  Analyzing Powers at the Indicated Angle and as a Function of Energy. Errors Shown are Purely Statistical. Triangles are measurements of Leemann et al. Squares are measurements of Forssmann et al.

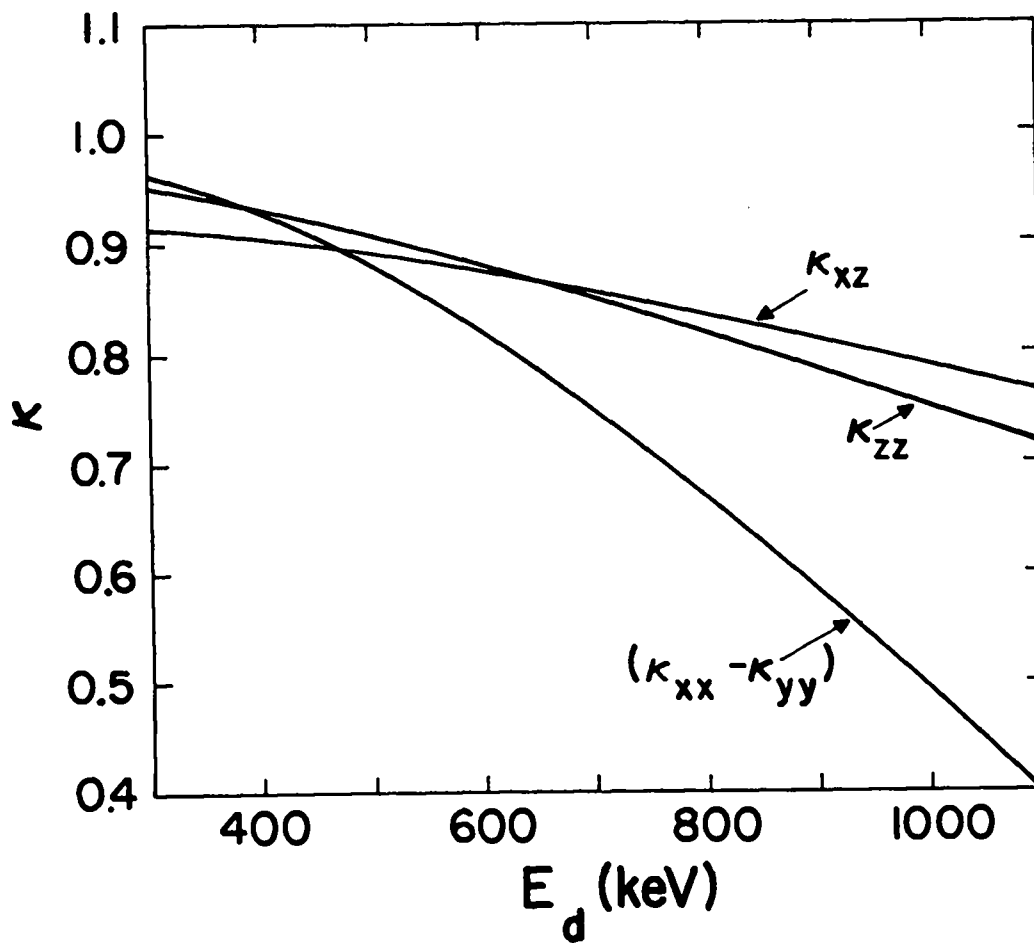


Fig. 17. Ratios of Observed Analyzing Powers to Values Which would Obtain if the Reaction Proceeded Completely through a  $j = 3/2^+$  Compound State.

to  $\kappa_{xz}$  and  $\kappa_{zz}$  above the 430-keV resonance confirms that partial waves higher than s waves contribute appreciably in this energy region.

For use of the  ${}^3\text{He}(\vec{d}, p){}^4\text{He}$  reaction as a deuteron tensor polarization analyzer, an "excitation" curve was obtained for each experimental situation by varying the machine energy. A machine energy corresponding to 80% of the peak yield was then chosen at which to measure polarization transfer. For these conditions, the vector analyzing power was less than 0.01. As will be seen in Chapter V, negligible vector analyzing power is a desirable characteristic for the measurement of second-rank deuteron polarizations.

## CHAPTER V

### MEASUREMENT OF PROTON-DEUTERON POLARIZATION TRANSFER

#### A. Experimental Data Collection Procedure

##### 1. Experimental arrangement

The experimental arrangement is shown schematically in Fig. 18. Although the apparatus was designed to measure the second-rank polarization components of recoil deuterons, one measurement of the outgoing vector component,  $p_x$ , was made at a laboratory angle of  $22\frac{1}{2}^\circ$  and the transfer coefficient  $K_x^{X'}$  was extracted.

A 50-150 nanoampere beam of  $\sim 90\%$  polarized protons was used to bombard the 6.4-mm diameter liquid nitrogen cooled  $D_2$  target cell operating at a pressure of 6.2 atm. The quantization axis,  $\hat{S}$ , of the polarized beam was chosen along one of the reaction initial (x,y,z) axes in order to obtain an incident beam with the desired maximum component of vector polarization,  $p_x$ ,  $p_y$ , or  $p_z$ . In practice, the beam quantization axis was aligned along the -x axis instead of the +x axis for the various measurements involving this component of incident beam polarization. The -x axis was used because the LASL spin precession and beam transport system makes this direction experimentally more convenient than the +x direction.

Recoil deuterons were slowed by Havar window foils and a suitable thickness of aluminum foil to  $\sim 700$  keV

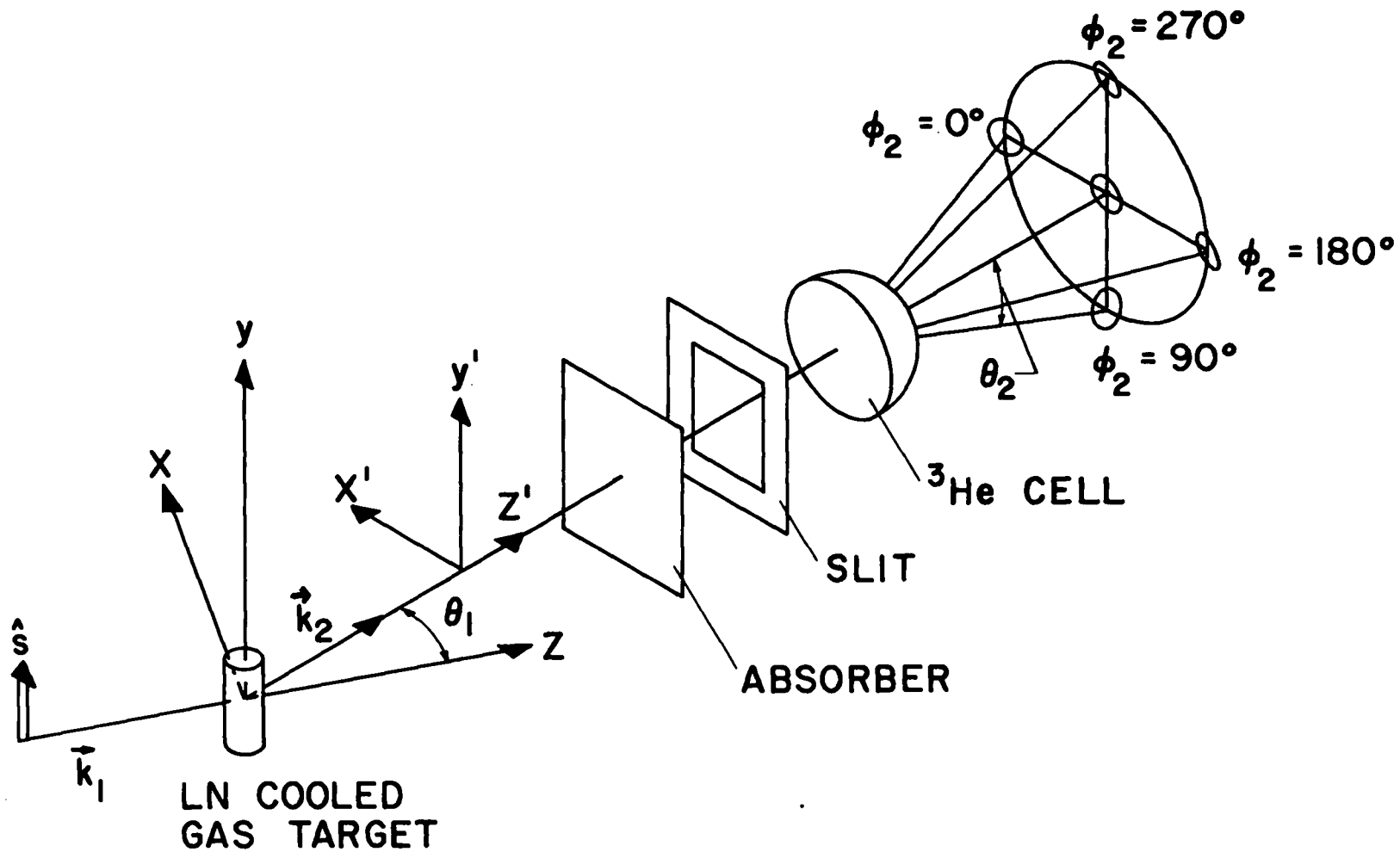


Fig. 18. Experimental Arrangement for  $D(\vec{p}, \vec{d})H$  Polarization Transfer.

(corresponding to a mean interaction energy of  $\sim 530$  keV) before entering the 2.54-cm diameter  $^3\text{He}$  cell where the  $^3\text{He}(\vec{d}, p)^4\text{He}$  reaction was used to determine deuteron tensor polarization. Counting rates were typically 100 to 1000 counts per hour per detector.

Under similar operating conditions the vector analyzing power has been shown (Chapter IV) to be less than 0.01. The zero degree detector has an effective  $A_{zz}$  of  $-0.883 \pm 0.021$  with the remaining analyzing tensors vanishing. The four detectors at  $54.7^\circ$  (c.m.) were found to have analyzing powers of  $-0.432 \pm 0.010$  and  $-0.601 \pm 0.013$  for  $\frac{1}{2}(A_{xx} - A_{yy})$  and  $A_{xz}$ , respectively, with  $A_{zz}$  estimated to be negligible ( $\lesssim 0.021$ ).

The one measurement of  $p_x$ , was made by removing the aluminum foils, thereby permitting higher energy deuterons to enter the  $^3\text{He}$  cell. At the higher energy, the vector analyzing power is sufficiently large to permit sensing of vector polarization. This measurement will be discussed in more detail later.

Tensor polarization transfer measurements were made at laboratory angles of  $0^\circ$ ,  $22\frac{1}{2}^\circ$ , and  $45^\circ$ . Measurements of tensor polarization made at  $22\frac{1}{2}^\circ$  utilized a polarized-to-unpolarized ratio technique to normalize detector yields in order to eliminate geometrical and target parameters, and current integration effects. Details of this technique will be discussed in a following section.

Measurements at  $0^\circ$  and  $45^\circ$  were also made using ratio techniques, but with polarized beams (spin-up-to-spin-down) only (Sa 73). As the details of this technique are discussed by Salzman et al., only a cursory description will be presented in this thesis.

The polarized-to-unpolarized technique appeared to be desirable in view of the larger ( $\sim 10$  to  $20$  times) unpolarized beam currents available. However, after one primary target failure, beam intensities for the unpolarized runs were limited to  $\sim 400$  nA. In addition to this problem, it became apparent that neutron fluxes were sufficiently high to cause probable detector damage. It was this problem which limited incident beam energies to less than  $\sim 9.5$  MeV and prompted a search for a more efficient method of data acquisition.

This search resulted in the spin-up-to-spin-down method. Computer techniques had to be used to extract transfer coefficients as the algebra is more complex than for the polarized-to-unpolarized method. However, the new method, for our case, resulted in run times of about 60% of those for the polarized-to-unpolarized method in order to achieve a given statistical precision. In addition, only about 20% as much radiation was delivered to the detectors. This method was first checked against measurements made at  $22\frac{1}{2}^\circ$  with the polarized-to-unpolarized

method for computational errors and then used exclusively for the  $0^\circ$  and  $45^\circ$  measurements.

## 2. Selection of machine energy via an excitation function

In order to make tensor polarization transfer measurements under "reproducible" conditions and ensure a negligible vector analyzing power, a procedure for selecting the machine energy was established. This procedure consisted of selecting an aluminum degrading foil of sufficient thickness so as to require an incident machine energy near some desired value. The aluminum foil was then inserted between the scattering chamber and entrance to the  $^3\text{He}$  cell by means of a phenolic foil holder. In view of the finite number of foil combinations available and the sensitivity of the  $^3\text{He}(d,p)^4\text{He}$  reaction near the 430-keV resonance, desired primary target center energies could only approximately be selected in advance.

Using an unpolarized beam, the machine energy was varied in 100 to 200 keV steps and an excitation function obtained from the yields. That machine energy corresponding to a yield which was 80% of the maximum value was then selected at which to obtain transfer data. This criterion resulted in acceptable count rates while restricting the vector analyzing power to less than 0.01.

Figure 19 illustrates a typical excitation function made at  $\theta_1 = 22\frac{1}{2}^\circ$  with  $28.50 \text{ mg/cm}^2$  of aluminum degrading foil. For nominal operating conditions (cell pressures, etc.) as discussed previously, a machine energy of 8.09 MeV corresponded to a target center energy of 7.9 MeV.

When maintaining a slit current balance near the entrance to the deuteron polarization transfer chamber, reproducibility in machine energy selection was typically to within about 10 keV. However, when refilling of the primary target cell was involved as on a week to week basis, reproducibility was typically to within about 60 keV. This difference was believed to be due to a non-reproducibility of target pressure ( $\Delta p \sim 100 \text{ Torr}$ ), beam steering effects, and the large magnification of small energy differences. For this reason, the excitation procedure was always followed just prior to the collection of transfer data.

In view of the smallness of the polarization functions in the reaction  $D(p, d)H$  (see Chapter III) and the sensitivity of the  ${}^3\text{He}(d, p){}^4\text{He}$  reaction to deuteron energy, excitation functions for this experiment were made with the  $0^\circ$  detector moved in close to the  ${}^3\text{He}$  cell in order to expedite that portion of the data collecting procedure. Ordinarily, the yield in the  $0^\circ$  detector depends on  $P^{z'z'}$  which may be large and energy dependent (see Eq. (5-4)). In this event, the sum of the yields in the four

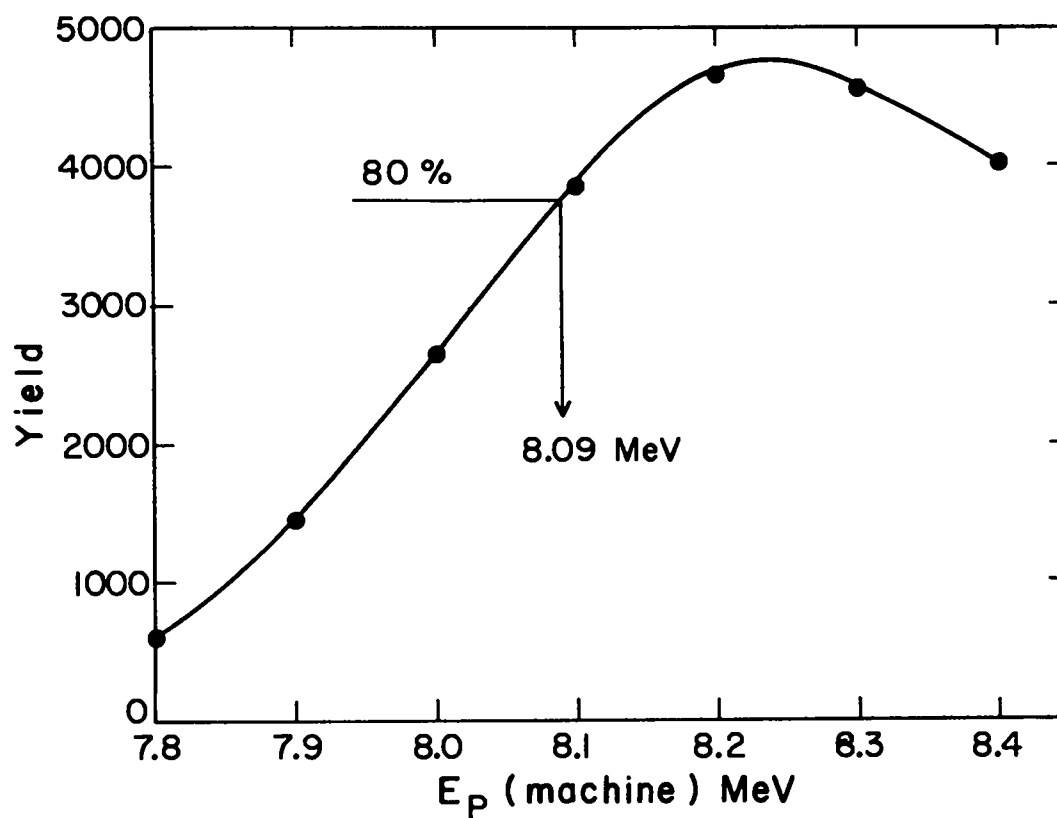


Fig. 19. Typical Excitation Function for D(p,d)H Polarization Transfer.

detectors at a center-of-mass angle near  $54.7^\circ$  should be used for the excitation function as the sum is approximately independent of polarization effects.

### 3. Data collection

The  $0^\circ$  measurements posed a particular problem in that the Faraday cup had to be rotated to a position out of the path of the incident beam thus permitting the beam to pass directly into the  $^3\text{He}$  cell. In order to ensure that the beam could not enter the  $0^\circ$  detector telescope an additional  $30 \text{ mg/cm}^2$  aluminum hemispherical "hat" was placed over the  $^3\text{He}$  cell. This was sufficient to stop beam protons without adversely affecting the high energy ( $\sim 17 \text{ MeV}$ ) reaction [ $^3\text{He}(d,p)^4\text{He}$ ] protons. In addition to this measure, the cryostat-target assembly was electrically insulated from the chamber via a teflon spacer and a LASL made kovar insulating seal soldered into the gas target filling lead. Current produced by secondary electron emission from the target was then monitored by the machine operator in lieu of that normally collected by the Faraday Cup. This was satisfactory as accurate current integration was not a requirement.

Also, the aluminum "hat" was used during the measurement of  $K_X^{X'}$  at  $22\frac{1}{2}^\circ$  at a machine energy of  $9.28 \text{ MeV}$  as the aluminum degrading foil had been removed and it was desirable to ensure that the higher energy deuterons

could not penetrate the  $^3\text{He}$  cell and initiate the reaction  $^{14}\text{N}(\text{d},\text{p})^{15}\text{N}$  although it was likely that for this particular case the two proton groups could have been distinguished.

Figure 20 illustrates typical mass and energy spectra for two of the detectors, L' and  $0^0$ , in the rotated position (Fig. 21b) for  $\theta_1 = 22\frac{1}{2}^\circ$  and at a machine energy of 8.09 MeV. These spectra were obtained with a 700 nA unpolarized incident beam in a time of 90 minutes. Mass spectra show the low energy background and high energy proton peak. Energy spectra for the detectors were determined on the basis of those events occurring within the gates set on their respective mass spectra. These spectra indicate that background did not pose a problem with regard to the collection of data. Hence, background corrections were not made.

It should be noted that the only requirement of the detection system was to identify and count protons from the  $^3\text{He}(\vec{\text{d}},\text{p})^4\text{He}$  reaction. What appears to be a double proton peak in the  $0^0$  detector is a result of a substantial fraction of the high energy protons penetrating the depleted region of the E detector due to an insufficient amount of slowing foil immediately in front of the detector telescope. With the addition of  $30\text{ mg/cm}^2$  more of aluminum the double peak characteristic went away.

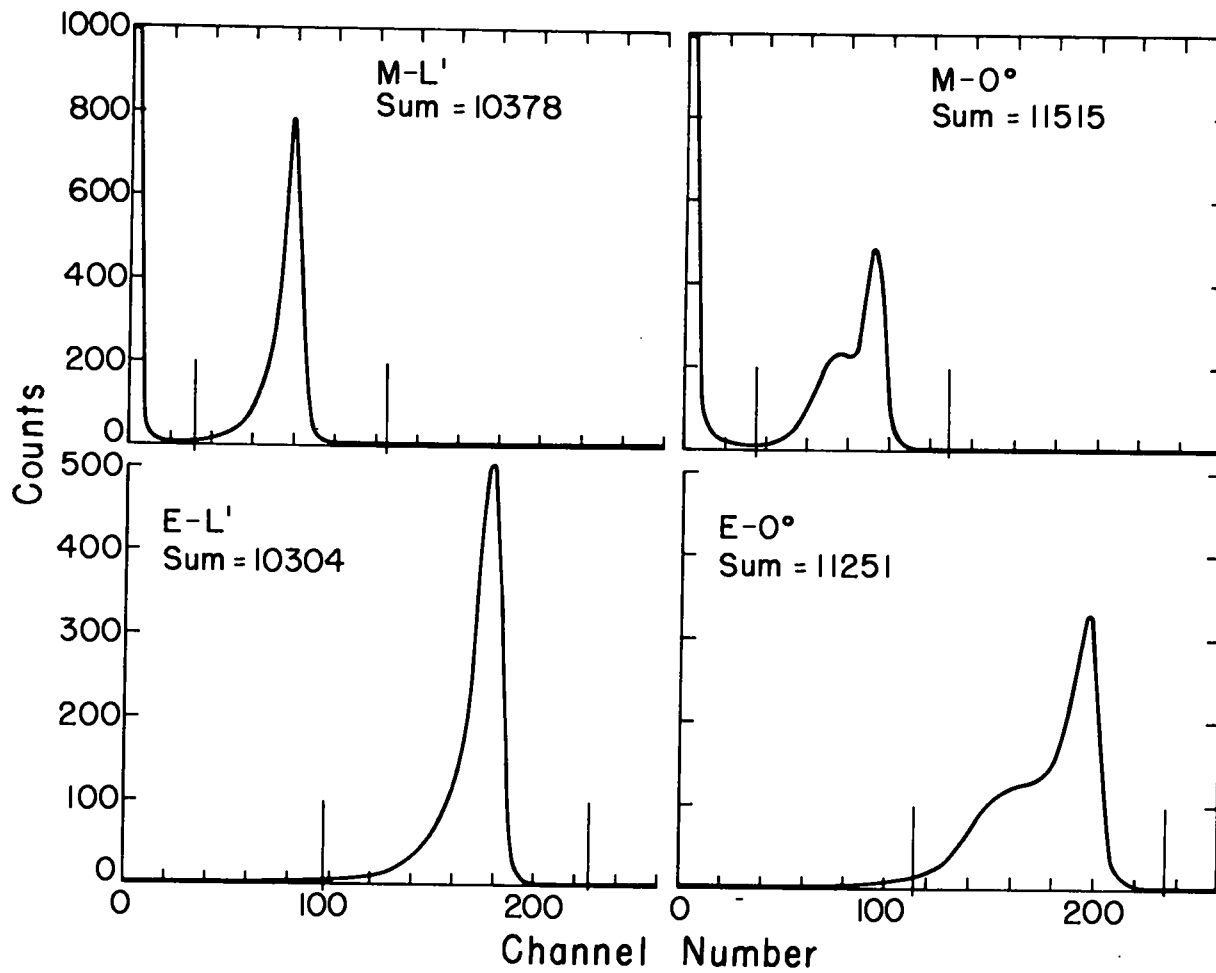


Fig. 20. Typical Mass and Energy Spectra for Unpolarized Run in  $D(p, \vec{d})H$  at 8.09 MeV.

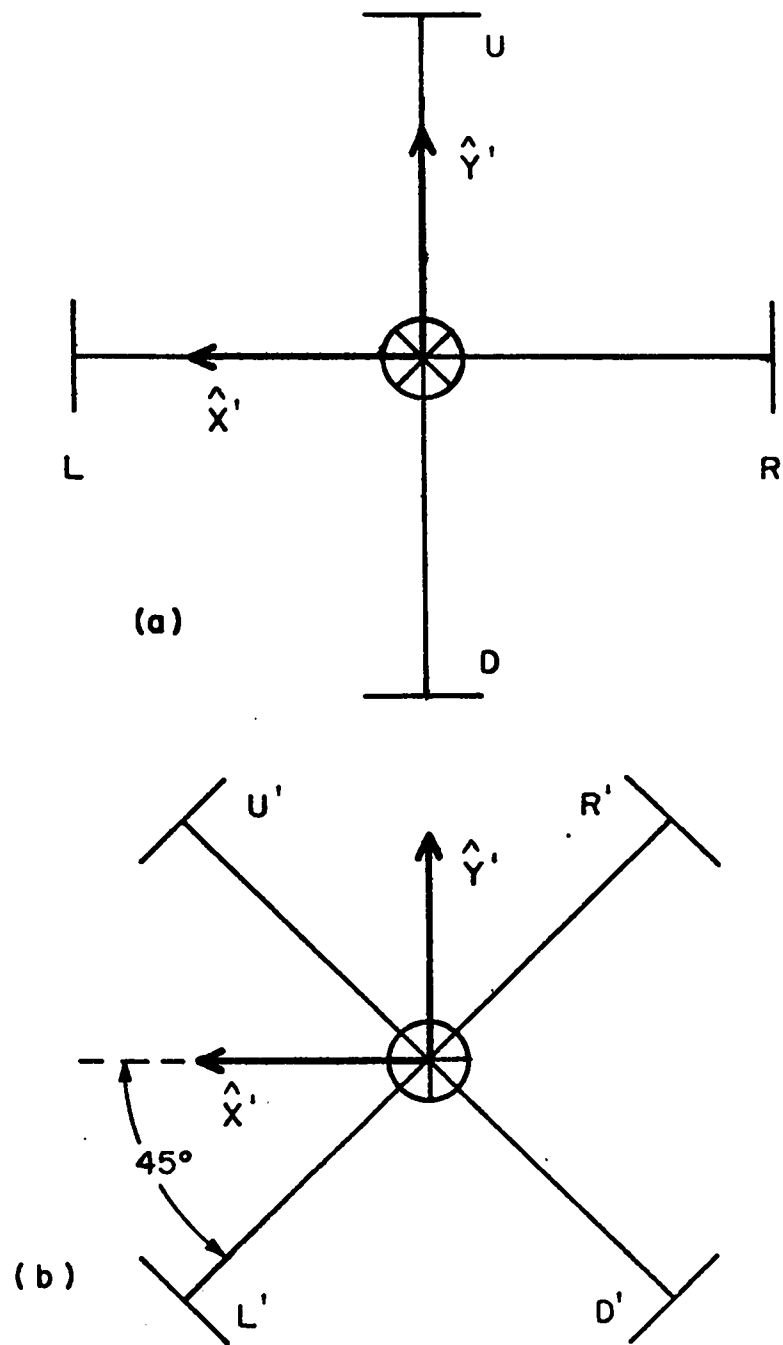


Fig. 21. Detector Orientation with Beam going into the Plane of the Page; a)  $0^\circ$  configuration and b) detector array rotated about  $z'$  axis through  $45^\circ$ .

B. Data Reduction Procedures

Observables for the reaction  $D(\vec{p}, \vec{d})H$  are given by Eq. (1-16). The K's are those quantities ultimately to be measured. Rewriting the cross section expression (Eq. (4-2)) appropriate for the  ${}^3\text{He}(\vec{d}, p){}^4\text{He}$  reaction as it applied here, one obtains

$$\begin{aligned}
 I(\theta_2, \varphi_2) = & I_0(\theta_2) \left( 1 + \frac{3}{2} p_y'' A_y(\theta_2) + \frac{2}{3} p_x'' z'' A_{xz}(\theta_2) \right. \\
 & + \frac{1}{6} (p_x'' x'' - p_y'' y'') (A_{xx}(\theta_2) - A_{yy}(\theta_2)) \\
 & \left. + \frac{1}{2} p_z'' z'' A_{zz}(\theta_2) \right) . \quad (5-1)
 \end{aligned}$$

Polarization quantities in this expression (indicated with double primes) are related to the polarization quantities of deuterons emerging from the primary scattering which are expressed in the outgoing deuteron laboratory helicity frame ( $x', y', z'$  system in Fig. 18) via the rotation

$$\begin{aligned}
 \vec{p}'' &= U \vec{p}' \\
 (pp)'' &= U(pp)' \tilde{U} ,
 \end{aligned}$$

where

$$U = \begin{pmatrix} \cos\varphi_2 & -\sin\varphi_2 & 0 \\ \sin\varphi_2 & \cos\varphi_2 & 0 \\ 0 & 0 & 1 \end{pmatrix} .$$

The resulting relations of interest are

$$\begin{aligned}
 p_y'' &= p_{x'} \sin\varphi_2 + p_{y'} \cos\varphi_2 \\
 p_x'' z'' &= p_{x' z'} \cos\varphi_2 - p_{y' z'} \sin\varphi_2
 \end{aligned}$$

$$(p_{x''x''} - p_{y''y''}) = (p_{x'x'} - p_{y'y'}) (\cos^2 \varphi_2 - \sin^2 \varphi_2) - 4p_{x'y'} \cos \varphi_2 \sin \varphi_2$$

$$p_{z''z''} = p_{z'z'} \quad (5-2)$$

These equations indicate the azimuthal angles at which detectors should be located in order to sense the various polarization components of deuterons emerging from the primary scattering or reaction.

Hence, with the detector array positioned as in Fig. 21a, one might expect to sense  $p_{x'}$ ,  $p_{y'}$ ,  $p_{x'z'}$ ,  $p_{y'z'}$ ,  $(p_{x'x'} - p_{y'y'})$ , and  $p_{z'z'}$ . With the array positioned as in Fig. 21b, one might expect to sense, in addition,  $p_{x'y'}$ , while sacrificing  $(p_{x'x'} - p_{y'y'})$ . It is also apparent that, if the analyzing reaction were sensitive to all of these tensors simultaneously, an additional experiment would be required to achieve separation of the tensors as there are more observables than there are detectors in the present scheme. It was for this reason that a zero vector analyzing power was desirable when measuring the second-rank observables. The effect of a nonzero vector analyzing power will become apparent shortly.

A  $p_y$  polarized incident beam cannot give rise to the outgoing components  $p_{x'y'}$  and  $p_{y'z'}$ , but may contribute to the component  $(p_{x'x'} - p_{y'y'})$ . Hence, for  $p_y$

incident beams the detector array was positioned as shown in Fig. 21a. On the other hand,  $p_x$  or  $p_z$  incident beams may not contribute to  $(p_{x'x'} - p_{y'y'})$  but may contribute to components  $p_{x'y'}$  and  $p_{y'z'}$ . For these runs the array was rotated about the  $z'$  axis through an angle of  $45^\circ$ .

In order to illustrate how the polarized-to-unpolarized technique was used, details will be given for the case in which the quantization axis of the polarized run was along the reaction initial  $y$  axis.

For an unpolarized beam Eq. (1-16) reduces to

$$\begin{aligned}
 I &= I_0 \\
 p_{y'} &= p^{y'} \\
 p_{x'z'} &= p^{x'z'} \\
 p_{x'x'} - p_{y'y'} &= p^{x'x'} - p^{y'y'} \\
 p_{z'z'} &= p^{z'z'} , \qquad (5-3)
 \end{aligned}$$

while the other observables are zero. With the aid of Eqs. (5-1) and (5-2) expressions for the yield in the left detector may be written

$$\begin{aligned}
 \mathcal{L} &= n_0 E \epsilon_L \Delta \Omega_L \left[ 1 + \frac{3}{2} p^{y'} A_y + \frac{2}{3} p^{x'z'} A_{xz} + \frac{1}{6} (p^{x'x'} - p^{y'y'}) \right. \\
 &\quad \left. \cdot (A_{xx} - A_{yy}) + \frac{1}{2} p^{z'z'} A_{zz} \right] \\
 &= n_0 E \epsilon_L \Delta \Omega_L C_L ,
 \end{aligned}$$

where  $n_0$  is the number of deuterons entering the  $^3\text{He}$  cell, given by  $n_0 = nN_1I_0G$ , for which  $n$  is the number of protons delivered in the incident beam,  $N_1$  is the density of deuterons ( $\#/cm^3$ ) in the primary target,  $I_0$  is the unpolarized differential cross section for the primary reaction, and  $G$  is a geometry factor including solid angle and the effective target thickness.  $E$  is an efficiency characteristic of the  $^3\text{He}$  cell ( $\sim 1 \times 10^{-6}$ ) and is given by  $E = N_2 t_{\text{eff}} \lambda_0$ , where  $N_2$  is the density of  $^3\text{He}$  atoms,  $t_{\text{eff}}$  is an effective cell thickness, and  $\lambda_0$  is the unpolarized differential cross section for the  $^3\text{He}(d,p)^4\text{He}$  reaction.  $\epsilon_L$  and  $\Delta\Omega_L$  refer to the efficiency of, and solid angle subtended by, the left detector (Fig. 21a). Similar expressions may be written for the remaining detectors:

$$\begin{aligned}
 \mathcal{R} &= n_0 E \epsilon_R \Delta\Omega_R \left[ 1 - \frac{3}{2} P^Y Y' A_Y - \frac{2}{3} P^{X'Z'} A_{XZ} + \frac{1}{6} (P^{X'X'} - P^{Y'Y'}) \right. \\
 &\quad \left. \cdot (A_{XX} - A_{YY}) + \frac{1}{2} P^{Z'Z'} A_{ZZ} \right] \\
 &= n_0 E \epsilon_R \Delta\Omega_R C_R \\
 \mathcal{U} &= n_0 E \epsilon_U \Delta\Omega_U \left[ 1 - \frac{1}{6} (P^{X'X'} - P^{Y'Y'}) (A_{XX} - A_{YY}) + \frac{1}{2} P^{Z'Z'} A_{ZZ} \right] \\
 &= n_0 E \epsilon_U \Delta\Omega_U C_U \\
 \mathcal{D} &= n_0 E \epsilon_D \Delta\Omega_D \left[ 1 - \frac{1}{6} (P^{X'X'} - P^{Y'Y'}) (A_{XX} - A_{YY}) + \frac{1}{2} P^{Z'Z'} A_{ZZ} \right] \\
 &= n_0 E \epsilon_D \Delta\Omega_D C_D
 \end{aligned}$$

$$\begin{aligned} \mathcal{J}(\theta_2=0^\circ) &= n_o E \epsilon_S \Delta \Omega_S \left[ 1 + \frac{1}{2} P^{z'z'} A_{zz}(0^\circ) \right] \\ &= n_o E \epsilon_S \Delta \Omega_S C_S . \end{aligned} \quad (5-4)$$

For an incident  $p_y$  polarized proton beam, Eq. (1-16) reduces to

$$\begin{aligned} I/I_o &= (1+p_y A_y) \\ (I/I_o) p_{x'} &= 0 \\ (I/I_o) p_{y'} &= P^{y'} + p_y K_y^{y'} \\ (I/I_o) p_{z'} &= 0 \\ (I/I_o) p_{x'y'} &= 0 \\ (I/I_o) p_{x'z'} &= P^{x'z'} + p_y K_y^{x'z'} \\ (I/I_o) p_{y'z'} &= 0 \\ (I/I_o) (p_{x'x'} - p_{y'y'}) &= (P^{x'x'} - P^{y'y'}) + p_y (K_y^{x'x'} - K_y^{y'y'}) \\ (I/I_o) p_{z'z'} &= P^{z'z'} + p_y K_y^{z'z'} . \end{aligned} \quad (5-5)$$

The ratio,  $I/I_o$ , was obtained from the experiments described in Chapter III.

Again using Eqs. (5-1) and (5-2) expressions may be written for the yield in each detector:

$$\begin{aligned} L &= n_1 E \epsilon_L \Delta \Omega_L \left[ 1 + \frac{3}{2} p_y A_y + \frac{2}{3} p_{x'z'} A_{xz} + \frac{1}{6} (p_{x'x'} - p_{y'y'}) \right. \\ &\quad \left. \cdot (A_{xx} - A_{yy}) + \frac{1}{2} p_{z'z'} A_{zz} \right] \end{aligned}$$

$$\begin{aligned}
R &= n_1 E \epsilon_R \Delta \Omega_R \left[ 1 - \frac{3}{2} p_{y'} A_y - \frac{2}{3} p_{x'z'} A_{xz} + \frac{1}{6} (p_{x'x'} - p_{y'y'}) \right. \\
&\quad \left. \cdot (A_{xx} - A_{yy}) + \frac{1}{2} p_{z'z'} A_{zz} \right] \\
U &= n_1 E \epsilon_U \Delta \Omega_U \left[ 1 - \frac{3}{2} p_{x'} A_x + \frac{2}{3} p_{y'z'} A_{xz} - \frac{1}{6} (p_{x'x'} - p_{y'y'}) \right. \\
&\quad \left. \cdot (A_{xx} - A_{yy}) + \frac{1}{2} p_{z'z'} A_{zz} \right] \\
D &= n_1 E \epsilon_D \Delta \Omega_D \left[ 1 + \frac{3}{2} p_{x'} A_x - \frac{2}{3} p_{y'z'} A_{xz} - \frac{1}{6} (p_{x'x'} - p_{y'y'}) \right. \\
&\quad \left. \cdot (A_{xx} - A_{yy}) + \frac{1}{2} p_{z'z'} A_{zz} \right] \\
S &= n_1 E \epsilon_S \Delta \Omega_S \left[ 1 + \frac{1}{2} p_{z'z'} A_{zz} (0^\circ) \right] . \tag{5-6}
\end{aligned}$$

It should be noted that  $n_0$  and  $n_1$  are most likely to be different. This difference can arise as a result of changes in incident beam polarization from run to run thereby changing the differential cross section of the primary reaction, and inaccurate current integration. In the present case the cross section for the polarized run is  $I = I_0(1+p_y A_y)$  while that for the unpolarized run is just  $I_0$ .

Forming ratios of the number of counts a detector received during the polarized run to the number received during the unpolarized run and multiplying each ratio by its corresponding constant ( $C_i$ ,  $i = L, R, U, D$ , or  $S$  of Eq. (5-4)), one obtains the following ratios which are, to a high degree, independent of detector efficiencies and solid angle:

$$\begin{aligned}
C_L \frac{I}{\mathcal{L}} = R_L &= \frac{n_1}{n_0} \left[ 1 + \frac{3}{2} p_{y'} A_y + \frac{2}{3} p_{x'z'} A_{xz} + \frac{1}{6} (p_{x'x'} - p_{y'y'}) \right. \\
&\quad \left. \cdot (A_{xx} - A_{yy}) + \frac{1}{2} p_{z'z'} A_{zz} \right] \\
C_R \frac{R}{\mathcal{R}} = R_R &= \frac{n_1}{n_0} \left[ 1 - \frac{3}{2} p_{y'} A_y - \frac{2}{3} p_{x'z'} A_{xz} + \frac{1}{6} (p_{x'x'} - p_{y'y'}) \right. \\
&\quad \left. \cdot (A_{xx} - A_{yy}) + \frac{1}{2} p_{z'z'} A_{zz} \right] \\
C_U \frac{U}{\mathcal{U}} = R_U &= \frac{n_1}{n_0} \left[ 1 - \frac{3}{2} p_{x'} A_x + \frac{2}{3} p_{y'z'} A_{xz} - \frac{1}{6} (p_{x'x'} - p_{y'y'}) \right. \\
&\quad \left. \cdot (A_{xx} - A_{yy}) + \frac{1}{2} p_{z'z'} A_{zz} \right] \\
C_D \frac{D}{\mathcal{D}} = R_D &= \frac{n_1}{n_0} \left[ 1 + \frac{3}{2} p_{x'} A_x - \frac{2}{3} p_{y'z'} A_{xz} - \frac{1}{6} (p_{x'x'} - p_{y'y'}) \right. \\
&\quad \left. \cdot (A_{xx} - A_{yy}) + \frac{1}{2} p_{z'z'} A_{zz} \right] \\
C_S \frac{S}{\mathcal{S}} = R_S &= \frac{n_1}{n_0} \left[ 1 + \frac{1}{2} p_{z'z'} A_{zz} (0^\circ) \right] \quad . \quad (5-7)
\end{aligned}$$

Outgoing polarization components may then be obtained from these ratios in a manner independent of the quantity  $n_1/n_0$ :

$$\begin{aligned}
p_{z'z'} &= \frac{2(R_L + R_R + R_U + R_D) - 8R_S}{(4R_S A_{zz} + R_L + R_R + R_U + R_D) A_{zz} (0^\circ)} \\
p_{y'z'} &= \frac{3(R_U - R_D)}{4(R_L + R_R + R_U + R_D)} \frac{(4 + 2p_{z'z'} A_{zz})}{A_{xz}} \\
&\quad + \frac{9}{4} \frac{p_{x'} A_y}{A_{xz}} \\
p_{x'z'} &= \frac{3(R_L - R_R)}{4(R_L + R_R + R_U + R_D)} \frac{(4 + 2p_{z'z'} A_{zz})}{A_{xz}} \\
&\quad - \frac{9}{4} \frac{p_{y'} A_x}{A_{xz}}
\end{aligned}$$

$$(p_{x',x'}, -p_{y',y'}) = \frac{3[(R_L+R_R)-(R_U+R_D)]}{R_L+R_R+R_U+R_D} \frac{(2+p_{z',z'}, A_{zz})}{(A_{xx}-A_{yy})}. \quad (5-8)$$

Equations given by Eq. (5-8) are completely general for a five detector system, one of which is at  $\theta_2 = 0^\circ$  while the remaining four are at an arbitrary polar angle but with azimuthal angles of  $0^\circ$ ,  $180^\circ$ ,  $270^\circ$ , and  $90^\circ$ , respectively. These equations exhibit desirable characteristics which are found in the  ${}^3\text{He}(\vec{d}, p){}^4\text{He}$  reaction, namely that  $A_y = 0$  and that  $A_{zz}$  vanish at some choice of polar angle though the latter is not absolutely necessary.

For operating conditions satisfied by the 80% criterion, the maximum contribution (assuming  $p_{x'} = p_{y'} = 1$ ) to  $p_{y',z'}$  and  $p_{x',z'}$  is less than 0.038 and is likely to be considerably smaller (i.e.,  $\sim 0.0038$ ) in the present experiment.

Equations similar to those in Eq. (5-8) obtain when the detector array is rotated  $45^\circ$  as in Fig. 21b, and new constants determined for the unpolarized run:

$$p_{y',z'} = \frac{3}{4\sqrt{2}} \frac{[(R_U+R_R)-(R_L+R_D)]}{(R_L+R_R+R_U+R_D)} \frac{(4+2p_{z',z'}, A_{zz})}{A_{xz}} + \frac{9}{4} \frac{p_{x'} A_y}{A_{xz}}$$

$$\begin{aligned}
p_{x',z'} &= \frac{3}{4\sqrt{2}} \frac{[(R_{U'}+R_{L'})-(R_{D'}+R_{R'})]}{(R_{L'}+R_{R'}+R_{U'}+R_{D'})} \frac{(4+2p_{z',z'}A_{zz})}{A_{xz}} \\
&\quad + \frac{9}{4} \frac{p_{y'}A_y}{A_{xz}} \\
p_{x',y'} &= \frac{3}{4} \frac{[(R_{U'}+R_{D'})-(R_{L'}+R_{R'})]}{(R_{L'}+R_{R'}+R_{U'}+R_{D'})} \frac{(4+2p_{z',z'}A_{zz})}{(A_{xx}-A_{yy})} . \quad (5-9)
\end{aligned}$$

The expression for  $p_{z',z'}$  remains unchanged. It is interesting to note that  $p_{y',z'}$  and  $p_{x',z'}$  are sensed with nearly equal efficiency with the detector array in either position.

A computer code, PØLTRSF, was written to process data obtained with this method. Statistical error analysis was handled numerically by the code.

Details of the spin-up-to-spin-down method were worked out for each case by first assuming  $A_y = 0$  and  $A_{zz}(54.7^\circ) = 0$ , then writing yield expressions for each detector for two different polarized runs. Ratios of the number of counts a detector received during the spin-up run to the number of counts received during the spin-down run were computed for each detector and iterative computer techniques used to extract the relevant polarization transfer coefficients. To the extent that the assumptions for  $A_y$  and  $A_{zz}(54.7^\circ)$  were correct, data obtained by the polarized-to-unpolarized method could be processed as a special case of the spin-up-to-spin-down method.

$K_X^{X'}$  was measured at a laboratory angle of  $22\frac{1}{2}^\circ$  by a spin-up-to-spin-down technique. For this measurement two 80 nA polarized runs were made at a machine energy of 9.28 MeV (corresponding to a target center energy of 9.08 MeV) with the quantization axis aligned or antialigned with the projectile helicity x axis. These will be referred to as  $p_x$  and  $p_{-x}$  beams, respectively. Without the aluminum degrading foil, recoil deuterons entering the  $^3\text{He}$  cell had an energy of  $\sim 5.8$  MeV giving a mean interaction energy of  $\sim 5.6$  MeV. At this energy the analyzing powers for the  $^3\text{He}(\vec{d},p)^4\text{He}$  reaction appropriate for use under these operating conditions ( $\theta_2(\text{c.m.}) \sim 61^\circ$ ) are approximately

$$A_y = -0.353 \pm 0.012$$

$$\frac{1}{2}(A_{xx} - A_{yy}) = 0.546 \pm 0.024$$

$$A_{zz} = 0.051 \pm 0.018 ,$$

where these numbers were obtained by interpolating the data of Gruebler et al. (Gr 71).

For the present case, Eq. (1-16) reduces to

$$I = I_0$$

$$p_{x'} = p_{x \frac{K_X^{X'}}{x}} \quad p_{x'z'} = p^{x'z'}$$

$$p_{y'} = p^{y'} \quad p_{y'z'} = p_{x \frac{K_Y^{Y'}}{x}}^{y'z'}$$

$$\begin{aligned}
p_{z'} &= p_x K_x^{z'} & (p_{x'x'} - p_{y'y'}) &= (P^{x'x'} - P^{y'y'}) \\
p_{x'y'} &= p_x K_x^{x'y'} & p_{z'z'} &= P^{z'z'} .
\end{aligned} \tag{5-10}$$

Since vector polarization gives rise to asymmetries in a plane normal to the vector and  $p_x$ , is the component of current interest, only the up and down detector yields need be considered here.

Again using Eqs. (5-1), (5-2), and (5-10) one can write expressions for the yields:

$$\begin{aligned}
U_+ &= n_+ E \epsilon_U \Delta \Omega_U \left[ 1 - \frac{3}{2} p_Q K_x^{x'} A_y + \frac{2}{3} p_Q K_x^{y'z'} A_{xz} \right. \\
&\quad \left. - \frac{1}{6} (P^{x'x'} - P^{y'y'}) (A_{xx} - A_{yy}) + \frac{1}{2} P^{z'z'} A_{zz} \right] \\
D_+ &= n_+ E \epsilon_D \Delta \Omega_D \left[ 1 + \frac{3}{2} p_Q K_x^{x'} A_y - \frac{2}{3} p_Q K_x^{y'z'} A_{xz} \right. \\
&\quad \left. - \frac{1}{6} (P^{x'x'} - P^{y'y'}) (A_{xx} - A_{yy}) + \frac{1}{2} P^{z'z'} A_{zz} \right] ,
\end{aligned} \tag{5-11}$$

where  $nE\epsilon\Delta\Omega$  means the same as in Eq. (5-4). The + has been used to indicate the quantization axis aligned with the x axis. The quenchable fractional value,  $p_Q = p_x$ , was 0.846. The remaining quantities mean the same as before.

With the quantization axis antialigned with the x axis,  $p_x = -p_Q$ , and the yields become

$$\begin{aligned}
U_- &= n_- E \epsilon_U \Delta \Omega_U \left( 1 + \frac{3}{2} p_Q K_x^{x'} A_y - \frac{2}{3} p_Q K_x^{y'z'} A_{xz} + \alpha \right) \\
D_- &= n_- E \epsilon_D \Delta \Omega_D \left( 1 - \frac{3}{2} p_Q K_x^{x'} A_y + \frac{2}{3} p_Q K_x^{y'z'} a_{xz} + \alpha \right) ,
\end{aligned} \tag{5-12}$$

where  $\alpha = \frac{1}{6}(P^{x'x'} - P^{y'y'})(A_{xx} - A_{yy}) + \frac{1}{2}P^{z'z'}A_{zz}$ . Notice again the mixing of vector and tensor polarizations as evidenced by the presence of both  $K_X^{x'}$  and  $K_X^{y'z'}$ . If one defines geometric means by

$$\begin{aligned} \mathcal{L} &= (D_+ U_-)^{\frac{1}{2}} \\ \mathcal{R} &= (D_- U_+)^{\frac{1}{2}}, \end{aligned} \quad (5-13)$$

and forms the asymmetry,  $\epsilon = - / +$ , then in terms of this asymmetry

$$3p_Q K_X^{x'} A_y = \epsilon(2+2\alpha) + \frac{4}{3}p_Q K_X^{y'z'} A_{xz}. \quad (5-14)$$

Values of  $(P^{x'x'} - P^{y'y'})$  and  $P^{z'z'}$  were obtained by interpolation of the data measured in Chapter III.  $K_X^{y'z'}$  was measured using the  ${}^3\text{He}(\vec{d}, p){}^4\text{He}$  reaction in the vicinity of the 430-keV resonance to be  $0.00 \pm 0.05$ .

Each run took  $\sim 40$  minutes with counts being recorded as follows:

$L_+$	$R_+$	$U_+$	$D_+$	$S_+$	$L_-$	$R_-$	$U_-$	$D_-$	$S_-$
109	131	197	153	84	147	142	137	163	75

Values used for  $\frac{1}{2}(P^{x'x'} - P^{y'y'})$  and  $P^{z'z'}$  were  $-0.090$  and  $0.030$ , respectively. This gave a value for  $K_X^{x'}$  of  $0.24 \pm 0.09$ .

### C. Results

Results of the second-rank outgoing deuteron polarization measured at  $22\frac{1}{2}^{\circ}$  are presented in Table 14. The polarization components are expressed in the laboratory reaction final coordinate system:  $\hat{y}'$  along  $\vec{k}_{in}(p)x\vec{k}_{out}(d)$ ,  $\hat{z}'$  along  $\vec{k}_{out}(d)$ , with  $\hat{x}'$  chosen to make a right-handed system. These data were obtained with the polarized-to-unpolarized method. All polarizations are small. Conservation of parity requires that  $p_{y',z'} = 0$  for the case of  $p_y$  incident beams. Measurements of this quantity are consistent with zero.

Polarization transfer coefficients may be extracted directly from the respective polarizations given in Table 14 with the aid of Eq. (1-16). The value of  $p_{y',z'}$  obtained with a  $p_{-x}$  beam at 7.87 MeV led to a transfer coefficient 2.7 standard deviations from zero. However, repeat measurements made with  $p_x$ ,  $p_y$ , and  $p_z$  beams at this energy by the spin-up-to-spin-down method produced five transfer coefficients in agreement with the earlier results and two transfer coefficients having poor agreement ( $\tau \cong 1.9$  standard deviations for  $K_x^{y'z'}$  and  $\frac{1}{2}(K_y^{x'x'} - K_y^{y'y'})$ ). The newer values are presented in Table 15 as they were obtained with higher statistical accuracy.

Table 14  
 Measured Outgoing Deuteron Polarizations Expressed in the Reaction  
 Final Coordinate System at a Laboratory Angle of  $22.5^\circ$

$\hat{S}$	$E_p^a)$ (MeV)	$E_p^b)$ (MeV)	$P_Q$	$P_{z'z'}$	$P_{y'z'}^c)$	$P_{x'z'}$	$1/2(P_{x'x'} - P_{y'y'})$	$P_{x'y'}$
$\hat{y}$	4.52	4.16	0.895	$0.053 \pm 0.051$	$0.005 \pm 0.040$	$0.061 \pm 0.040$	$-0.054 \pm 0.041$	
"	5.48	5.17	0.863	$0.085 \pm 0.050$	$-0.010 \pm 0.039$	$0.055 \pm 0.039$	$-0.063 \pm 0.040$	
"	6.38	6.11	0.889	$0.070 \pm 0.050$	$-0.009 \pm 0.039$	$0.111 \pm 0.039$	$-0.046 \pm 0.040$	
"	8.09	7.87	0.896	$0.062 \pm 0.050$	$0.001 \pm 0.039$	$0.019 \pm 0.040$	$-0.122 \pm 0.040$	
$-\hat{x}$	4.47	4.10	0.904	$0.049 \pm 0.041$	$0.007 \pm 0.031$	$-0.005 \pm 0.031$		$0.026 \pm 0.032$
"	5.41	5.10	0.901	$0.110 \pm 0.044$	$0.001 \pm 0.034$	$0.033 \pm 0.034$		$-0.008 \pm 0.035$
"	6.32	6.05	0.895	$0.016 \pm 0.056$	$0.055 \pm 0.042$	$0.017 \pm 0.042$		$0.017 \pm 0.043$
"	8.09	7.87	0.853	$-0.087 \pm 0.062$	$0.119 \pm 0.044$	$0.014 \pm 0.045$		$-0.017 \pm 0.046$
"	9.28	9.08	0.874	$-0.077 \pm 0.065$	$-0.001 \pm 0.047$	$0.107 \pm 0.047$		$0.032 \pm 0.049$
$\hat{z}$	4.47	4.10	0.905	$0.106 \pm 0.040$	$-0.062 \pm 0.031$	$0.042 \pm 0.031$		$0.037 \pm 0.032$
"	5.41	5.10	0.898	$0.104 \pm 0.043$	$-0.061 \pm 0.034$	$0.017 \pm 0.034$		$-0.030 \pm 0.035$
"	6.32	6.05	0.888	$0.013 \pm 0.046$	$0.015 \pm 0.035$	$0.014 \pm 0.035$		$0.004 \pm 0.036$
"	8.09	7.87	0.830	$0.029 \pm 0.062$	$0.098 \pm 0.046$	$0.057 \pm 0.046$		$-0.046 \pm 0.048$
"	9.28	9.08	0.861	$0.002 \pm 0.060$	$-0.068 \pm 0.045$	$0.056 \pm 0.045$		$0.003 \pm 0.047$

a) Proton lab energy (Machine).

b) Proton lab energy at the deuterium gas cell center.

c) For  $\hat{S}$  along  $\hat{y}$ , this observable is required to be zero.

Table 15  
Analyzing Power, Polarization Functions, and Vector to Tensor Polarization  
Transfer Coefficients for D(p,d)H Elastic Scattering

$E_p$ (MeV)	$\theta_d^{\text{lab}}$ (deg)	$A_y^p$	$P_{xz}$	$\frac{1}{2}(P_{xx} - P_{yy})$	$P_{zz}$	$K_x^{y'z'}$	$K_x^{x'y'}$
6.7	45	-0.055	0.008	-0.035	-0.094	0.04±0.04	0.06±0.04
8.3	45	-0.058	0.008	-0.035	-0.094	-0.04±0.05	0.03±0.06
4.1	22.5	-0.033	0.029	-0.051	0.053	-0.01±0.04	-0.03±0.04
5.1	22.5	-0.047	0.020	-0.077	0.058	0.00±0.04	0.01±0.04
6.1	22.5	-0.059	0.031	-0.087	0.056	-0.06±0.05	-0.02±0.05
7.9	22.5	-0.086	0.028	-0.087	0.038	0.03±0.03	-0.03±0.03
9.1	22.5	-0.100	0.025	-0.090	0.030	0.00±0.05	-0.04±0.05
3.6	0	a)	a)	a)	a)	0.03±0.03	a)-0.03±0.03
5.3	0	a)	a)	a)	a)	-0.02±0.03	a) 0.02±0.03
6.8	0	a)	a)	a)	a)	-0.07±0.03	a)-0.03±0.03
7.8	0	a)	a)	a)	a)	-0.04±0.03	a)-0.03±0.03

$E_p$ (MeV)	$\theta_d^{\text{lab}}$ (deg)	$K_y^{x'z'}$	$\frac{1}{2}(K_y^{x'x'} - K_y^{y'y'})$	$K_y^{z'z'}$	$K_z^{y'z'}$	$K_z^{x'y'}$
6.7	45	0.03±0.04	0.02±0.04	-0.05±0.05	0.04±0.05	-0.05±0.05
8.3	45	0.01±0.04	-0.09±0.05	-0.05±0.06	-0.02±0.05	-0.07±0.05
4.1	22.5	0.04±0.04	0.00±0.05	0.00±0.06	-0.07±0.03	0.04±0.04
5.1	22.5	0.04±0.04	0.02±0.05	0.03±0.06	-0.07±0.04	-0.03±0.04
6.1	22.5	0.08±0.04	0.05±0.04	0.01±0.06	0.02±0.04	0.00±0.04
7.9	22.5	0.03±0.03	0.08±0.03	-0.01±0.04	0.06±0.03	0.00±0.03
9.1	22.5				-0.08±0.05	0.00±0.05

a) Required to be zero by angular momentum conservation.

Table 15 also contains values of the proton analyzing power and deuteron polarization functions used in the reduction of the polarization transfer data. These values were obtained by interpolation of the data presented in Chapter III. The errors of these quantities are not given, but are somewhat less than 0.01 including both statistical and systematic effects.

The various vector-to-tensor polarization transfer coefficients are consistent with zero, in view of the errors, but effects of the order of  $\sim 0.05$  cannot be ruled out. This limit is to be compared to the range of possible values of  $\pm 1$  for observables relating strictly to vector polarization,  $\pm 2$  for  $K_y^{z'z'}$ , and  $\pm 3/2$  for the remaining vector-to-tensor transfer coefficients.

In addition to the data presented in Table 15, two runs were made at  $0^\circ$  at 3.61 MeV with  $p_z$  and  $p_{-z}$  beams and the transfer coefficients  $K_z^{x'y'}$  and  $K_z^{y'z'}$  extracted. Both these observables are required to be zero at  $0^\circ$ .  $K_z^{y'z'}$  is required to be zero as it is an odd function of scattering angle. Requirement that  $K_z^{x'y'}$  be zero at zero degrees is a result of the y axis ( $\vec{k}_{in} \times \vec{k}_{out}$ ) being undefined (note:  $\hat{y} = \hat{y}'$ ,  $\hat{x} = \hat{x}'$ , and  $\hat{z} = \hat{z}'$ ). For this case it is completely general to choose "up" as the y axis and "left" as the x axis. Or, an equally good choice would have been to choose "left" as the y axis and "down" as the x axis. This is equivalent to a  $90^\circ$  rotation

about the z axis for which  $y \rightarrow x$ ,  $x \rightarrow -y$ . Hence,  $K_z^{x'y'} = K_z^{-y'x'} = -K_z^{y'x'} = -K_z^{x'y'} = 0$  which follows from the definition of this observable in terms of the operators given in Chapter I. The measured values were consistent with zero.

$K_x^{x'}$  measured at  $\theta_{\text{lab}} = 22\frac{1}{2}^\circ$  and  $E_p = 9.08$  MeV was found to be  $0.24 \pm 0.09$ . This value is consistent with the value of 0.180 (Ga 72) calculated with the phase shifts of Christian and Gammel (Ch 53) at  $E_p = 9.66$  MeV at  $\theta_{\text{lab}} = 22\frac{1}{2}^\circ$ . This agreement indicates that their phase shifts contain the correct relative quartet and doublet state contributions to the scattering amplitude.

#### D. Summary

##### 1. Experimental

In the present experiment, it has been demonstrated that experiments in which polarization transfer coefficients relating to various outgoing deuteron second-rank polarizations are to be measured are feasible.

Currently available polarized beam intensities necessarily require a compromise in energy and angular resolution in order to achieve acceptable counting rates. The present geometry proved satisfactory in this regard.

It was desirable, for reasons already demonstrated, that a deuteron tensor polarization analyzer having zero vector analyzing power be used. The  ${}^3\text{He}(\vec{d}, p){}^4\text{He}$  reaction

has this characteristic in the vicinity of the 430-keV resonance and had previously been used by experimenters (Se 64, Mc 65, Yo 65, Iv 65) to measure outgoing deuteron second-rank polarizations resulting from unpolarized incident beams. As this reaction is very sensitive to deuteron energy, and the slowing process magnifies small energy differences, a technique was sought for which beam steering and evenness of illumination effects could not appreciably shift the centroid of proton production within the  ${}^3\text{He}$  cell. Successful elimination of detector efficiencies and solid angle factors were dependent on this requirement which necessarily required at least two runs, one of which was for normalization purposes. The ten detector yields thus generated could be combined in a number of ways in order to extract various outgoing polarization components. A technique was chosen in which current integration effects were eliminated, both in the polarized-to-unpolarized ratio method and in the spin-up-to-spin-down ratio method.

For later experiments (Oh 73a, Oh 73b) on  ${}^4\text{He}(\vec{d}, \vec{d}){}^4\text{He}$  and  ${}^3\text{He}(\vec{d}, \vec{d}){}^3\text{He}$  polarization transfer where effects were found to be large, a more accurate knowledge of the effective analyzing powers for the  ${}^3\text{He}(\vec{d}, p){}^4\text{He}$  reaction was required in view of the highly asymmetrical energy and intensity variation of the illumination of the  ${}^3\text{He}$  cell. Numerical calculations made with a modified version

of YIELD (listed in Appendix C) showed that the analyzing powers were always within 1% of a given value, provided that the calculations were carried out at a point corresponding to a given yield level of the excitation curve. We chose the 80% level because it was sufficiently high to give reasonable counting rates while still maintaining a negligible vector analyzing power. Although a higher  ${}^3\text{He}$  density would have increased counting rates, a compensating level less than the 80% level would have been required for  $A_y \approx 0$ .

Some features of the present design were never fully utilized: the capability of rotating the primary chamber through  $\pm 110^\circ$  and the detector array through a full  $360^\circ$  (although techniques using this kind of capability have been successfully used in the measurement of analyzing powers).

The most severe problem encountered was due to larger than expected neutron fluxes. This placed an upper limit on operating energies of  $\sim 9.5$  MeV which in turn limited the angular range of the experiment. Future experimental designs should allow for a beam stop far removed from the detector array. In addition, since energy degrading foils were not frequently interchanged, a design in which the primary target,  ${}^3\text{He}$  cell, and detector array are all inside vacuum might prove more satisfactory. This would extend downward the low energy limit for each angle and

extend upward the angular range for which data could be obtained as the chamber exit window could be eliminated. The entrance foil to the  $^3\text{He}$  cell could then be made of foil considerably thinner than the  $5\text{-mg/cm}^2$  Havar which was used. The thicker entrance foil was needed in order to withstand the negative pressure differential encountered during the filling process.

The full range of polar angle adjustment in the detector array was never used though an initial small adjustment was made.

In any event, the measurement of polarization transfer coefficients requires that additional analyzing power and polarization experiments be performed. The complexity of the experiments increases rapidly as the spin structure of the reacting particles becomes more complex,

## 2. Theoretical

Nucleon-deuteron scattering has been the subject of intensive investigation in recent years. This interest has arisen as a result of the nucleon-deuteron problem being the simplest of multi-nucleon systems. Extensive reviews of the experimental data on nucleon-deuteron scattering have been given by Seagrave (Se 70) for differential cross sections and by Haeberli (Ha 70) for polarizations and other spin observables. Several attempts to deduce phase shifts have been made (Ch 53, Ar 67, Tr 67, Va 67, Pu 68, Br 70, Ja 70), the most recent of which is

the one by Gruebler et al. (Gr 72).

Recent calculations of nucleon-deuteron observables have been made (Av 71, Aa 72, Do 72, Pi 72a, Pi 72b, Pi 73) by solving numerically the Faddeev-Lovelace three body integral equations (Fa 61, Lo 64) for a given set of potentials. Depending upon the complexity of the potentials used, the calculations have either been exact or have made use of perturbative techniques.

Aarons and Sloan (Aa 72) calculated nucleon and deuteron polarizations using an exact three-body calculation with non central, spin dependent, two-body forces of separable form. These calculations led to vector polarizations which were too small and of the wrong angular shape compared to the data. Second rank polarizations agreed only qualitatively with the data. Lack of agreement became more pronounced with decreasing nucleon energy. The calculations of Doleschall were of a similar nature.

Pieper (Pi 72a) calculated vector-to-vector polarization transfer coefficients (Wolfenstein parameters) in  $D(\vec{p}, \vec{p})D$  elastic scattering as well as nucleon and deuteron polarizations. He used a two-potential formula for separable S-, P-, and D-wave nucleon-nucleon forces. The S-wave part of the calculation was treated exactly while the P- and D-waves were included to first order as a perturbation. For one set of potential parameters the nucleon polarizations agreed reasonably well, the deuteron

vector polarizations tended to be large by ~50%, while the second rank polarizations were in complete disagreement--presumably because of a lack of a  ${}^3S_1$ - ${}^3D_1$  tensor force in the calculation. Lack of agreement of vector polarizations became more pronounced with increasing nucleon energy. The Wolfenstein parameters appeared large and sensitive to the potential parameters used. The calculations show that scattering amplitudes that produce only slightly different elastic cross sections produce significantly different polarizations and other spin observables. Later calculations (Pi 72b) made with the inclusion of the  ${}^3S_1$ - ${}^3D_1$  tensor force did produce qualitative agreement of the rank two polarizations.

Quite recently, calculations of  $K_x^{x'y'}$  and  $K_y^{x'z'}$  as well as  $K_x^{x'}$ ,  $K_y^{y'}$ , and  $K_z^{x'}$  for  $D(\vec{p}, \vec{d})H$  have been made (Pi 73). These vector-to-tensor polarization transfer observables, though small, do show a single "bump" at a c.m. angle near  $120^\circ$  (corresponding to an outgoing deuteron laboratory angle of  $30^\circ$ ; an angle within the range of capability of the deuteron polarization transfer chamber). However, vector-to-vector polarization transfer observables appear large and may be sensitive to potential parameters. Should this be the case, then perhaps additional polarization transfer experiments of the vector-to-vector type should be performed.

The single measurement of  $K_x^{x'}$  reported here disagrees from the calculated value by two-standard-deviations. It is not yet known whether this disagreement is significant.

## APPENDIX A

### MEASUREMENT OF ANALYZING POWERS IN REACTIONS INDUCED BY POLARIZED DEUTERONS VIA THE RATIO METHOD

At the time the experiments described in this thesis were in progress, two methods of measuring analyzing powers in reactions induced by polarized deuterons were in use at LASL. Since that time additional schemes have been developed (Oh 73c). The first of the older methods has been reported elsewhere (La 71). The second, known as the Ratio Method, has not yet been reported but was used for the measurement of the analyzing powers for the reaction  $H(\vec{d}, p)D$  described in Chapter III. Each of the methods utilize the "cube" scattering chamber and is dependent on the flexibility of the polarized ion source with regard to selection of magnetic substates and quantization axis direction.

The most general form of the differential cross section expression for parity conserving reactions induced by a polarized spin-1 beam is (Oh 73c)

$$I(\theta, \varphi) = I_0(\theta) \left[ 1 + \frac{3}{2} p_y A_y + \frac{2}{3} p_{xz} A_{xz} + \frac{1}{3} p_{xx} A_{xx} + \frac{1}{3} p_{yy} A_{yy} + \frac{1}{3} p_{zz} A_{zz} \right], \quad (A-1)$$

where  $I_0(\theta)$  is the unpolarized cross section at the scattering angle  $\theta$ , the p's are the beam polarization

quantities [expressed in the reaction initial coordinate system (see Chapter IV)]. In order to obtain the polarization components appropriate for use in Eq. (A-1), the rotation given by Eq. (4-3) must be used.

In view of the overcompleteness of the Goldfarb operators, the operator relation  $\rho_{xx} + \rho_{yy} + \rho_{zz} = 0$  can be used to rewrite the terms involving these tensors in various ways (Oh 73c), e.g.,

$$\sum_{i=x,y,z} p_{ii} A_{ii} = \frac{1}{2}(p_{jj} - p_{kk})(A_{jj} - A_{kk}) + \frac{3}{2} p_{\ell\ell} A_{\ell\ell}, \quad (A-2)$$

where  $j, k, \ell$  are  $x, y, z$  in any order.

The Ratio Method utilizes polarized  $m_I = 1$  and  $m_I = 0$  deuteron beams with the quantization axis perpendicular to the beam direction ( $\beta = 90^\circ$ ) for the measurement of  $A_y$ ,  $A_{yy}$ , and  $A_{xx}$ . For this configuration,

$$\begin{aligned} p_y &= p_z \cos\varphi \\ p_{xz} &= 0 \\ p_{xx} &= \frac{1}{2}(3\sin^2\varphi - 1)p_{zz} \\ p_{yy} &= \frac{1}{2}(3\cos^2\varphi - 1)p_{zz} \\ p_{zz} &= -\frac{1}{2} p_{zz}, \end{aligned} \quad (A-3)$$

where  $p_z$  and  $p_{zz}$  are the vector and tensor polarization of the incident beam for the respective magnetic substate (see Chapter I).

Using Eqs. (A-2) and (A-3) in Eq. (A-1) with  $\phi = 0$ , 180, 270, and 90° corresponding to left, right, up, and down, respectively, one can write expressions for the yield in each of the four detectors:

$$\begin{aligned}
 L &= nN\Omega_L I_0 \left( 1 + \frac{3}{2} p_Z A_y + \frac{1}{2} p_{ZZ} A_{yy} \right) \\
 R &= nN\Omega_R I_0 \left( 1 - \frac{3}{2} p_Z A_y + \frac{1}{2} p_{ZZ} A_{yy} \right) \\
 U &= nN\Omega_U I_0 \left( 1 + \frac{1}{2} p_{ZZ} A_{xx} \right) \\
 D &= nN\Omega_D I_0 \left( 1 + \frac{1}{2} p_{ZZ} A_{xx} \right), \tag{A-4}
 \end{aligned}$$

where  $n$  is proportional to the amount of charge delivered,  $N$  is the target density (number of nuclei/cm<sup>2</sup>),  $\Omega$  is the solid angle subtended by the detector,  $I_0$  is the unpolarized differential cross section, and the  $A$ 's are the analyzing powers to be determined.

Then, utilizing yields from the two runs (assuming  $p_Z = p_{ZZ} = p_Q$  for  $m_I = 1$  and  $p_Z = 0.012 p_Q$ ;  $p_{ZZ} = -1.966 p_Q$  for  $m_I = 0$ , where  $p_Q$  is the quenchable percentage), expressions in terms of the analyzing powers may be obtained:

$$\begin{aligned}
 \frac{3}{2} p_Q A_y &= \frac{2.966(L_1 - R_1)}{(L_0 + R_0) + 1.966(L_1 + R_1)} \\
 p_Q A_{yy} &= \frac{2[(L_1 + R_1) - (L_0 + R_0)]}{(L_0 + R_0) + 1.966(L_1 + R_1)}
 \end{aligned}$$

$$p_{QA_{xx}} = \frac{[2(U_1+D_1)-(U_0+D_0)]}{(U_0+D_0)+1.966(U_1+D_1)}, \quad (A-5)$$

where the subscripts refer to the magnetic substate used.

In practice, a two- or four-fold rotational sequence of the cube was used for each magnetic substate and geometric means were computed for the yields in Eq. (A-5). This procedure serves to eliminate the effects of non-identical detector efficiencies and geometries.

For a determination of  $A_{xz}$ , the quantization axis was placed at  $45^\circ$  ( $\beta = 45^\circ$ ) with respect to  $\vec{k}_{in}$  and a single  $m_I = 0$  run was taken. Using Eqs. (A-2) and (4-3) in Eq. (A-1), one can again write expressions for the yield in each detector:

$$\begin{aligned} L &= nN\Omega_L \left(1 + \frac{3\sqrt{2}}{2} p_{ZA_y} - \frac{1}{4} p_{ZZA_{xx}}\right) \\ R &= nN\Omega_R \left(1 - \frac{3\sqrt{2}}{2} p_{ZA_y} - \frac{1}{4} p_{ZZA_{xx}}\right) \\ U &= nN\Omega_U \left(1 + \frac{1}{2} p_{ZZA_{xz}} - \frac{1}{4} p_{ZZA_{yy}}\right) \\ D &= nN\Omega_D \left(1 - \frac{1}{2} p_{ZZA_{xz}} - \frac{1}{4} p_{ZZA_{yy}}\right). \end{aligned} \quad (A-6)$$

The most efficient way in which to obtain  $A_{xz}$  is to use a twofold ( $180^\circ$ ) rotational sequence of the cube with an  $m_I = 0$  beam to obtain

$$p_{ZZA_{xz}} = \frac{2(U_0 - D_0)}{U_0 + D_0} \left(1 - \frac{1}{4} p_{ZZA_{yy}}\right),$$

where geometric means have again been used. Notice that a prior knowledge of  $A_{yy}$  is required before  $A_{xz}$  can be obtained.

Advantages and disadvantages of this method were briefly discussed in Chapter III.

## APPENDIX B

### LOW ENERGY ANALYZING POWER MEASUREMENTS

#### IN THE REACTION ${}^3\text{He}(\vec{d}, p){}^4\text{He}$

Measurements presented here represent an early attempt at determining the analyzing powers for the  ${}^3\text{He}(\vec{d}, p){}^4\text{He}$  reaction at low energies. Data were obtained in the cube scattering chamber by the use of Rapid Method (La 71) with  $\beta$ , the angle between  $\hat{s}$  and  $\vec{k}_{in}$ , set at  $54.7^\circ$ . This permitted simultaneous measurements of  $A_y$ ,  $A_{xz}$ , and  $\frac{1}{2}(A_{xx} - A_{yy})$  in a manner independent of current integration.

A 1-nA polarized beam of deuterons was used to bombard a 2.66-cm diameter  ${}^3\text{He}$  cell operating at a pressure of 760 Torr. Entrance and exit windows of the cell were 2.1-mg/cm<sup>2</sup> Havar foil, respectively. Detector telescopes consisted of  $\Delta E$  and E surface barrier detectors of thickness 330  $\mu$  and 1000  $\mu$ , respectively.

Results of these measurements are presented in Table 16. The errors listed in the table are purely statistical. It is estimated that all errors are at least as large as 0.01. One of the large uncertainties is that of the beam polarization as the accuracy of the quench ratio method (Oh 71a) is at present uncertain at very low beam energies. Also, no attempt has been made to correct the data for multiple scattering which can result in a

Table 16

Analyzing Power Measurements For The Reaction  ${}^3\text{He}(\vec{d},p){}^4\text{He}$  For  
 $1.03\text{MeV} \leq E_d \leq 4.00\text{MeV}$

$E_d$ (MeV)	$\theta_p^{\text{lab}}$ (deg)	$\theta_{\text{c.m.}}$ (deg)	$A_y$	$A_{xz}$	$\frac{1}{2}(A_{xx}-A_{yy})$
1.03	30	32.1	0.039±0.010	-0.335±0.006	-0.061±0.007
1.03	45	48.0	0.043±0.012	-0.442±0.008	-0.110±0.005
1.03	55	58.5	0.014±0.014	-0.474±0.012	-0.193±0.012
1.03	75	79.1	0.051±0.017	-0.442±0.015	-0.372±0.014
1.03	90	94.2	0.031±0.014	-0.238±0.013	-0.572±0.011
1.03	105	109.1	-0.008±0.012	0.139±0.011	-0.694±0.010
1.62	30	32.6	0.078±0.004	-0.281±0.006	-0.015±0.006
1.62	55	59.3	0.106±0.006	-0.398±0.009	0.017±0.009
1.62	75	80.1	0.044±0.011	-0.536±0.016	-0.197±0.016
1.62	90	95.3	0.020±0.022	-0.388±0.019	-0.444±0.018
1.62	105	110.1	-0.034±0.022	-0.033±0.021	-0.668±0.018
1.62	125	129.3	-0.023±0.014	0.585±0.020	-0.731±0.018
1.62	145	148.0	0.002±0.010	0.945±0.014	-0.444±0.014
2.18	30	33.0	0.090±0.005	-0.312±0.008	-0.014±0.008
2.18	55	60.0	0.093±0.015	-0.348±0.011	0.152±0.012
2.18	75	80.8	0.046±0.008	-0.590±0.012	0.027±0.012
2.18	90	96.0	-0.004±0.009	-0.522±0.013	-0.284±0.013
2.18	105	110.8	-0.025±0.011	-0.136±0.016	-0.606±0.015
2.18	125	130.0	0.004±0.010	0.557±0.015	-0.762±0.013
2.18	145	148.5	0.025±0.009	0.918±0.012	-0.474±0.012
2.88	30	33.4	0.089±0.004	-0.480±0.006	-0.082±0.006
2.88	45	49.9	0.100±0.006	-0.317±0.008	0.125±0.009
2.88	55	60.6	0.078±0.006	-0.295±0.008	0.312±0.009
2.88	75	81.6	-0.006±0.007	-0.544±0.010	0.248±0.011
2.88	90	96.9	-0.019±0.008	-0.551±0.011	-0.070±0.011
2.88	105	111.6	-0.008±0.013	-0.250±0.019	-0.446±0.018
4.00	30	34.0	-0.027±0.005	-0.813±0.007	-0.252±0.007
4.00	45	50.6	-0.032±0.006	-0.384±0.009	0.117±0.010
4.00	55	61.5	-0.055±0.007	-0.281±0.010	0.469±0.011
4.00	75	82.7	-0.090±0.008	-0.404±0.011	0.657±0.012
4.00	90	98.0	-0.052±0.009	-0.445±0.013	0.403±0.014
4.00	105	112.7	0.062±0.010	-0.390±0.015	-0.139±0.015

larger effective scattering angle than that at which the detectors are set.

Comparison of our results with the measurements of Gruebler et al. (Gr 71) have been made at 2.8 and 4.0 MeV where direct comparison could be made. Agreement with  $A_y$  was good except at  $\theta_{\text{lab}} = 75^\circ$  and  $90^\circ$ . In addition, there appeared to be systematic differences in  $A_y$  at 4 MeV. Agreement of  $\frac{1}{2}(A_{xx} - A_{yy})$  was fair, but again there appeared to be systematic differences in the 4 MeV data. There was considerable disagreement on the measurement of  $A_{xz}$  at both energies.

It is interesting to compare the 1.03 MeV data obtained here at  $\theta_{\text{c.m.}} = 58.5^\circ$  with the respective analyzing powers at this angle and energy as extracted from the thick geometry experiment described in Chapter IV. Agreement with  $A_y$  is good. The calculated values of  $A_{xz}$  and  $\frac{1}{2}(A_{xx} - A_{yy})$  are -0.524 and -0.253, respectively, as compared to the measured values here of  $-0.474 \pm 0.012$  and  $-0.193 \pm 0.012$ , respectively. The estimated seven percent uncertainty in energy in the thick geometry experiment is not sufficient alone to achieve agreement. However, when this possibility is considered in addition to an estimated 4% depolarization of the beam at this energy (Oh 73d), agreement can be obtained.

## APPENDIX C

### FINITE GEOMETRY COMPUTER CODE, YIELD

YIELD was a computer code written to integrate over the thick geometry which prevailed in the deuteron polarization transfer apparatus.

An incremental yield at a detector may be written as  $\Delta y = nN\sigma t\Delta\Omega$ , where  $n$  is the number of particles in an increment of incident beam,  $N$  is the target density ( $\#/cm^3$ ),  $\sigma$  is a cross section ( $cm^2$ ),  $t$  is the target thickness (cm), and  $\Delta\Omega$  is the solid angle subtended by the detecting area.

For the present case:

$n = n(E', a_1) da_1 dE'$ , the number of deuterons in a given energy bin which enter the  ${}^3\text{He}$  cell through a particular incremental area and

$$\sigma = \frac{I_{\text{tot}}(\text{c.m.})}{4\pi} \frac{d\sigma_{\text{lab}}}{d\sigma_{\text{c.m.}}}, \text{ the laboratory polarized}$$

differential cross section and

$t = ds$ , an increment of deuteron path length in the  ${}^3\text{He}$  cell (corresponding to a 25 keV increment as used here) and

$$\Delta\Omega = \frac{da_2}{r^2}, \text{ where } da_2 \text{ is an incremental area at}$$

a detector and  $r^2$  is the distance between  $ds$  and

$da_2$ . The total yield in a detector is then given by

$$Y = \int_{E'} \int_{a_1} \int_{0^*}^{E_1} \int_{a_2} n(E', a_1) \frac{I_{\text{tot}}(\text{c.m.})}{4\pi} \frac{d\sigma_{\text{lab}}}{d\sigma_{\text{c.m.}}} .$$

$$\begin{aligned}
 & [1 + 3/2 p_y A_y + 2/3 p_{xz} A_{xz} + 1/6 (p_{xx} - p_{yy}) (A_{xx} - A_{yy}) \\
 & + 1/2 p_{zz} A_{zz} ] \cdot \frac{1 dE'}{\epsilon r^2} da_1 dE da_2,
 \end{aligned}
 \tag{C-1}$$

where  $\epsilon = -\frac{1}{N} \cdot \frac{dE}{ds}$ , the definition of the stopping

cross section, has been substituted for  $ds/dE$ .

The asterisk on the middle integral means it was

terminated when the deuterons had less than  $\Delta E/2$

keV left, or when they reached the far side of the

${}^3\text{He}$  cell.

Several versions were used depending on the nature of the questions being asked. In the  ${}^3\text{He}(\overset{*}{d}, p){}^4\text{He}$  calibration experiment, one version was used to calculate the excitation function illustrated in Fig. 13 by calculating a yield in the zero degree detector for each incident unpolarized deuteron distribution. Additional outputs included average interaction energies and average interaction center-of-mass angles.

Later versions were used to determine the analyzing powers for the  ${}^3\text{He}(\overset{*}{d}, p){}^4\text{He}$  reaction (see Chapter IV) which were required to reproduce the experimentally observed ratios (i.e., Eq. (4-5)). It was intended that the code could have been modified to unfold, from the thick geometry, the various polarization transfer coefficients should the need arise. However, in view of the smallness of the p-d polarization effects, the modification was not made. The version listed here was used to determine effective thick

geometry analyzing powers to be used in the  $^4\text{He}(\vec{d},\vec{d})^4\text{He}$  experiment (Oh 73a) for various conditions of  $^3\text{He}$  cell illumination and outgoing deuteron energy distributions.

Inputs to the version of YIELD listed here are:

CARD 1 NX, NY, NR, NDET1, NDET

NX and NY are the number of divisions into which the  $^3\text{He}$  cell entrance is divided, NR is the number of concentric circular elements into which each detecting area is divided, NDET1 is the number of the first detector, and NDET is the number of detectors in the array.

CARD 2 NANG

There are NR values to be read in. Each value gives the number of angular increments into which the corresponding ring of detecting area is to be further divided.

CARD 3 YTH

YTH gives the angular dependence of the deuteron yield entering the  $^3\text{He}$  cell (permitting unevenness of illumination calculations)

CARD 4 ETH

ETH gives the angular dependence of

the central energy of the deuteron distributions entering each incremental area of the  $^3\text{He}$  cell.

(Kinematics and subsequent magnifications of small energy differences during the slowing process permits deuterons of higher energy to enter the small angle side of the  $^3\text{He}$  cell than those which enter the large angle side)

CARD 5 YL, B, ZF

YL is the height and B is the width of the  $^3\text{He}$  cell entrance (inches). ZF is the distance from the  $^3\text{He}$  cell entrance to the origin of the analyzing reaction coordinate system (i.e. the point at which the detectors are aimed).

CARD 6 RO, PHE3, THE3, RO1

RO is the radius of the  $^3\text{He}$  cell (inches). PHE3 is the absolute cell pressure (p.s.i.). THE3 is the cell temperature ( $^{\circ}\text{C}$ ), and RO1 is the distance from the primary reaction to the  $^3\text{He}$  cell entrance (inches).

CARD 7 SDET

SDET is the distance from the origin of the analyzing reaction to the respective detectors (inches).

CARD 8 DDET

DDET is the diameter of the useful detecting surface for the respective detectors.

CARD 9 TH2, PHIDET1, DPHI, TH1

TH2 is the laboratory polar angle at which the NDET-1 detectors are set, PHIDET1 is the azimuthal angle of the first detector, DPHI is the azimuthal angular separation, and TH1 is the laboratory scattering angle of the primary reaction.

YIELD then calculated the coordinates of the centroid of each incremental area and stored them for future use in calculating  $r^2$  and the rotated polarization quantities appropriate for use in Eq. (C-1).

Cross section data for the  ${}^3\text{He}(d,p){}^4\text{He}$  reaction were taken from Ya 53, interpolated in 20 keV increments, and input as data. Stopping cross section data for deuterons in helium were taken from Wh 58, again interpolated in 20 keV increments and input as data.

Because the integration scheme was the heart of the

program, polarization quantities appropriate for each incremental cross section were determined from initial beam polarizations by the use of vector dot and cross products. These could be determined and the "rotation" effected much more rapidly than in the usual way of evaluating trigonometric functions

Included at the end of the program listing is a set of sample input data. This particular version was for an unpolarized incident beam. Ordinarily, incident beam polarization quantities must be read in.

```

PROGRAM YIELD(INPUT,OUTPUT)
COMMON AAXYY, AAXZ, AAY, AAZZ, AV1(3), AV2(3), A1(100,3),
1     A2(9,25,3), B, BD(3), D, DA1, DA2(9), DDET(9), DPHI, E,
2     ECENTR, ENG(15), FXXPXX, FYPX, FYPY, FZZPZZ, LL, NANG(6),
3     NDA1, NDA2, NDET, NENG, NR, NX, NY, PHI, PHIDET1, PX,
4     PXXYY, PXY, PXZ, PY, PYZ, PZZ, R(3), RD(3), RXIOEPS, S,
5     SDET(9), SIGMA, THCM, TH2, XI, XK(3), XNP(3), YINC(15), YL,
6     ZF, FXXPXY, FXZPXZ, FXZPYZ,
7     AXXYYAV(9), AXZAVG(9), AYAVG(9), AZZAVG(9), FXXPXXA(9),
7     FXXPYA(9), FXZPXZA(9), FXZPYZA(9), FYPXA(9), FYPYA(9),
8     FZZPZZA(9), SYCM(9), SYE(9), YELD(9),
9     EAVG(9), EDE(25), EDH(25,5), ETH(5),
0     THCM(9), XKX(100,3), XNPX(100,3), YDE(25), YDH(25,5),
1     YTH(5)
DIMENSION XTOT(90),EPSLON(90)
1 FORMAT(10I5)
2 FORMAT(12F6,3)
5 FORMAT(1H1)
111 FORMAT(38H ENERGY SUBDIVISION SET FOR 5 INCR ONLY )
112 FORMAT(5H ESET 12F10,3)
314 FORMAT(59X,9H TIMIT=,F13,3,16H CALLED FINITE,I7)
400 FORMAT(4H NX=,I3,2X3HNY=,I3,3X3HNR=,I3,13H FIRST DET=,I3,12H
1LAST DET=,I3)
401 FORMAT(16X,5HNANG=,I3,20(2X,I3))
402 FORMAT(4H YL=,F6,3,3X2HB=,F6,3,3X3HZF=,F6,3,3X3HDE=,F4,0)
403 FORMAT(4H RO=,F6,3,3X5HPHE3=,F6,2,3X5HTHE3=,F6,2,3X4HR01=,F6,3)
404 FORMAT(20H DETECTOR DISTANCES ,F6,3,8(3X,F6,3))
405 FORMAT(20H DETECTOR DIAMETERS ,F6,3,8(3X,F6,3))
406 FORMAT(24H 8 DETECTORS AT TH(LAB)=,F6,2,5X,23HCHAMBER SET AT TH(LA
1B)=,F6,2)
407 FORMAT(23H FIRST DETECTOR AT PHI=,F6,2)
408 FORMAT(28H 8 DETECTORS SPACED BY DPHI=,F6,2)
410 FORMAT(5H DA1=,F6,4,3X7HDA2(I)=,9(2X,F6,4))
412 FORMAT(//)
413 FORMAT(32H YIELD VS THETA AT HE3 ENTRANCE .7F10,3)

```

```

414 FORMAT(32H ENERGY VS THETA AT HE3 ENTRANCE,7F10.3)
415 FORMAT(110H D  EAVG      YIELD  THCM      AY      AXZ  AXXZZ      AZZ
1      PX      PY      PXZ      PYZ  PXXYY      PXY      PZZ
)
416 FORMAT(I2,F6.0,F11.2,F7.2,11F7.3)
417 FORMAT(7F10.3)
850 FORMAT(41H INCREMENTAL AREA COORDINATES AT ENTRANCE )
852 FORMAT(10X,1H(,F8.4,1H,,F8.4,1H,,F8.4,1H))
853 FORMAT(39H INCREMENTAL AREA COORDINATES AT DET.           15)
855 FORMAT(23H INITIAL BEAM DIRECTION )
856 FORMAT(40H INCREMENTAL NORMALS TO FIRST SCATTERING )
858 FORMAT(40H INCREMENTAL BEAM DIRECTIONS AT ENTRANCE )
      PRINT 5
602 READ 1,NX,NY,NR,NDET1,NDET
      IF (NX.LE.0) GO TO 603
      READ 1,(NANG(I),I=1,NR)
C  READ YIELD AND ENERGY VS THETA OF FIRST SCATTERING
      READ 2,(YTH(I),I=1,NX)
      READ 417,(ETH(I),I=1,NX)
      PRINT 413,(YTH(I),I=1,NX)
      PRINT 414,(ETH(I),I=1,NX)
      PRINT 400,NX,NY,NR,NDET1,NDET
      PRINT 401,(NANG(I),I=1,NR)
      READ 2,YL,B,ZF
      DE=25.
      PRINT 402,YL,B,ZF,DE
      READ 2,RO,PHE3,THE3,RO1
      PRINT 403,RO,PHE3,THE3,RO1
      READ 2,(SDET(I),I=1,NDET)
      PRINT 404,(SDET(I),I=1,NDET)
      READ 2,(DDET(I),I=1,NDET)
      PRINT 405,(DDET(I),I=1,NDET)
      F=2.54
      YL=YL*F
      B=B*F
      ZF=ZF*F

```

```

RO=RO*F
R01=R01*F
DO 3 I=1,NDET
SDET(I)=SDET(I)*F
3 DDET(I)=DDET(I)*F
READ 2,TH2,PHIDET1,DPHI,TH1
PRINT 406,TH2,TH1
PRINT 407,PHIDET1
PRINT 408,DPHI
F=0.0174532925
C F=3.1415926536/180.
TH1=TH1*F
TH2=TH2*F
PHIDET1=PHIDET1*F
DPHI=DPHI*F
XNHE3=6.025*PHE3/14.7/(273.16+THE3)/82.3*1.E+23
NDA1=NX*NY
NDA2=0
DO 4 I=1,NR
4 NDA2=NDA2+NANG(I)
CALL SETUP2
PRINT 410,DA1,(DA2(I),I=1,NDET)
PRINT 850
DO 851 I=1,NDA1
851 PRINT 852,(A1(I,J),J=1,3)
DO 900 JJ=NDET1,NDET
PRINT 853, JJ
DO 854 I=1,NDA2
854 PRINT 852,(A2(JJ,I,J),J=1,3)
900 CONTINUE
DATA XTOT/0.,0.,.255,2.58,9.,21.,40.,67.6,105.,153.,210.,274.,344.,
1,417.,495.,540.,672.,761.,834.,887.,920.,934.,929.,906.,867.,820.,
2771.,723.,678.,637.,600.,568.,540.,515.,492.,470.,448.,427.,406.,3
387.,370.,355.,342.,330.,320.,310.,301.,293.,285.,277.,270.,263.,25
47.,251.,245.,239.,234.,229.,224.,219.,215.,211.,207.,203.,200.,196

```

5.,193.,190.,187.,184.,181.,179.,177.,174.,172.,170.,168.,166.,164.  
6,163.,161.,159.,158.,156.,155.,154.,152.,151.,149.,148./  
DATA EPSLON/,05,3.26,4.70,5.69,6.27,6.71,7.12,7.19,7.27,7.22,7.21,  
17.13,6.96,6.73,6.48,6.23,6.02,5.84,5.69,5.55,5.43,5.31,5.19,5.07,4  
2.95,4.83,4.71,4.59,4.48,4.36,4.26,4.16,4.07,3.99,3.91,3.84,3.78,3.  
371,3.65,3.60,3.54,3.49,3.43,3.38,3.33,3.28,3.23,3.18,3.13,3.09,3.0  
44,3.00,2.95,2.91,2.87,2.83,2.79,2.75,2.71,2.68,2.64,2.61,2.57,2.54  
5,2.51,2.48,2.45,2.42,2.4,2.37,2.35,2.33,2.31,2.29,2.28,2.26,2.25,2  
6.24,2.23,2.22,2.21,2.20,2.20,2.19,2.19,2.18,2.18,2.17,2.16,2.15/

C DETERMINATION OF INITIAL BEAM DIRECTION(UNIT VECTOR)

BD(1)=-SIN(TH1)

BD(2)=0.

BD(3)=COS(TH1)

PRINT 855

PRINT 852,BD(1),BD(2),BD(3)

C INITIALIZE INITIAL YIELDS AND ENERGIES ON HE3 CELL ENTRANCE

TOTINC=1.E+09

NENG=5

FNY=NY

DO 100 NX1=1,NX

DO 100 NY1=1,NY

INDEX=NX1+NX\*(NY1-1)

EDE(INDEX)=ETH(NX1)

100 YDE(INDEX)=TOTINC\*YTH(NX1)/FNY

DO 101 J=1,NDA1

ECENTR=EDE(J)

SIGMA=398942.0/(1100.0+0.6636\*ECENTR)

C

C ENERGY SUBDIVISION FOR NORMAL DISTRIBUTION, 5 INCREMENTS

IF(NENG,NE,5) PRINT 111

ENG(1)=ECENTR-1.9386\*SIGMA

ENG(2)=ECENTR-0.9210\*SIGMA

ENG(3)=ECENTR

ENG(4)=ECENTR+0.9210\*SIGMA

ENG(5)=ECENTR+1.9386\*SIGMA

```

        YINC(1)=668.0
        YINC(2)=2417.0
        YINC(3)=3830.0
        YINC(4)=2417.0
        YINC(5)=668.0
        DO 110 I=1, 5
        IF(ENG(I).LE.0.0) YINC(I)=0.0
110 CONTINUE
        PRINT 112,ECENTR,SIGMA, (ENG(I),I=1,5), (YINC(I),I=1,5)
C
        TERM=YDE(J)*0.0001
        DO 102 K=1,NENG
        EDH(J,K)=ENG(K)
102 YDH(J,K)=YINC(K)*TERM
101 CONTINUE
C INITIALIZE INCREMENTAL BEAM DIRECTIONS ON HE3 CELL ENTRANCE
        DO 23 I=1,NDA1
        DIST=1.0/SQRT(A1(I,1)**2+A1(I,2)**2+(A1(I,3)+R01+ZF)**2)
        XKX(I,1)=A1(I,1)*DIST
        XKX(I,2)=A1(I,2)*DIST
        XKX(I,3)=(A1(I,3)+R01+ZF)*DIST
C CALCULATION OF INCREMENTAL NORMALS TO FIRST SCATTERING
        AV1(1)=XKX(I,1)
        AV1(2)=XKX(I,2)
        AV1(3)=XKX(I,3)
        CALL CROSS(BD,AV1,AV2)
        AV2DIST=1.0/SQRT(AV2(1)**2+AV2(2)**2+AV2(3)**2)
        XNPX(I,1)=AV2(1)*AV2DIST
        XNPX(I,2)=AV2(2)*AV2DIST
23 XNPX(I,3)=AV2(3)*AV2DIST
        PRINT 858
        PRINT 852, ((XKX(I,J),J=1,3),I=1,NDA1)
        PRINT 856
        PRINT 852, ((XNPX(I,J),J=1,3),I=1,NDA1)
        PRINT 5

```

```
PX=0.
PY=0.
PXY=0.
PXZ=0.
PYZ=0.
PXXYY=0.
PZZ=0.
DO 18 I=1,NDET
AYAVG(I)=0.
AXZAVG(I)=0.
AXXYYAV (I)=0.
AZZAVG(I)=0.
FYPXA(I)=0.
FYPYA(I)=0.
FXZPXZA(I)=0.
FXZPYZA(I)=0.
FXXPXXA(I)=0.
FXXPXYA(I)=0.
FZZPZZA(I)=0.
SYE(I)=0.
SYCM(I)=0.
18 YELD(I)=0.
KCFIN=0
KC=0
CALL SECOND(START)
DO 10 M=1,NENG
DO 10 J=1,NDA1
YD=YDH(J,M)
IF (YD.LE.0.0) GO TO 10
610 CONTINUE
R(1)=A1(J,1)
R(2)=A1(J,2)
R(3)=A1(J,3)
E=EDH(J,M)
14 IF (E-0.5*DE.LE.0.0) GO TO 10
```

```

IF (R(1)**2+R(2)**2+(R(3)+ZF)**2-R0**2.GE.0.0) GO TO 10
KENN=0.05*E
KEN=KENN+1
IF(KEN.GE.90) KEN=90
KENP1=KEN+1
TERM=(E-20.0*FLOAT(KENN))*0.05
XTOTX=(XTOT(KEN)+(XTOT(KENP1)-XTOT(KEN))*TERM)*(1.E-27)
C IF EVER KEN=90, THEN KENP1=91, THIS WILL CAUSE TROUBLE ABOVE.
EPS=(1.E+18)/(EPSLON(KEN)+(EPSLON(KENP1)-EPSLON(KEN))*TERM)
RXIOEPS=XTOTX*EPS
DS2=DE*EPS/XNHE3
DX=DS2*XKX(J,1)
DY=DS2*XKX(J,2)
DZ=DS2*XKX(J,3)
IF(KC)10,13,15
13 R(1)=R(1)+0.5*DX
R(2)=R(2)+0.5*DY
R(3)=R(3)+0.5*DZ
GO TO 16
15 R(1)=R(1)+DX
R(2)=R(2)+DY
R(3)=R(3)+DZ
16 KC=KC+1
DO 17 L=NDET1,NDET
DO 17 K=1,NDA2
RD(1)=A2(L,K,1)
RD(2)=A2(L,K,2)
RD(3)=A2(L,K,3)
XK(1)=XKX(J,1)
XK(2)=XKX(J,2)
XK(3)=XKX(J,3)
XNP(1)=XNPX(J,1)
XNP(2)=XNPX(J,2)
XNP(3)=XNPX(J,3)
KCFIN=KCFIN+1

```

```

CALL FINITE2
DYELD =YD *XI*DA2(L)*DE/((RD(1)-R(1))**2+(RD(2)-R(2))**2+(RD(
13)-R(3))**2)
YELD(L)=YELD(L)+DYELD
AYAVG(L)=AYAVG(L)+DYELD*AAV
AXZAVG(L)=AXZAVG(L)+DYELD*AAXZ
AXXYAV(L)=AXXYAV(L)+DYELD*AAXXY
AZZAVG(L)=AZZAVG(L)+DYELD*AAZZ
FYPXA(L)=FYPXA(L)+DYELD*FYPX
FYPYA(L)=FYPYA(L)+DYELD*FYPY
FXZPXZA(L)=FXZPXZA(L)+DYELD*FXZPXZ
FXZPYZA(L)=FXZPYZA(L)+DYELD*FXZPYZ
FXXPXXA(L)=FXXPXXA(L)+DYELD*FXXPXX
FXXPXYA(L)=FXXPXYA(L)+DYELD*FXXPX
FZZPZZA(L)=FZZPZZA(L)+DYELD*FZZPZZ
SYCM(L)=SYCM(L)+DYELD*THCM
17 SYE(L)=SYE(L)+DYELD*E
E=E-DE
GO TO 14
10 CONTINUE
PRINT 415
DO 21 I=NDET1,NDET
OOYELD=1.0/YELD(I)
SAY =AYAVG (I)*OOYELD
SAXZ =AXZAVG (I)*OOYELD
SAXXY=AXXYAV(I)*OOYELD
SAZZ =AZZAVG (I)*OOYELD
SPX =FYPXA (I)*OOYELD
SPY =FYPYA (I)*OOYELD
SPXZ =FXZPXZA(I)*OOYELD
SPYZ =FXZPYZA(I)*OOYELD
SPXXY=FXXPXXA(I)*OOYELD
SPXY =FXXPXYA(I)*OOYELD
SPZZ =FZZPZZA(I)*OOYELD
THCMA(I)=SYCM (I)*OOYELD/F

```

```

EAVG (I)=SYE (I)*00YELD
21 PRINT416,I,EAVG(I),YELD(I),THCMA(I),SAY,SAXZ,SAXXYY,SAZZ,SPX,SPY,
1SPXZ,SPYZ,SPXXYY,SPXY,SPZZ
CALL SECOND(END)
TIMIT=END-START
PRINT 314,TIMIT,KCFIN
PRINT 412
GO TO 602
603 CONTINUE
STOP
END
SUBROUTINE SETUP2
COMMON AAXXYY, AAXZ, AAY, AAZZ, AV1(3), AV2(3), A1(100,3).
1      A2(9,25,3), B, BD(3), D, DA1, DA2(9), DDET(9), DPHI, E.
2      ECENTR, ENG(15), FXXPXX, FYPX, FYPY, FZZPZZ, LL, NANG(6),
3      NDA1, NDA2, NDET, NENG, NR, NX, NY, PHI, PHIDET1, PX,
4      PXXYY, PXY, PXZ, PY, PYZ, PZZ, R(3), RD(3), RXIOEPS, S,
5      SDET(9), SIGMA, THCM, TH2, XI, XK(3), XNP(3), YINC(15), YL,
6      ZF
C  NX      NO. OF INCREMENTS ALONG BASE OF HE3 CELL ENTRANCE
C  NY      NO. OF INCREMENTS ALONG HEIGHT OF HEO CELL ENTRANCE
C  NDA1    NO. OF HE3 CELL ENTRANCE INCREMENTAL AREAS
C  NDA2    NO. OF DETECTOR INCREMENTAL AREAS
C  NR      NO. OF RADIUS INCREMENTS
C  NDET    NO. OF DETECTORS
C  YL      HEIGHT OF HE3 CELL ENTRANCE
C  B       BASE OF HE3 CELL ENTRANCE
C  ZF      DISTANCE HE3 CELL ENTRANCE IS IN FRONT OF ORIGIN
C  TH2     ANGLE AT WHICH POLAR DETECTORS ARE SET
C  PHIDET1 AZIMUTHAL ANGLE OF FIRST DETECTOR
C  DPHI    AZIMUTHAL ANGLE INCREMENT BETWEEN DETECTORS
C  NANG    NO. OF ANGLE INCREMENTS (1 NO. FOR EACH RADIUS INCREMENT)
C  SDET    DISTANCE TO DETECTOR
C  DDET    DIAMETER OF DETECTOR COLLIMATOR
C  DA1     SIZE OF HE3 CELL ENTRANCE INCREMENTAL AREA (RETURN)

```

```

C DA2    SIZE OF DETECTOR INCREMENTAL AREA (RETURN)
C A1     COORDINATES OF HE3 CELL ENTRANCE INCREMENTAL AREAS (RETURN)
C A2     COORDINATES OF DETECTOR INCREMENTAL AREAS (RETURN)
C COMPUTE HE3 ENTRANCE COORDINATES
  A=YL*B
  DA1=A/NDA1
  DX=B/NX
  DY=YL/NY
  A1(1,1)=0.5*(B-DX)
  A1(1,2)=0.5*(YL-DY)
  A1(1,3)=-ZF
  KK=0
  TERM1=A1(1,1)
  TERM2=A1(1,2)
  TERM3=A1(1,3)
  DO 1 LL=1,NY
    II=LL-1
    DO 1 MM=1,NX
      JJ=MM-1
      KK=KK+1
      A1(KK,1)=TERM1-JJ*DX
      A1(KK,2)=TERM2-II*DY
    1 A1(KK,3)=TERM3
C COMPUTE COORDINATES OF 54.7 DEG DETECTORS
  II=NDET-1
  PHI=PHIDET1
  DO 3 LL=1,II
    S=SDET(LL)
    D=DDET(LL)
    CALL DETDIV
  3 PHI=PHI-DPHI
C COMPUTE COORDINATES OF 0.0 DEG DETECTOR
  TH2=0.
  PHI=0.
  S=SDET(NDET)

```

```

D=DDET(NDET)
LL=NDET
CALL DETDIV
RETURN
END

```

```

SUBROUTINE DETDIV

```

```

COMMON AAXXY, AAXZ, AAY, AAZZ, AV1(3), AV2(3), A1(100,3),
1      A2(9,25,3), B, BD(3), D, DA1, DA2(9), DDET(9), DPHI, E,
2      ECENTR, ENG(15), FXXPXX, FYPX, FYPY, FZZPZZ, LL, NANG(6),
3      NDA1, NDA2, NDET, NENG, NR, NX, NY, PHI, PHIDET1, PX,
4      PXXYY, PXY, PXZ, PY, PYZ, PZZ, R(3), RD(3), RXIOEPS, S,
5      SDET(9), SIGMA, THCM, TH, XI, XK(3), XNP(3), YINC(15), YL,
6      ZF

```

```

C LL      NUMBER OF DETECTOR UNDER CONSIDERATION
C NR      NUMBER OF RADIUS INCREMENTS
C TH      POLAR ANGLE OF DETECTOR
C PHI     AZIMUTHAL ANGLE OF DETECTOR
C NDA2    NUMBER OF DETECTOR INCREMENTAL AREAS
C NDET    NUMBER OF DETECTORS
C S       DISTANCE TO DETECTOR
C D       DIAMETER OF DETECTOR COLLIMATOR
C NANG    NUMBER OF ANGLE INCREMENTS(1 NO. FOR EACH RADIUS INCREMENT)
C DA2     SIZE OF DETECTOR INCREMENTAL AREA (RETURN)
          A=0.7853981634*D**2
C          A=3.14159/4.*D**2
          DA2(LL)=A/NDA2
          W=COS(TH)
          X=SIN(TH)
          Y=COS(PHI)
          Z=SIN(PHI)
          R1=0.
          JJ=0
          ZCM=S
          DO 4 II=1,NR
          BETA=0.

```

```

MM=NANG(II)
DBETA=6.2831853072/FLOAT(MM)
DBETA=2.*3.1415926536/MM
ALPHA=DBETA
R2=SQRT(2.*DA2(LL)/ALPHA+R1**2)
IF(MM=1)5,6,7
6 RCM=0.
GO TO 8
7 RCM=2./3.*(R2*R2+R1*R2+R1*R1)/(R1+R2)
8 CONTINUE
TERM2=0.5*DBETA
DO 3 NN=1,MM
ALPHA=BETA+DBETA
JJ=JJ+1
TERM=ALPHA-TERM2
XCM=RCM*COS(TERM)
YCM=RCM*SIN(TERM)
TERM=XCM*W
TERM3=ZCM*X
A2(LL,JJ,1)=TERM*Y-YCM*Z+TERM3*Y
A2(LL,JJ,2)=TERM*Z+YCM*Y+TERM3*Z
A2(LL,JJ,3)=ZCM*W-XCM*X
3 BETA=BETA+DBETA
4 R1=R2
GO TO 9
5 PRINT 10
10 FORMAT(62H TROUBLE,CANNOT DIVIDE DETECTOR AREA INTO ZERO INCREMENT
1S,MM=0)
9 RETURN
END
SUBROUTINE FINITE2
COMMON AAXYY, AAXZ, AAY, AAZ, AV1(3), AV2(3), A1(100,3),
1 A2(9,25,3), B, BD(3), D, DA1, DA2(9), DDET(9), DPHI, E,
2 ECENTR, ENG(15), FXXPXX, FYPX, FYPY, FZZPZZ, LL, NANG(6),
3 NDA1, NDA2, NDET, NENG, NR, NX, NY, PHI, PHIDET1, PX,

```

```

4      PXXYY, PXY, PXZ, PY, PYZ, PZZ, R(3), RD(3), RXIOEPS, S,
5      SDET(9), SIGMA, THCM, TH2, XI, XK(3), XNP(3), YINC(15), YL,
6      ZF, FXXPY, FXZPXZ, FXZPYZ
      DIMENSION XN(3), RR(3), C(3)
C  XK      DIRECTION OF BEAM (UNIT VECTOR)
C  E       ENERGY OF BEAM
C  XNP     DIRECTION OF NORMAL TO FIRST SCATTERING
C  PX, PY  VECTOR POLARIZATION
C  PXY, PXZ, PYZ, PXXYY, PZZ
C          TENSOR POLARIZATION.
C  FKXZ, FKXXYY, FKZZ
C          ANALYZER SCALING CONSTANTS
C  RXIOEPS RATIO OF UNPOLARIZED X-SECTION TO STOPPING POWER
C  R       COORDINATES OF SOURCE POINT
C  RD      COORDINATES OF DETECTION POINT
C  XI      CALCULATED (POLARIZED) CROSS SECTION
      ABSRR=0.0
      DO 10 II=1,3
      RR(II)=RD(II)-R(II)
10     ABSRR=RR(II)**2+ABSRR
      OOABSRR=1.0/SQRT(ABSRR)
      DO 20 II=1,3
20     RR(II)=RR(II)*OOABSRR
      CALL CROSS(XK,RR,XN)
      SINTH=SQRT(XN(1)**2+XN(2)**2+XN(3)**2)
C  COMPUTE DIRECTION OF NORMAL TO SECOND SCATTERING (UNIT VECTOR)
      IF (SINTH-1.E-10.GT.0.0) GO TO 40
      COSTH=1.0
      COSPH=1.0
      SINPH=0.0
      GO TO 70
40     DO 30 II=1,3
30     XN(II)=XN(II)/SINTH
      CALL DOT(XK,RR,COSTH)
C  COMPUTE AZIMUTHAL ANGLE

```

```

CALL CROSS(XN,XNP,C)
CALL DOT(C,XK,SINPH)
CALL DOT(XN,XNP,COSPH)
70 TERM=1.0/(E+18353.50718)
AA=.319850048*E*TERM
BB=.080491985*E*TERM
TERM2=1.0+0.697617304*18353.50718*TERM
CC=.120566056*TERM2
DD=.479091908*TERM2
FS=SQRT(DD/BB-SINTH**2)
FJACOB=(BB*(COSTH+FS)**2)/SQRT(AA*CC)/FS
XXIO=0.25*RXIOEPS*0.318309886*FJACOB
C XXIO=RXIOEPS/4./3.14159*FJACOB
SCMTH=SQRT(BB*(COSTH+FS)**2/DD)*SINTH
TH=ASIN(SCMTH)
CCMTH=COS(TH)
THCM=ASIN(SCMTH)
AAY=0.0
IF(SINTH.LT.0.5) GO TO 80
AAY=-1.34097E-05*(1.-1.9191*E*(1.-.17544E-02*E*(1.-.94999E-03*E)))
80 FKXZ=.95204*(1.-.13217E-03*E*(1.-.16387E-03*E*(1.-.26618E-02*E)))
AAXZ=-1.5*FKXZ*SCMTH*CCMTH
FKXXYY=.9522*(1.+ .38082E-03*E*(1.-.32989E-02*E*(1.-.31137E-03*E)))
AAXXYY=-1.5*FKXXYY*SCMTH**2
FKZZ=.95230*(1.+ .16733E-03*E*(1.-.38401E-02*E*(1.-.41051E-03*E)))
AAZZ=-.5*FKZZ*(3.*CCMTH**2-1.)
FYPX=1.5*SINPH*AAY
FXZPXZ=COSPH*AAXZ/1.5
FYPY=1.5*COSPH*AAY
FXZPYZ=-SINPH*AAXZ/1.5
FXXPXX=(COSPH**2-SINPH**2)*AAXXYY/6.0
FXXPXY=-4.0*SINPH*COSPH*AAXXYY/6.0
FZZPZZ=0.5*AAZZ
XI=XXIO*(1.0+PY*FYPY+PX*FYPX+PXZ*FXZPXZ+PYZ*FXZPYZ +PXXYY*FXXPXX+
1PXY*FXXPXY+PZZ*FZZPZZ)

```

C IN THIS VERSION PY=PX=PXZ=PYZ=PXXYY=PLY=PZZ=0.0 IF THIS WILL ALWAYS  
 C BE TRUE, THEN THE STATEMENT ABOVE SHOULD BE CHANGED ETC.

```

RETURN
END
SUBROUTINE DOT(A,B,D)
DIMENSION A(3),B(3)
D=A(1)*B(1)+A(2)*B(2)+A(3)*B(3)
RETURN
END
SUBROUTINE CROSS(A,B,C)
DIMENSION A(3),B(3),C(3)
C(1)=A(2)*B(3)-A(3)*B(2)
C(2)=A(3)*B(1)-A(1)*B(3)
C(3)=A(1)*B(2)-A(2)*B(1)
RETURN
END
  
```

166

	3	3	2	1	9					
	1	4	8							
1,000	1,000	1,000								
635,000		635,000		635,000						
.750	.250	.280								
.5	70.3	22.2		3.672						
3.1	3.1	3.1		3.1	3.1	3.1	3.1	3.1	3.1	3.1
.83	.83	.83		.83	.83	.83	.83	.83	.83	.83
+54.00	+00.00	-45.00		+30.00						

## ACKNOWLEDGMENTS

The author would like to express his sincere appreciation to Dr. William G. Simon of the University of Wyoming for his advice and assistance, and to Dr. Gerald G. Ohlsen of Los Alamos Scientific Laboratory for his encouragement, council, and guidance in the experimental work and writing of the thesis, and to Dr. P. W. Keaton, Jr., of LASL for his supervision during the early stages of apparatus design and construction in Dr. Ohlsen's absence.

Gratitude is extended to the University of Wyoming and to Associated Western Universities for financial support, and to LASL for providing for the use of facilities.

Thanks are due Ben Roybal (LASL/P-9) for drafting most of the shop drawings; Ray Squires and staff (LASL/P-12) for machining the deuteron polarization transfer chamber and associated parts; Lloyd Catlin (P-9) for his technical assistance in assembly and installation of the transfer chamber; Dr. G. C. Salzman for his assistance in data collection and computer programming for the spin-up-to-spin-down polarization transfer data reduction technique; and Mrs. Judy Elder for typing the manuscript.

In addition, the author would like to express special thanks to his parents for their love and encouragement; and to his wife Nancy and three sons for the love, patience, and understanding extended during his graduate career.

## REFERENCES

- (Aa 72) J. C. Aarons, and I. H. Sloan, Nucl. Phys. A182 (1972) 369.
- (Al 51) A. J. Allen, J. F. Nechaj, K. H. Sun, and B. Jennings, Phys. Rev. 81 (1951) 538.
- (Ar 67) J. Arvieux, Nucl. Phys. A102 (1967) 513.
- (Ar 69) D. D. Armstrong, J. G. Beery, E. R. Flynn, W. S. Hall, P. W. Keaton, Jr., and M. P. Kellogg, Nucl. Instr. Meth. 70 (1969) 69.
- (Av 71) Y. Avishai and A. S. Rinat, Phys. Lett. 37B (1971) 487.
- (Be 58) J. S. Bell and F. Mandl, Proc. Phys. Soc. A71 (1958) 272 and 867.
- (Bl 52) R. J. Blin-Stoyle, Proc. Phys. Soc. A65 (1952) 452.
- (Br 66) L. Brown, H. A. Christ, and H. Rudin, Nucl. Phys. 79 (1966) 459.
- (Br 70) R. Brünig, B. Zeitnitz, and J. Arvieux, Polarization Phenomena in Nuclear Reactions, ed. H. H. Barschall and W. Haeberli (University of Wisconsin Press, Madison, 1971) p. 445
- (Ch 53) R. S. Christian and J. L. Gammel, Phys. Rev. 91 (1953) 100.
- (Cl 67) T. B. Clegg and W. Haeberli, Nucl. Phys. A95 (1967) 608.
- (Da 52) R. H. Dalitz, Proc. Phys. Soc. A65 (1952) 175.
- (Do 72) P. Doleschall, Phys. Lett. 38B (1972) 298.
- (Fa 61) L. D. Faddeev, JETP (Sov. Phys.) 12 (1961) 1014.
- (Fo 71) B. Forssmann, G. Graf, H. Schober, and H. P. Jochim, Polarization Phenomena in Nuclear Reactions, ed. H. H. Barschall and W. Haeberli (University of Wisconsin Press, Madison, 1971) p. 537.

- (Ga 59) A. Galonsky, H. B. Willard, and T. A. Welton, Phys. Rev. Lett. 2 (1959) 349.
- (Ga 70) J. L. Gammel, P. W. Keaton, Jr., and G. G. Ohlsen, Los Alamos Scientific Laboratory Report LA-4492-MS (1970).
- (Ga 71) J. L. Gammel, P. W. Keaton, Jr., and G. G. Ohlsen, Polarization Phenomena in Nuclear Reactions, ed. H. H. Barschall and W. Haeberli (University of Wisconsin Press, Madison, 1971) p. 411.
- (Ga 72) J. L. Gammel, D. C. Dodder, and K. Witte, private communication.
- (Go 58) L. J. B. Goldfarb, Nucl. Phys. 7 (1958) 622.
- (Go 59) L. J. B. Goldfarb, Nucl. Phys. 12 (1959) 657.
- (Gr 66) W. Grüebler, W. Haeberli, and P. Extermann, Nucl. Phys. 77 (1966) 394.
- (Gr 71) W. Grüebler, V. König, A. Ruh, P. A. Schmelzbach, R. E. White, and P. Marmier, Nucl. Phys. A176 (1971) 631.
- (Gr 72) W. Grüebler, V. König, R. E. White, P. Risler, A. Ruh, P. A. Schmelzbach, and P. Marmier, private communication, submitted for publication
- (Ha 70) W. Haeberli, Three-Body Problem in Nuclear and Particle Physics, ed. J. S. C. McKee and P. M. Rolph (North-Holland, Amsterdam, 1970) p. 188.
- (Iv 67) M. Ivanovich, Ph.D. Thesis, Australian National University, 1967.
- (Ja 66) J. F. Janni, Air Force Weapons Laboratory Report AFWL-TR-65-150 (Sept. 1966).
- (Ja 70) S. Jaccard, J. Piffaretti, R. Viennet, and J. Weber, Polarization Phenomena in Nuclear Reactions, ed. H. H. Barschall and W. Haeberli (University of Wisconsin Press, Madison, 1971) p. 448.
- (Ke 71) P. W. Keaton, Jr., D. D. Armstrong, L. L. Catlin, and G. G. Ohlsen, "A Study of Systematic Errors in Nuclear Polarization Measurements," Los Alamos Scientific Laboratory, 1971, (unpublished).

- (La 69) G. P. Lawrence, G. G. Ohlsen, and J. L. McKibben, Phys. Lett. 28B (1969) 594.
- (La 71) G. P. Lawrence, G. G. Ohlsen, J. L. McKibben, P. W. Keaton, Jr., and D. D. Armstrong, Polarization Phenomena in Nuclear Reactions, ed. H. H. Barschall and W. Haeberli (University of Wisconsin Press, Madison, 1971) p. 855.
- (Le 71) C. Leemann, H. Bürgisser, P. Huber, U. Rohrer, H. Paetz Gen. Shieck, and F. Seiler, Ann. Phys. (N. Y.) 66 (1971) 810.
- (Li 71) W. W. Lindstrom, R. Garrett, and U. Von Mollendorff, Nucl. Instr. Meth. 93 (1971) 387.
- (Lo 64) C. Lovelace, Phys. Rev. 135 (1964) B1225.
- (Lo 73) P. A. Lovoi, G. C. Salzman, G. G. Ohlsen, C. K. Mitchell, and W. Gruebler, "Polarization Transfer in  $^3\text{He}(d,d)^3\text{He}$  Elastic Scattering", (1973) submitted to Phys. Rev. C
- (Mc 65) L. C. McIntyre, Jr., Ph.D. Thesis, University of Wisconsin, 1965.
- (Mc 67) L. C. McIntyre, Jr., and W. Haberli, Nucl. Phys. A91 (1967) 369.
- (Mc 71) J. L. McKibben, G. P. Lawrence, and G. G. Ohlsen, Polarization Phenomena in Nuclear Reactions, ed. H. H. Barschall and W. Haeberli (University of Wisconsin Press, Madison, 1971) p. 828.
- (Oh 70) G. G. Ohlsen, Los Alamos Scientific Laboratory Report LA-4451 (1970).
- (Oh 71a) G. G. Ohlsen, J. L. McKibben, G. P. Lawrence, P. W. Keaton, Jr., and D. D. Armstrong, Phys. Rev. Lett. 27 (1971) 599.
- (Oh 71b) G. G. Ohlsen, "Lecture Notes," (1971) p. 19 (unpublished).
- (Oh 72a) G. G. Ohlsen, J. L. Gammel, and P. W. Keaton, Jr., Phys. Rev. C 5 (1972) 1205.
- (Oh 72b) G. G. Ohlsen, Rep. Prog. Phys. 35 (1972) 717.

- (Oh 73a) G. G. Ohlsen, G. C. Salzman, C. K. Mitchell, W. G. Simon, and W. Gruebler, "Polarization Transfer in  $^4\text{He}(d,d)^4\text{He}$  Elastic Scattering", (1973) submitted to Phys. Rev.
- (Oh 73b) G. G. Ohlsen, and P. W. Keaton, Jr., Nucl. Instr. & Meth. 109 (1973) 41.
- (Oh 73c) G. G. Ohlsen, P. A. Lovoi, G. C. Salzman, U. Meyer-Berkhout, C. K. Mitchell, and W. Gruebler, "Analyzing Power for d- $^4\text{He}$  Elastic Scattering at 12.0, 14.0, and 17.0 MeV", (1973) submitted to Phys. Rev.
- (Pi 72a) S. C. Pieper, Nucl. Phys. A193 (1972) 529.
- (Pi 72b) S. C. Pieper, Phys. Rev. C 6 (1972) 1157.
- (Pi 73) S. C. Pieper, (private communication, to be published)
- (Pu 68) R. D. Purrington and J. L. Gammel, Phys. Rev. 168 (1968) 1174.
- (Re 53) H. Reynolds, D. Dunbar, W. Wenzel, and W. Whaling, "The Stopping Cross Section of Gasses for Protons, 30-600 keV," Phys. Rev. 92 (1953) 742.
- (Sa 58) G. R. Satchler, Nucl. Phys. 8 (1958) 65.
- (Sa 73) G. C. Salzman, C. K. Mitchell, and G. G. Ohlsen, "Techniques for Polarization Transfer Coefficient Determination", Nucl. Instr. Meth. 109 (1973) 61.
- (Se 64) F. Seiler, S. E. Darden, L. C. McIntyre, and W. G. Weitkamp, Nucl. Phys. 53 (1964) 65.
- (Se 65) E. Segre, Nuclei and Particles, W. A. Benjamin, Inc. (N. Y.), (1965) Chapter II
- (Se 70) J. D. Seagrave, Three-Body Problem in Nuclear and Particle Physics, ed. J. S. C. McKee and P. M. Rolph (North-Holland, Amsterdam, 1970) p. 41
- (Si 59) E. A. Silverstein, Nucl. Instr. Meth. 4 (1959) 60.
- (Si 71) M. Simonius, Polarization Phenomena in Nuclear Reactions, ed. H. H. Barschall and W. Haeberli (University of Wisconsin Press, Madison, 1971) p. 401

- (St 69) V. S. Starkovich, Ph.D. Thesis, University of Wyoming, 1969; Los Alamos Scientific Laboratory Report LA-4191 (1969)
- (Th 52) T. Thompson, "Effect of Chemical Structure on Stopping Powers of High Energy Protons," Ph.D. Thesis, University of California, UCRL-1910 (1952).
- (Tr 67) W. Trachslin, L. Brown, T. B. Clegg, and R. S. Seyler, Phys. Lett. 25B (1967) 585.
- (Va 67) W. T. H. van Oers, and K. W. Brockman, Jr., Nucl. Phys. A92 (1967) 561.
- (Wh 58) W. Whaling, Encyclopedia of Physics, ed. S. Flugge (Springer-Verlag, Berlin, Gottingen, Heidelberg, 1958) Vol. XXXIV p. 193.
- (Wh 72) R. E. White, W. Gruebler, V. König, R. Risler, A. Ruh, P. A. Schmelzbach, and P. Marmier, Nucl. Phys. A180 (1972) 593.
- (Wo 52) L. Wolfenstein and J. Ashkin, Phys. Rev. 85 (1952) 947.
- (Wo 56) L. Wolfenstein, Ann. Rev. Nucl. Sci. 6 (1956) 43.
- (Ya 53) J. L. Yarnell, R. H. Loveberg, and W. R. Stratton, Phys. Rev. 90 (1953) 295.
- (Yo 65) P. G. Young, Ph.D. Thesis, Australian National University, 1965.